Structural and functional analysis of the HOPS tethering complex at the yeast vacuole

Dissertation zur Erlangung des Grades

Doktor der Naturwissenschaften

(Dr. rer. nat)

eingereicht am Fachbereich Biologie/ Chemie der

Universität Osnabrück

von

Cornelia Bröcker

Osnabrück, März 2011

Hauptberichterstatter:	Prof. Dr. Christian Ungermann
Berichterstatter:	apl. Prof. Dr. Siegfried Engelbrecht-Vandré

Table of Contents

I. Publications and manuscripts

Ostrowicz*, C.W., **Bröcker*, C.**, Ahnert, F., Nordmann, M., Lachmann, J., Peplowska, K., Perz, A., Auffarth, K., Engelbrecht-Vandré, S., Ungermann, C. (2010) Defined subunit arrangement and rab interactions are required for functionality of the HOPS tethering complex. Traffic. 11(10):1334-46.

Nordmann, M., Cabrera, M., Perz, A., **Bröcker, C.**, Ostrowicz, C.W., Engelbrecht-Vandré, S., Ungermann, C. (2010) The Mon1-Ccz1 complex is the GEF of the late endosomal Rab7 homolog Ypt7. Current Biology. 20(18):1654-9.

Cabrera, M., Langemeyer, L., Mari, M., Rethmeier, R., Orban, I., Perz, A., **Bröcker, C.**, Griffith, J., Klose, D., Steinhoff, H.J., Reggiori, F., Engelbrecht-Vandré, S., Ungermann, C. (2010) Phosphorylation of a membrane curvature-sensing motif switches function of the HOPS subunit Vps41 in membrane tethering. Journal of Cell Biology. 191(4):845-59.

Balderhaar*, H.J.k., Arlt*, H., Ostrowicz, C.W., **Bröcker, C.**, Sündermann, F., Brandt, R., Babst, M., Ungermann, C. (2010) The Rab GTPase Ypt7 is linked to retromer-mediated receptor recycling and fusion at the yeast late endosome. Journal of Cell Science. 123(23):4085-94.

Bröcker, C., Engelbrecht-Vandré, S., Ungermann, C., (2010) Multisubunit tethering complexes and their role in membrane fusion. Current Biology. 20(21):R943-54.

* these authors distributed equally to the respective works.

II. Summary

A prominent feature of eukaryotic cells is their compartmentalization. Distinct organelles are maintained and interconnected via transport vesicles. For this purpose, vesicles pinch off at a donor membrane and fuse with the target membrane to release their cargo. Defined transport routes between the organelles ensure delivery of the correct cargo to the target organelle.

For fusion of transport vesicles within the endocytic pathway two related tethering complexes together with their corresponding Rab GTPases and SNAREs[1] are responsible. The CORVET[2] complex shares four of its six subunits with HOPS[3] and is involved in fusion of early endosomes, where it interacts with the Rab GTPase Vps21. The vacuolar HOPS complex functions as the Rab GTPase Ypt7 effector, and is involved in fusion of endosomes and AP-3 vesicles, which are transported from the Golgi to the vacuole by omitting the endosmes, with the vacuole. In addition, HOPS mediates the homotypic fusion of vacuoles. An intermediate complex between CORVET and HOPS (i-CORVET), which might be a transition state, contains one CORVET- and one HOPS-specific subunit.

In my PhD thesis, I focused on the functional and structural analysis of the HOPS complex. Therefore, I purified HOPS from a *Saccharomyces cerevisiae* overexpression strain. The purified HOPS complex was functional and could stimulate vacuole fusion *in vitro*. The same approach was used to examine HOPS assembly from subcomplexes. I reconstituted the entire HOPS from a tetrameric and a dimeric subcomplex.

I could also show that the HOPS-specific subunit Vps39 is indispensable for HOPS activity, and that its absence was partially compensated for by the CORVET homologous subunit Vps3 in i-CORVET. This complex showed the same binding specificity to Ypt7-GTP as HOPS, but was unable to rescue fusion of fusion-deminished vacuoles. The fusion of these inhibited vacuoles was stimulated by HOPS addition, but the postulated function of Vps39 as recruitmentfactor for Ypt7 from within the complex was excluded.

To investigate the HOPS structure single subunits of HOPS were GFP-tagged or contained internal deletions. With this approach, I could on the one hand reduce tethering activity by interfering with HOPS stability and functionality. On the other

hand HOPS fusion activity was reduced via deletion of a membrane-binding domain. The mechanisms of fusion inhibition and stimulation are still not clarified and need to be further elucidated.

I finally analyzed the fusion-active HOPS by electron microscopy in cooperation with the Stefan Raunser group (Max-Planck insitute, Dortmund, Germany). HOPS exhibits an elongated dumb-bell like shape with a flexible arm. We used two different GFP-tagged versions to localize the Rab binding site and the SNARE binding site in the complex. After single particle analysis and class averaging we solved the two-dimensional structure. Via negative staining and tilting of the grid inside the microscope we determined the three-dimensional structure of single particles at low resolution. This work is still in progress.

---

[1] Soluble N-ethylmaleimide sensitive protein receptors

[2] Class C Core vacuole endosome tethering

[3] Homotypic fusion and vacuole protein sorting

III. Zusammenfassung

Eine bedeutsame Eigenschaft eukaryotischer Zellen ist ihre Kompartimentierung. Die verschiedenen Organellen sind über Transportvesikel miteinander verbunden, die von einer Donormembran abgeschnürt werden und mit einer Zielmembran fusionieren, um ihr Cargo abzuliefern. Definierte Transportwege zwischen den Organellen gewährleisten die Auslieferung des korrekten Cargo zum Zielorganell.

Für die Fusion von Transportvesikeln im endozytischen Weg sind zwei ähnliche *Tethering* Komplexe und ihre zugehörigien Rab GTPasen und SNAREs verantwortlich. Der CORVET Komplex, der vier von sechs Untereinheiten mit dem HOPS Komplex gemein hat, ist an Fusionen mit dem frühen Endosom beteiligt, wo er mit der Rab GTPase Vps21 interagiert. Der vakuoläre HOPS Komplex ist der Effektor der Rab GTPase Ypt7 und an der Fusion von Endosomen und AP-3 Vesikeln, die vom Golgi unter Umgehung des Endosoms zur Vakuole transportiert werden, mit der Vakuole beteiligt. Der HOPS Komplex vermittelt zudem die homotypische Vakuolenfusion. Ein Intermediatkomplex zwischen CORVET und HOPS (i-CORVET), der möglicherweise einen Übergangszustand darstellt, enthält eine CORVET- und eine HOPS-spezifische Untereinheit.

In meiner Doktorarbeit fokussierte ich mich auf die funktionelle und strukturelle Analyse des HOPS Komplexes. Ich konnte HOPS aus einem *Saccharomyces cerevisiae* Überexpressionsstamm aufreinigen. Der aufgereinigte HOPS war funktionell und konnte die *in vitro* Vakuolenfusion stimulieren. Mit dem gleichen Ansatz wurde die Assemblierung von HOPS aus Unterkomplexen analysiert. Ich konnte aus einem tetrameren Unterkomplex zusammen mit einem dimeren Unterkomplex den gesamten HOPS rekonstituieren und seine Aktivität nachweisen.

Ich konnte weiterhin zeigen, dass Vps39 unersätzlich für die HOPS Aktivität ist und dessen Fehlen nur teilweise durch die homologe CORVET Untereinheit Vps3 im i-CORVET kompensiert wurde. Dieser Komplex zeigte die gleiche Bindungsspezifität für Ypt7-GTP wie HOPS, konnte allerdings die Fusion von fusions-inhibierten Vakuolen nicht retten. Die Fusion der inhibierten Vakuolen wurde hingegen durch HOPS-Zugabe stimuliert, allerdings wurde die postulierte Funktion von Vps39, als Faktor zur Rekrutierung von Ypt7, innerhalb des Komplexes ausgeschlossen.

Um die Struktur des HOPS zu analysieren, stellte ich HOPS Komplexe her, bei denen einzelne Untereinheiten mit Epitopen (GFP) markiert wurden, oder Deletionen enthielten. Mit Hilfe dieses Ansatzes konnte ich einerseits die HOPS *Tethering* Aktivität durch Beeinflussung der Stabilität und Funktionalität reduzieren. Andererseits wurde die Fusionsaktivität von HOPS durch entfernen einer Membranbindedomäne erhöht. Die Mechanismen der Fusionsinhibition und –stimulation sind noch nicht vollständig aufgeklärt und müssen weiter analysiert werden.

Ich analysierte schließlich den fusionsaktiven HOPS unter dem Elektronenmikroskop in Kooperation mit der Gruppe von Stefan Raunser (MPI, Dortmund, Deutschland). Der HOPS besitzt eine hantelförmige Struktur mit einem flexiblen Arm. Wir verwendeten HOPS Komplexe mit zwei GFP-Epitopen, um die Rab-Bindestelle und die SNARE-Bindestelle im Komplex zu lokalisieren. Mit Hilfe von Einzelpartikel-Analysen und *Class Averaging* konnten wir die zweidimensionale Struktur lösen. Durch Negativ-Färbung und Neigen des HOPS-beladenen Gitters im Mikroskop wurde die dreidimensionale Struktur einzelner Partikel analysiert. Diese Arbeit ist noch nicht vollständig abgeschlossen.

1. Introduction

1.1 The eukaryotic endomembrane system

In contrast to prokaryotes, eukaryotic cells contain morphological distinct organelles designed for specific cellular requirements. Each organelle is surrounded by a bilayered membrane, which differs in protein and lipid composition. The organelles of the endomembrane system (ER, Golgi, Endosomes and vacuole/lysosome) are required for protein and lipid processing, sorting and degradation. On their way through these organelles, proteins and lipids are processed and thereby activated and afterwards recycled or degraded. Small bilayered vesicles mediate protein transport through organelles. They are transported either along the cytoskeleton or diffuse freely to reach their target organelle. For sorting of proteins and lipids into the correct transport vesicle and for vesicle release, a fission machinery is required. Vesicles only fuse with the correct target organelle by help of a dedicated fusion machinery. Organelles therefore contain specific sets of proteins and lipids for fission and fusion of transport vesicles.

1.1.1 Intracellular transport pathways and their organelles

The organelles of the endomembrane system and some transport pathways are summarized in Figure 1.1. The nomenclature in the following chapters is used according to the *Saccharomyces cerevisiae* nomenclature and is compared to higher eukaryotes, where indicated. In this study the model organism *S. cerevisiae* was used since genetic manipulations are easy to conduct. Many proteins and their functions within the endomembrane system are conserved from yeast to mammalians. Even though general mechanisms exist from yeast to human, some specific features of the endomembrane system are only present in yeast.

1.1.1.1 The endoplasmatic reticulum (ER)

During biosynthesis proteins are translated on free ribosomes and released into the cytosol or alternatively co-translationally released into the endoplasmatic reticulum (ER), the first sorting and processing organelle in the endomembrane system. It is directly connected to the nucleus, where gene expression is regulated. Proteins destined for cellular compartments or the extracellular space, contain a specific signal peptide, which targets them to the ER and through the secretory pathway. They are

released into the ER lumen or incorporated into the ER membrane, if they contain a transmembrane domain. Already at this stage, the topology of the protein in the membrane is determined and does not change during further transport. Proteins are also modified in the ER by addition of different carbohydrate chains before they are routed by vesicular transport to the Golgi apparatus.

1.1.1.2 The Golgi apparatus (Golgi)

The Golgi is an organelle consisting of stacked cisternae, where proteins are further modified and processed before getting sorted via transport vesicles to the plasma membrane, the endosomal compartment or the vacuole (Figure 1.1). Newly synthesized proteins are transported in COPII-coated vesicles to the *cis*-Golgi and are further processed by traveling through the Golgi stacks. Traffic between these Golgi cisternae takes place in an anterograde and a retrograde manner and is supported by long coiled-coil proteins (coiled-coil tether, see 1.2.2.1). During this transport, proteins are further glycosylated or proteolytically cleaved to mature into their active form. At the *trans*-Golgi network (TGN), cargo is enriched in specific sites ensuring the correct sorting into different transport vesicles.

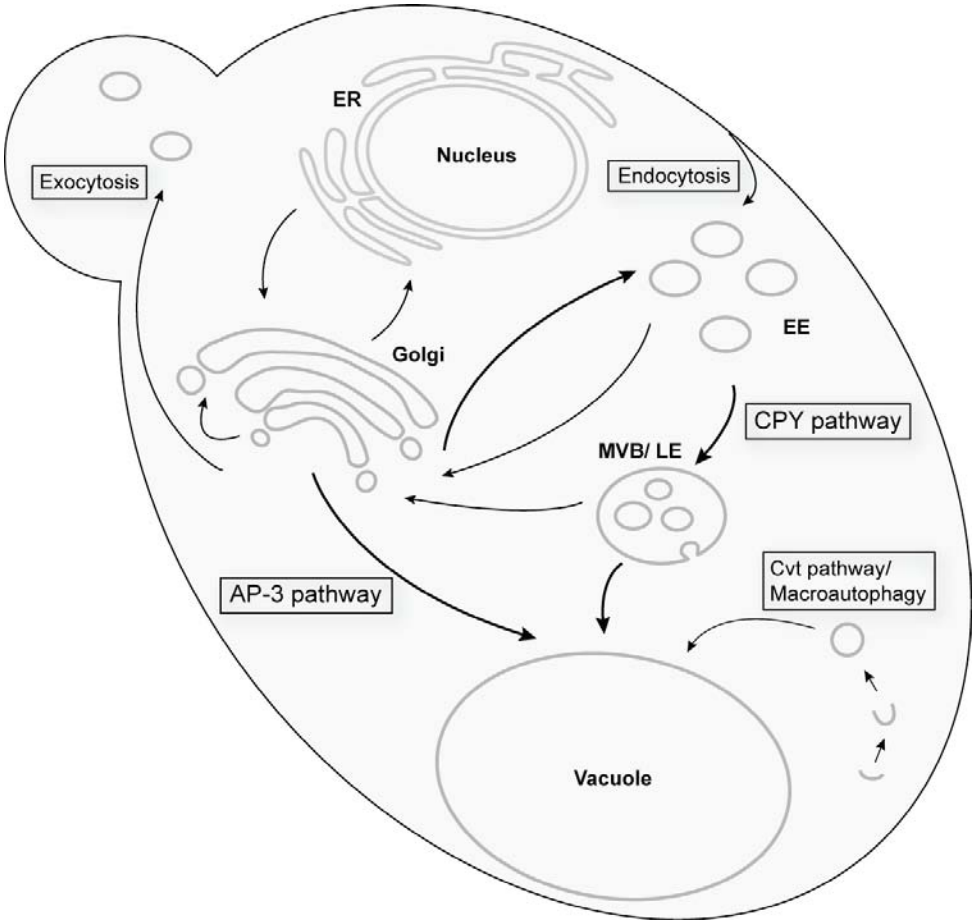

Figure 1.1: Overview of the intracellular trafficking pathways. Some trafficking pathways are highlighted by rectangles. Synthesized proteins are transported from ER to Golgi, where they are sorted into early endosomes and are further routed via the CPY pathway to the vacuole. Other Golgi-derived proteins are directly transported to the vacuole bypassing the endosomal compartment. This pathway is named after its adaptor protein complex 3, AP-3 pathway. Proteins endocytosed from the plasma membrane are transported via the endosomal compartment to the vacuole. Cytoplasmic proteins are engulfed by a membrane of unknown origin and traffic via the Cvt pathway or in autophagosomes (macroautophagy) to the vacuole. ER, endoplasmatic reticulum; EE, early endosome; MVB/LE, multivesicular body/ late endosome; CPY, carboxypeptidase Y; AP-3 adaptor protein complex-3 (Figure modified after Bröcker et al., 2010).

1.1.1.3 The endosomal compartment

The endosomal compartment constitutes the third sorting device along the protein transport pathway. During endocytosis, proteins from the extracellular space or integral plasma membrane proteins are incorporated into secretory vesicles. Fusion of these vesicles generates the early endosomal compartment. Golgi-derived vesicles carrying lysosomal components fuse with early endosomes to deliver their content (Figure 1.1). Interestingly, in plants the endosomes seem to directly evolve from the TGN (Sztul and Lupashin, 2006; Robinson et al., 2008).

Hydrolytic enzymes and proteins destined for degradation in the vacuole are retained in early endosomes, whereas other proteins are recycled back to the TGN with the help of the retromer complex (see 1.1.2.1), (Seaman et al., 2005). The early

endosomal compartment matures into the more acidic late endosomal compartment, where the assembled ESCRT machinery (see 1.1.2.2; Figure 1.2) forms intralumenal vesicles, which are then also called multivesicular bodies (MVBs) (Hurley and Emr, 2006). After fusion of the MVB with the vacuole, intralumenal vesicles are degraded in the vacuolar lumen.

1.1.1.4 Transport pathways to the vacuole

The biosynthetic transport pathway from TGN via endosomes to the vacuole is termed after one of its cargo proteins CPY (carboxypeptidase Y) pathway (Rothman et al., 1989; Stevens et al., 1982). Many lipases and hydrolases are transported via this pathway to the vacuole (Figure 1.1). Vesicles with different origins fuse with early and late endosomes, which then carry a mixture of endocytosed proteins and proteins derived from the Golgi, all destined for the vacuole. Before reaching the vacuole endosomes mature through different stages accompanied by changes in protein and lipid content. After fusing with the vacuole proteins and lipids are degraded or proteolytically cleaved for activation. A small group of vacuolar resident proteins, e.g. alkaline phosphatase Pho8 (ALP), the SNAREs (**s**oluble **N**-ethylmaleimide-sensitive **a**ttachment protein **re**ceptor) Vam3 and Nyv1 and the casein kinase Yck3, travel to the vacuole more directly by omitting the endosomal compartment (Darsow et al., 1998; Reggiori and Pelham, 2002; Sun et al., 2004; Wen et al., 2006). This pathway is termed AP-3 pathway, after its adaptor protein complex-3 (Figure 1.1).

Two other pathways, the Cvt (cytoplasm to vacuole targeting) and the macroautophagy pathway use similar sets of proteins and lipids to transport cargo to the vacuolar lumen (Klionsky et al., 1992; Klionsky et al., 2005; Scott et al., 1997; Scott et al., 1996; Scott et al., 2000). In both pathways, a double membrane of unknown origin engulfs organelles and cytosolic material, which is packed into a vesicle during membrane maturation. Cvt vesicles and autophagosomes finally fuse with the vacuole (Klionsky et al., 2005). Despite these similarities, the Cvt pathway is a biosynthetic pathway, where proteins (like aminopeptidase I) are transported to their functional compartment, whereas the macroautophagy pathway is a catabolic pathway, induced during starvation to ensure the survival of the cell (Figure 1.1).

The numerous pathways underline the highly dynamic nature of the vacuole (Weisman et al., 2006). Vesicles from different origins with different sets of cargo fuse with the vacuole. Additionally, the vacuole itself can fragment during cytokinesis

or as stress response. During cell division, vacuolar vesicles are transported into the emerging bud, where they fuse homotypically, thus maintaining a low copy number of this organelle (Conradt et al., 1992; Weisman et al., 1987; Weisman and Wickner, 1988).

1.1.2 Sorting devices in the CPY pathway

The CPY and AP-3 pathways are two parallel transport routes from Golgi to the vacuole. Since the CPY pathway is used for the majority of cargo proteins, two essential checkpoints for regulation and sorting at the endosomal compartment are described in more detail.

1.1.2.1 Retromer complex

The retromer complex is the first sorting device in the endosomal compartment. It consists of a heteropentameric complex that associates with the cytosolic face of endosomes and mediates retrograde transport of Golgi-derived transmembrane cargo from endosomes back to the TGN. The best-characterized, recycled transmembrane protein is Vps10, the receptor for carboxypeptidase Y (Marcusson et al., 1994; Seaman et al., 2005). The main role of this receptor in the CPY pathway is to bind newly synthesized CPY and deliver it, packed into vesicles, to the vacuole for activation. After release of CPY into the endosomal lumen, the receptor is transported back to the TGN in a retromer-dependent manner.

The retromer complex can be divided into two distinct parts. A dimeric portion, consisting of Vps5 and Vps17, is responsible for recruiting retromer to endosomes, and a trimeric subcomplex (Vps26, Vps29 and Vps35) recognizes the cargo (Horazdovsky et al., 1997; Seaman et al., 1998; Arghi et al., 2004; Hierro et al., 2007). Both, Vps5 and Vps17 and their mammalian orthologs SNX1/2 and SNX6/7 (sorting nexins), contain BAR (**B**in/ **A**mphiphysin/ **R**vs) domains that can drive tubule formation and - by recruiting the cargo recognition complex - effectively coordinate cargo sorting and tubule carrier formation for recycling to the TGN (Gallop et al., 2005; Carlton et al., 2004; Figure 1.2, left part). In addition, the cargo recognition complex interacts with the Rab GTPase Ypt7, which seems to be an important factor in assembly of the complex and in coordination of cargo recycling (Nakada-Tsukui et al., 2005; Rojas et al., 2008; Seaman et al., 2009; Balderhaar et al., 2010).

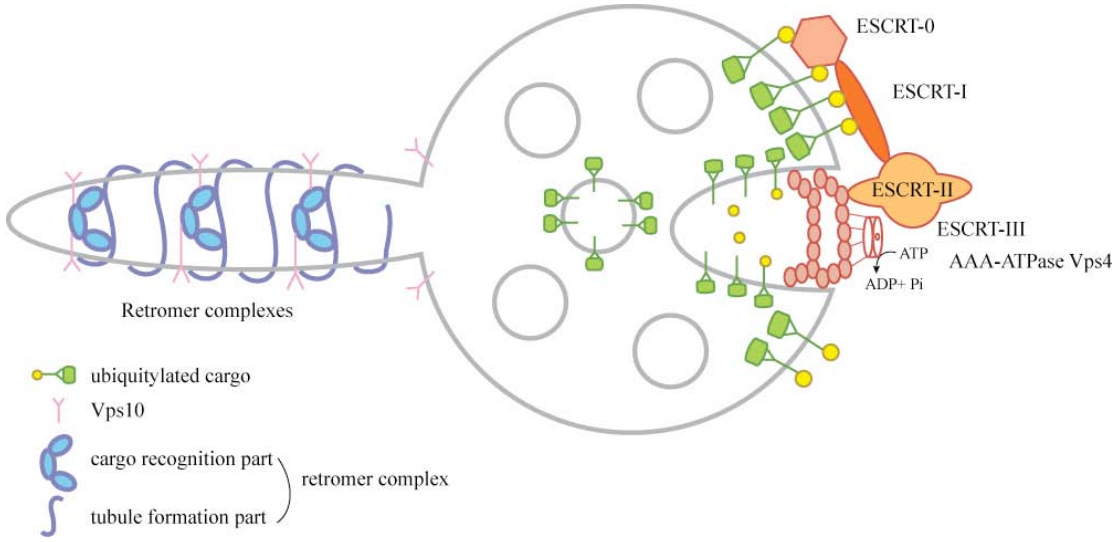

Figure 1.2: Sorting devices at the endosome. The retromer complex assembles from two subcomplexes (a cargo recognition portion and a tubule formation portion) and forms tubules to recycle the CPY receptor Vps10 (left part). The ESCRT machinery assembles stepwise by recognizing ubiquitylated cargo and recruiting the ESCRT complexes (right part). After the formation of intralumenal vesicles carrying selected cargo, they are pinched off by the AAA-ATPase Vps4. Thereafter the ESCRT machinery disassembles.

1.1.2.2 ESCRT machinery

Whereas the retromer rescues transmembrane proteins from the limiting membrane of the endosome for recycling back to the TGN, the ESCRT (**E**ndo**s**omal **C**omplex **R**equired for **T**ransport) machinery functions in the sorting of transmembrane proteins from the endosomal membrane into intralumenal vesicles (Bonifacino and Hurley, 2008; Figure 1.2, right part). Members of the ESCRT machinery recognize monoubiquitin- or lysine-63-linked polyubiquitin chains attached to cargo proteins. The recycling of ubiquitylated cargo is then inhibited and the endosomal membrane is deformed, allowing cargo to be sorted into endosomal invaginations. The ESCRT machinery catalyses the abscission of these invaginations with the help of the AAA-ATPase Vps4. As a result, intralumenal vesicles (ILVs) with sorted cargo are formed (Raiborg and Stenmark, 2009; Figure 1.2).

The ESCRT machinery consists of four complexes, called ESCRT-0 to ESCRT-III. They bind to the endosomal membrane in a well-defined order, recruiting one after the other (Teis et al., 2008). ESCRT-0 initiates cargo sorting into ILVs by recognizing and enriching the ubiquitylated cargo, whereby ESCRT-I is recruited. Afterwards ESCRT-II is recruited. Finally, ESCRT-III deforms the membrane, which leads to invaginations of the endosomal membrane (Teis et al., 2008). The invaginations are pinched off after the activation of the AAA-ATPase Vps4, which

results in the disassembly of ESCRT-III and the formation of the multivesicular body (MVB) (Lata et al., 2008; Figure 1.2).

The distinct activities of retromer and ESCRT contribute to the biochemical and structural remodeling that occur during maturation from early to late endosomes/MVBs. The opposing effect of both sorting devices on the endosomal membranes is essential for regulation of protein sorting.

1.2 Principles of vesicular tethering and fusion*

Transport vesicles, which pinched off a donor membrane, are targeted to the acceptor membrane to be consumed at their correct destination. They must either bring along or acquire the machinery necessary for fusion. Fusion of transported vesicles at their destination membrane requires the coordinated action of Rab GTPases, tethering complexes and SNAREs (Figure 1.3). After tethering, SNAREs from opposing membranes bring the two bilayers into close proximity by folding into specific four-helix-bundle complexes, which subsequently lead to fusion and lipid mixing of the bilayers (Jahn and Scheller, 2006; see 1.4). Tethers are thought to bridge membranes by binding to Rab GTPases as well as SNAREs and thus prepare them for fusion. Tethers may have additional membrane-binding modules to stabilize their interaction with Rabs and SNAREs. This general principle is widely accepted, even though it is surprising that in most cases no direct proof for a tethering function exists.

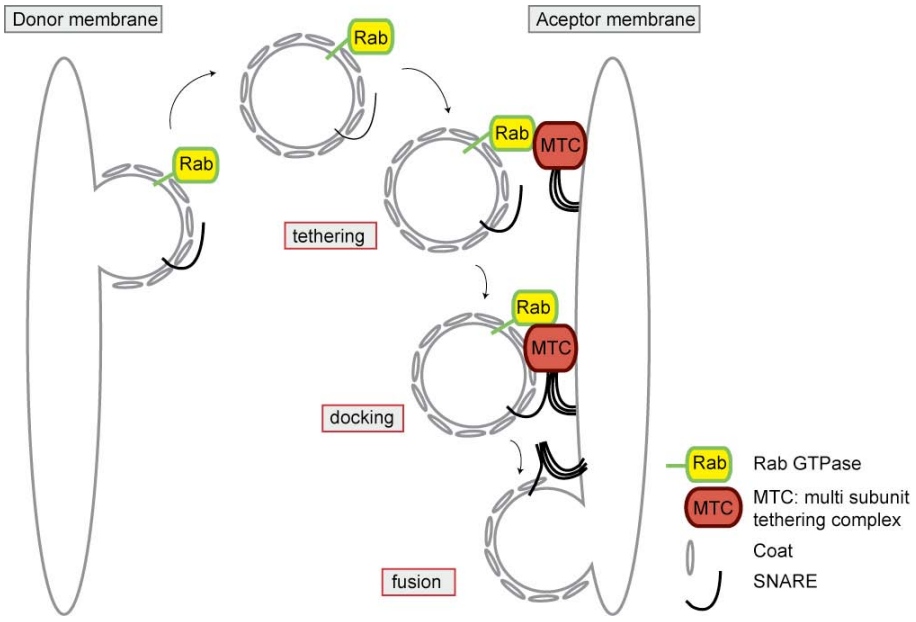

Figure 1.3: Coordinated action of Rab GTPases, multisubunit tethering complex (MTC) and SNAREs during vesicle budding and fusion. A vesicle is pinched off a donor membrane and transported to the acceptor membrane. After tethering via the interaction between Rab GTPase and MTC, *trans*-SNARE complexes are formed prior to vesicle fusion. The consecutive steps of tethering, docking and SNARE-mediated fusion are indicated (Figure from Bröcker et al., 2010)

1.2.1 Priming of vesicles to the target organelle*

To initiate the fusion reaction of a vesicle with the target organelle, Rab GTPases need to be activated. They are small GTP-binding proteins with low intrinsic GTP-hydrolysis and GDP-release activities (Barr and Lambright, 2010). Rabs serve as molecular switches, which exist in two conformations, depending on their nucleotide content (Behnia and Munro, 2005; Barr and Lambright, 2010; Bos et al., 2007). In their GDP-form, Rabs can be extracted from membranes by the Gdi1 protein (GDP-dissociation inhibitor), which chaperones the Rab in the cytosol. The recruitment to membranes requires displacement of Gdi1, potentially via a GDF (Gdi1-displacement factor), and subsequent activation by a GEF (GDP/GTP exchange factor) (Figure 1.4). These two activities may be comprised in one and the same protein (Schöbel et al., 2009). In their GTP-form, Rabs interact with their effectors, until their conversion back into the inactive GDP-form by a GAP (GTPase activating protein; Figure 1.4).

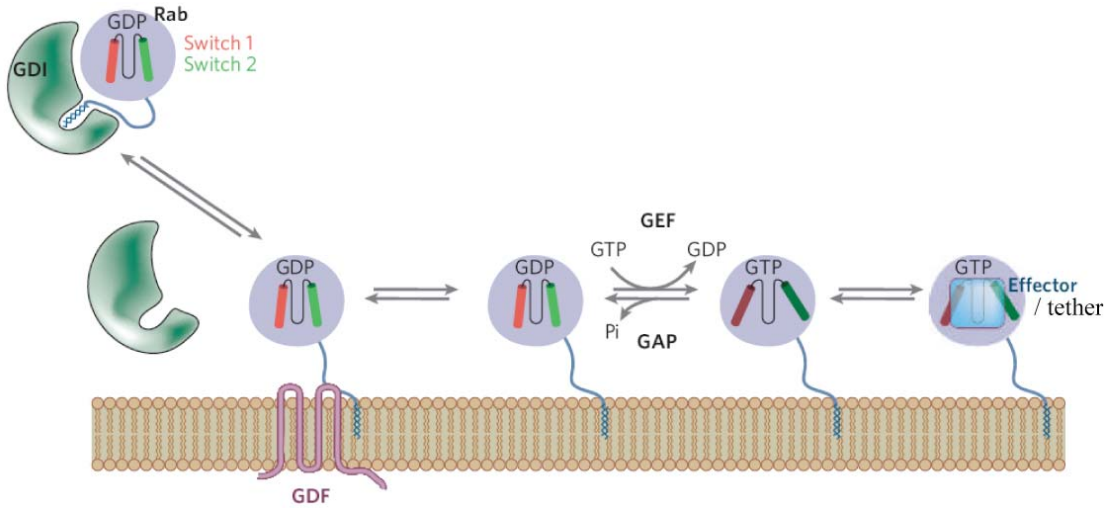

Figure 1.4: Model of the Rab cycle between cytosol and membrane. The cytosolic GDP-bound (inactive) Rab is chaperoned by Gdi1. By replacing Gdi1 for GDF, the Rab is recruited to membranes, where it is activated by the GEF. To be inactivated, the bound GTP is hydrolyzed to GDP with the help of the GAP and the Rab is released back into the cytosol. (Adopted from Behnia and Munro, 2005).

To function in fusion, Rabs in their GTP-loaded form interact with tethering factors (Cai et al., 2007). The cooperation between Rabs and tethering factors is necessary for vesicle capturing and tightly coupled to fusion of vesicles (Cai et al., 2007). Nevertheless, not all vesicles seem to be loaded with a Rab GTPase (e.g. AP-3 vesicles). Their tethering to the target organelle might be mediated by recognition of its coat by the respective tethering complex (see below; Figure 1.5).

1.2.2 Tethering of vesicles to the target organelle*

Two classes of tethering complexes have been characterized in eukaryotes: elongated coiled-coil tethers and multisubunit tethering complexes (MTCs, Figure 1.5). Both act as effectors of a Rab GTPase and are believed to mediate the initial and reversible contact between a vesicle and the acceptor organelle.

*1.2.2.1 Role of coiled-coil tethers**

Coiled-coil tethers are large hydrophilic dimeric proteins with two globular heads and predicted long coiled-coil domains in between (Gillingham and Munro, 2003; Sztul and Lupashin, 2006). Due to their size (up to >3000 residues (Gillingham and Munro, 2003)), they can bridge distances of more than 200nm (Figure 1.5). Most coiled-coil tethers have been found in the Golgi and were termed 'golgins', but some are present at endosomes (e.g. EEA1), which, at least in plants, are part of the *trans*-Golgi network (Robinson et al., 2008; Niemes et al., 2010). The function of golgins and other coiled-coil tethers has been analyzed in recent reviews (Gillingham and Munro, 2003; Sztul and Lupashin, 2006). Coiled-coil tethers can associate with membranes via one of three different modes:

1.) They bind to adaptors like the small GTPase Arf or Arf-like proteins via their carboxy-terminal GRIP domains (e.g. Golgin-245 and GMAP-210) (Panic et al., 2003; Panic et al., 2003b).
2.) They contain a carboxy-terminal transmembrane domain (e.g. Giantin and CASP), (Gillingham et al., 2002), or
3.) they bind directly to specific lipids (EEA1) (Simonsen et al., 1998).

Coiled-coil tethers, however, also carry binding sites at their amino-terminal regions. GMAP-210 for instance binds via its carboxy-terminal domain to Arf1-GTP on membranes and contains in addition an amino-terminal ALPS (amphipathic lipid packaging sensor) motif, which is able to bind to highly curved membranes (Drin et al., 2007, see also 1.2.2.4.3). Using a truncated GMAP-210 tether, Antonny et al. could reconstitute tethering between Arf1-GTP loaded large liposomes and small liposomes (Drin et al., 2008). This tether may thus capture small vesicles from one Golgi cisterna and release them for fusion with the next one (Drin et al., 2008). Alternatively, the protein may generate contacts between the cisternae by taking advantage of its ability to bind both, flat membranes (via the GTPase Arf1) and highly curved membranes at the edges of the Golgi cisternae (via its ALPS motif). Coiled-

coil tethers could thus be responsible for the stacking of the Golgi and might protrude from the Golgi in a tentacle-like manner.

The coiled-coil sequence is not just required for bridging distances but it contains multiple binding sites for Rab GTPases (Hayes et al., 2009; Sinka et al., 2008; Figure 1.5). Golgins may thus provide a Rab-binding and releasing matrix, which could facilitate local transport of Rab-loaded vesicles through the Golgi stacks (Sinka et al., 2008).

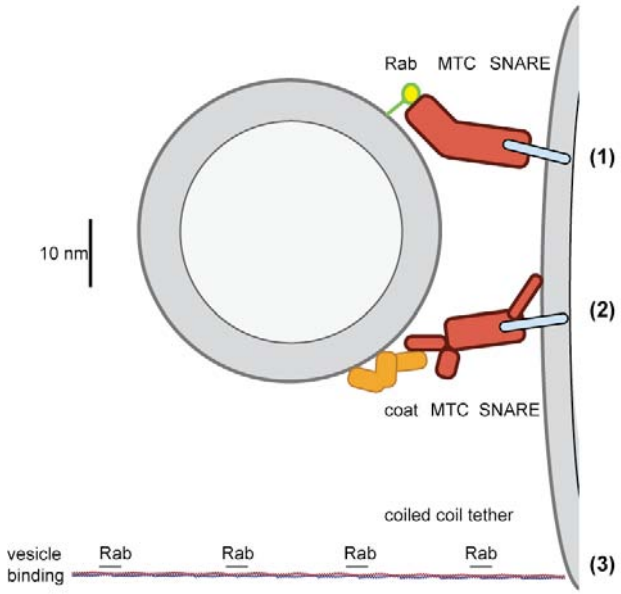

Figure 1.5: Role of tethers in vesicle recognition and fusion. Three different modes of tethering at the organelle membranes. All structures are drawn to scale. The indicated vesicle is 70nm in diameter. MTCs (red) are scaled according to the published Dsl1 complex structure (pdb: 3k8p), the coat based on available AP-2 structures (pdb: 2kjt, 2iv8), the Rab corresponds to Ypt7 (pdb: 1ky2), the SNARE complex was sized according to pdb: 3ipd. Due to its hypervariable domain, it may reach out > 10nm from the surface of the vesicle. The depicted coiled-coil tether contains 1000 residues. Three modes of interactions are shown: MTC-mediated bridging (1) via Rab-GTP (yellow) and SNAREs (blue) or (2) via coat recognition and SNAREs. Coiled-coil tethers (3) have membrane-binding sites at both ends, and multiple Rab-interaction domains along their entire length (Hayes et al., 2009; Sinka et al., 2008; Picture from Bröcker et al., 2010).

*1.2.2.2 Role of multisubunit tethering complexes**

The second group of tethers along the endomembrane system and at the plasma membrane are the MTCs. They consist of multisubunit protein complexes and constitute a much more divergent family of proteins with three to ten subunits, which differ in size between 50 and 140kDa per subunit (Figure 1.6). This suggests a combination of several functions within one protein complex. Due to their multiple subunits, elongated MTCs may span distances up to 30nm, sufficient to capture vesicles, but much shorter than the >200nm distances coiled-coil tethers can span (Figure 1.5). In general, MTCs seem to combine the recognition of membranes via

Rab GTPases with their subsequent SNARE-mediated fusion (Figure 1.5, (1)). Binding to the Rab in its GTP form occurs in most cases via a so-called effector subunit. Moreover, tethering complexes cooperate with SNARE proteins and may even proofread their assembly.

Initially, MTCs were considered to form a divergent family of proteins with multiple evolutionary origins, although some similarities were noticed early on (Whyte and Munro, 2001). The composition of MTCs seems to differ between species, suggesting that some subunits may perform specialized functions in some organisms (Koumandou et al., 2007). However, recent structural observations and sequence comparisons rather suggest a more coherent picture (Munson and Novick, 2006; Richardson et al, 2009; Ren et al., 2009; Nickerson et al., 2009; Zink et al., 2009), which allows to sort MTCs into two general groups: (i) those required for membrane fusion with organelles of the secretory pathway (Dsl1p, COG, GARP, Exocyst (recently renamed 'CATCHR' for **c**omplex **a**ssociated with **t**ethering **c**ontaining **h**elical **r**ods)) and (ii) those of the endolysosomal pathway (CORVET and HOPS). In addition, eukaryotic cells contain the TRAPP complex acting as multisubunit GEF, which does not fit into any of the two previous categories, but rather combines coat recognition with tethering (Figures 1.5, (2) and 1.6).

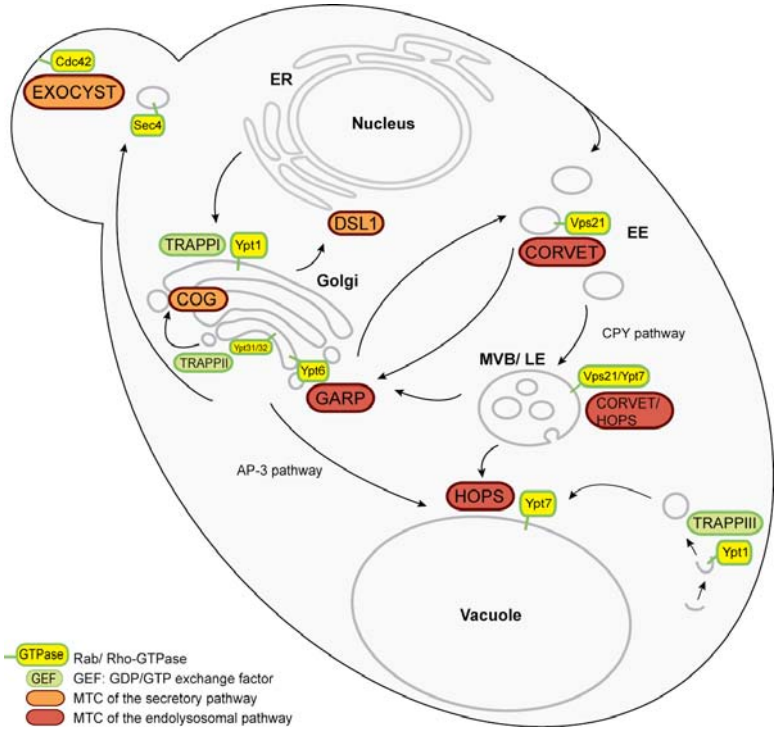

Figure 1.6: Overview of intracellular trafficking pathways and the involved tethering complexes with their corresponding GTPases. MTCs are indicated in orange (secretory pathway) and red (endolysosomal pathway). Rabs are indicated in yellow. (Picture from Bröcker et al., 2010).

*1.2.2.3. Tethers between endosome and lysosome/vacuole**

The 700kDa MTCs CORVET and HOPS operate sequentially between endosome and lysosome (Nickerson et al., 2009; Figure 1.6). Due to four shared subunits (the Class C proteins Vps11, Vps16, Vps18 and Vps33) and two additional homologous subunits, the structure of the two hexamers is probably very similar (Ostrowicz et al., 2010; Plemel, 2011). Moreover, all subunits except the Sec1 homologue Vps33 share a similar domain arrangement, which likely consists of an amino-terminal β-propeller domain and a carboxy-terminal α-solenoid domain (Nickerson et al., 2009). Their structure thus resembles subunits of the nuclear pore complex; structural parallels in comparison with coat proteins have been discussed (Brohawn et al., 2008; Plemel et al., 2011). It is also noteworthy that the shared subunits Vps11 and Vps18 both carry carboxy-terminal RING domains, which are important for CORVET and HOPS function (Rieder et al., 1997). The E3-ubiquitin ligase activity of mammalian hVps18 also requires this domain (Yogosawa et al., 2005).

1.2.2.3.1 The CORVET complex

CORVET is most likely required for fusion of Golgi-derived vesicles with the endosome (Raymond et al, 1990; Chen et al., 1996). In addition to the just mentioned four Class C subunits, CORVET contains two specific subunits, Vps3 and Vps8 (Peplowska et al., 2007), with which it binds the Rab GTPase Vps21 (Markgraf et al., 2009; Plemel et al., 2011). Vps8 is the third subunit of the CORVET complex with a carboxy-terminal RING domain. Vps3, the other CORVET specific subunit, also binds to Vps21 (Peplowska et al., 2007; Plemel et al., 2011), though its precise role within the complex remains to be determined. It is likely that CORVET interacts with endosomal SNAREs via Vps33, and may thus couple Vps21-GTP binding to SNARE assembly (Figure 1.5 (1)).

1.2.2.3.2 The HOPS complex

The HOPS complex is required for several fusion events at the late endosome and the vacuole, including the fusion of autophagosomes, multivesicular bodies (MVBs), Golgi-derived adaptor-protein complex (AP)-3 vesicles, and the homotypic fusion of vacuoles (Radisky et al., 1997; Wurmser et al., 2000). The two HOPS-specific subunits, Vps41 and Vps39, interact with Ypt7 (Wurmser et al., 2000; Brett et al., 2008; Plemel et al., 2011). Vps41 binds to Ypt7-GTP as its effector subunit, both, from within the HOPS complex as well as on its own (Ostrowicz et al., 2010; Plemel

et al., 2011), whereas Vps39 can interact with Ypt7 independently of its nucleotide state[1] (Plemel et al., 2011; Ostrowicz et al., 2010; Wurmser et al., 2000), but is not the GEF of Ypt7 (Nordmann et al., 2010). Functional studies on yeast vacuole fusion indicate that HOPS is able to promote tethering by binding Ypt7-GTP and the vacuolar SNAREs Vam3, Vam7 and Vti1 (Stroupe et al., 2009; Hickey et al., 2009).

[1]: the corresponding experiments leading to this statement are presented in the results (3.1.5.1) and are already mentioned here for completeness.

1.3 Principles of multisubunit tethering function*

1.3.1 Recruitment of MTCs to membranes*

How are MTCs recruited to membranes? All MTCs are peripheral membrane proteins, which seem to associate with membranes via the coordinated interaction with Rab GTPases and SNAREs. As almost all MTCs (except the Dsl1 complex) interact with Rab-GTP via a specific effector subunit, Rab activation and MTC recruitment are likely linked (Figure 1.5 (1)). MTCs may either associate with membranes via Rab-GTP as preassembled units or they may assemble on membranes as a prerequisite of tethering. Alternatively, MTCs interact with the coat of a vesicle and SNAREs on the target membrane (Figure 1.5 (2)). This leaves then the question, at which state during transport the coat of a vesicle is disassembled.

The Golgi-localized COG complex interacts with the Rab GTPase Ypt1 via Cog2 and Cog3 (Suvorova et al., 2002), and potentially also with Rab6 (Sun et al., 2007; Starr et al., 2010). The Rab binding site in the COG complex lies within the Cog2-Cog3 subcomplex (Suvorova et al., 2002). Potentially, the two-lobed structure of COG may allow binding to multiple Rabs and thus coordinate retrograde trafficking within the Golgi (Ungar et al., 2006). In mammalian cells, Rab33 and Rab6 act sequentially and COG depletion can be compensated for by depletion of Rab33, suggesting that Rab33 and COG cooperate in the same pathway (Starr et al., 2010). Whether COG assembly or dynamics of its two lobes is linked to Rab recognition is currently unknown.

Likewise, GARP binds specifically to the Rab Ypt6 via its subunit Vps52 (Siniossoglou et al., 2001; Siniossoglou et al., 2002). As GARP is purified as a heterotetramer, it remains unclear if binding to Ypt6 is linked to the assembly of the complex.

For the Exocyst, the link between GTPase binding and assembly is an open question, although several studies shed light on Exocyst recruitment to vesicles. Exocyst seems to assemble from two subcomplexes, which are recruited initially onto exocytic vesicles and the recipient plasma membrane (Figure 1.7, upper panel). Exocytic vesicles initially contain the Rab Ypt31/32, but require the Rab Sec4 for binding to the Exocyst. Ypt31/32 is replaced by Sec4, which is coupled to the recruitment and assembly of the Exocyst complex. During transport from the Golgi to the plasma membrane, Ypt32-GTP recruits, assisted by phosphoinositide-4-phosphate (PI-4-P), the Sec4 exchange factor Sec2 (Ortiz et al., 2002; Mizuno-Yamasaki et al., 2010). Upon loss of PI-4-P, presumably caused by a PI-4-phosphatase, Sec2 is activated and generates Sec4-GTP, which recruits Sec15 to the exocytic vesicles (Mizuno-Yamasaki et al., 2010; Guo et al., 1999). Most of the remaining Exocyst subunits also arrive via vesicular transport, presumably by subsequent binding to Sec15 (Boyd et al., 2004). At the plasma membrane, Exocyst subunits bind Rho and Ral GTPases (Roumanie et al., 2005; Wu et al., 2008). At least two Exocyst subunits, Exo70 and Sec3, bind to Rho GTPases (Rho3, Rho1 and Cdc42) and PI-4,5-P_2 (Liu et al., 2007; Hamburger et al., 2006; He et al., 2007; Yamashita et al., 2010; Zhang et al., 2008; Baek et al., 2010). However, it is not yet clear if the complex acts as one unit or assembles upon vesicle docking to the plasma membrane (Munson and Novick, 2006).

Similarly, the Rab exchange on endosomes may accompany the assembly/recruitment of CORVET and HOPS (Figure 1.7, lower panel). As mentioned above, both complexes differ in their Rab interacting subunits. During endocytosis and on endosomes, the mammalian exchange factor Rabex5 activates Rab5, which can bind multiple effectors, including the coiled-coil tether EEA1 (Christoforidis et al., 1999). In yeast, the CORVET complex also binds Vps21 (Rab5 homolog) via its subunits Vps8 (Peplowska et al., 2007; Markgraf et al., 2009; Abenza et al., 2010; Pawelec et al., 2010) or Vps3 (Plemel et al., 2011; F.A., H.J.k.B, D.O. unpublished). Endosomes (and the related phagosomes) mature by undergoing Rab exchange (Rink et al., 2005), whereby Ypt7 (Rab7 homolog) replaces Vps21 in a process that is aided by the Mon1-Ccz1 complex (Poteryaev et al., 2010; Kinchen et al., 2010), which was recently identified as the Ypt7 GEF (Nordmann et al., 2010). Due to a change in the Rab composition on endosomes, CORVET is replaced by HOPS, which binds Ypt7 via its subunit Vps41 (Brett et al., 2008; Ostrowicz et al.,

2010; Plemel et al., 2011; Figure 1.7, lower panel)[2]. Such an exchange may occur by sequential replacement of the CORVET-specific subunits Vps3 and Vps8 for the HOPS-specific Vps41 and Vps39 or by replacing one entire complex for the other (Peplowska et al., 2007). Intriguingly, overexpression of the CORVET subunit Vps3 displaces Vps39 from the HOPS complex (Peplowska et al., 2007), suggesting that these tethering complexes may undergo a dynamic turnover. However, neither for HOPS nor for CORVET it is currently known whether the complex assembles on endosomes or remains as one entity throughout endosomal maturation.

Among all tethering complexes, the Dsl1 complex is the only exception with respect to Rab binding since this complex apparently does not require any Rab for its recruitment. This is likely due to the fact that the ER is the starting point of the secretory pathway and is not subject of constant remodeling due to organelle maturation. As maturation of organelles is tightly linked to Rab exchange cascades, Rab recruitment and tethering function are connected to almost all subsequent organelles.

[2]: the corresponding experiments leading to this statement are presented in the results (3.1.5.1) and are already mentioned here for completeness.

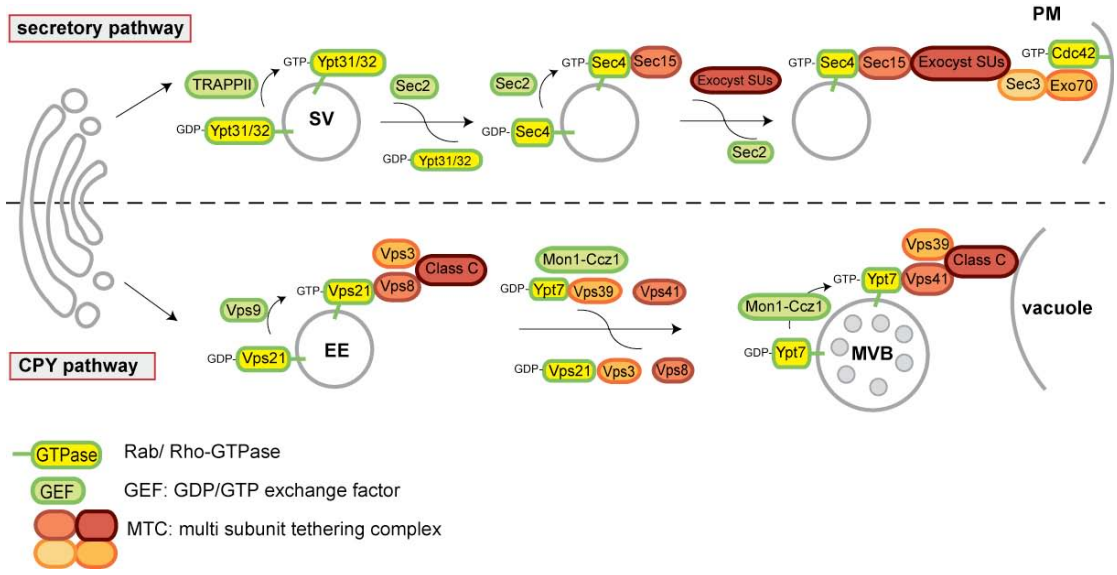

Figure 1.7: Recruitment of tethering complexes during vesicle maturation. Models that compare Rab exchange on secretory vesicles (SV) and endosomes (EE, MVB), which is accompanied by the recruitment of MTCs. Upper panel: Ypt32-GTP recruits the next GEF Sec2, which in turn promotes Ypt32 displacement. The next Rab Sec4 is in turn recruited and activated, which results in the recruitment of Exocyst subunits (e.g. Sec15), and Sec2 displacement. Exocyst may then assemble during tethering. Lower panel: Vps21-GTP recruits CORVET. During maturation, the Vps21 GEF is displaced, and CORVET may be remodeled into HOPS, while Ypt7 is activated via the Mon1-Ccz1 GEF complex. HOPS then mediates tethering with the vacuole. (Picture from Bröcker et al., 2010).

1.3.2 Recognition of vesicle coats by MTCs*

Once MTCs are recruited to membranes, how do they recognize vesicles? One possibility is that tethers interact directly with the Rab GTPase or with the coat (Figure 1.5 (1), (2); Angers et al., 2010). If the coat is indeed one binding site, then it has to be maintained, at least partially, to provide an interaction surface. Indeed, the time when a coat (COPII, COPI, clathrin etc.) is shed is unclear.

Several MTCs have binding sites for the coat. The Dsl1 complex interacts with the COPI coat via a binding site that is also needed to stabilize interactions within the COPI coat (Zink et al., 2009; Kraynack et al., 2005). Thus, the Dsl1 complex may tether vesicles by recognition of the COPI coat, and assist in uncoating prior to vesicle fusion. Likewise, COG may bind COPI vesicles via the coat, as depletion of COG and COPI result in a similar phenotype (Smith et al., 2009).

Neither for GARP nor Exocyst coat interactions have been reported. Potentially, Exocyst can bridge membranes by assembling from its two parts, one of which is present on exocytic vesicles, and thus initiate fusion (Munson and Novick, 2006; Figure 1.8, upper panel).

At the yeast vacuole, the HOPS complex is required for several distinct fusion reactions, including late endosomes and Golgi-derived AP-3 coated vesicles. The Rab effector subunit Vps41 has a dedicated function in the AP-3 pathway by binding to the ear domain of the δ-subunit Apl5 (Darsow et al., 2001; Rehling et al., 1999). The vacuole casein kinase Yck3, which is transported via the AP-3 pathway to the vacuole (Sun et al., 2004), phosphorylates Vps41, and controls Vps41 function in the AP-3 pathway (Cabrera et al., 2009; LaGrassa et al., 2005). As Vps41 function seems to be restricted to the late endosome and vacuolar membrane, the interaction of Apl5 with Vps41 might be required to tether AP-3 coated vesicles to vacuoles (Angers et al., 2009), (Figure 1.5 (2)). This tethering is controlled by Vps41 phosphorylation (Cabrera et al., 2009), and Apl5 indeed partially localizes to the vacuole membrane (Angers et al., 2009). A phosphorylation-based switch mechanism that allows Vps41 to distinguish between fusion of late endosomes and fusion of AP-3 vesicles with the vacuole is described below. For CORVET, potential interactions with coats have not been reported.

1.3.2.1 The ALPS motif of Vps41

Vps41 acts as Ypt7 effector subunit of HOPS and is recruited to late endosomes (Brett et al., 2008; Cabrera et al., 2009). Here, the curvature-sensing motif (ALPS (**a**mphipathic **l**ipid **p**ackaging **s**ensor)) of Vps41 is inserted into the highly curved endosomal membrane. This motif, initially identified in GMAP-210, is able to bind highly curved membranes (Bigay et al., 2005; Drin et al., 2007; Drin et al., 2008). Upon fusion of late endosomes with the vacuole Vps41 ALPS motif is no longer able to insert into the lower curved vacuolar membrane. Here, the casein kinase Yck3 gets access to phosphorylation sites within the ALPS motif. Additionally, the binding site for Apl5 is now available and AP-3 vesicles can bind, allowing for its tethering to the vacuole (Cabrera et al., 2010; Figure 1.8). At the late endosome, where Vps41 ALPS motif is inserted into the membrane, the binding site to Apl5 is blocked, preventing tethering of AP-3 vesicles with late endosomes/MVBs.

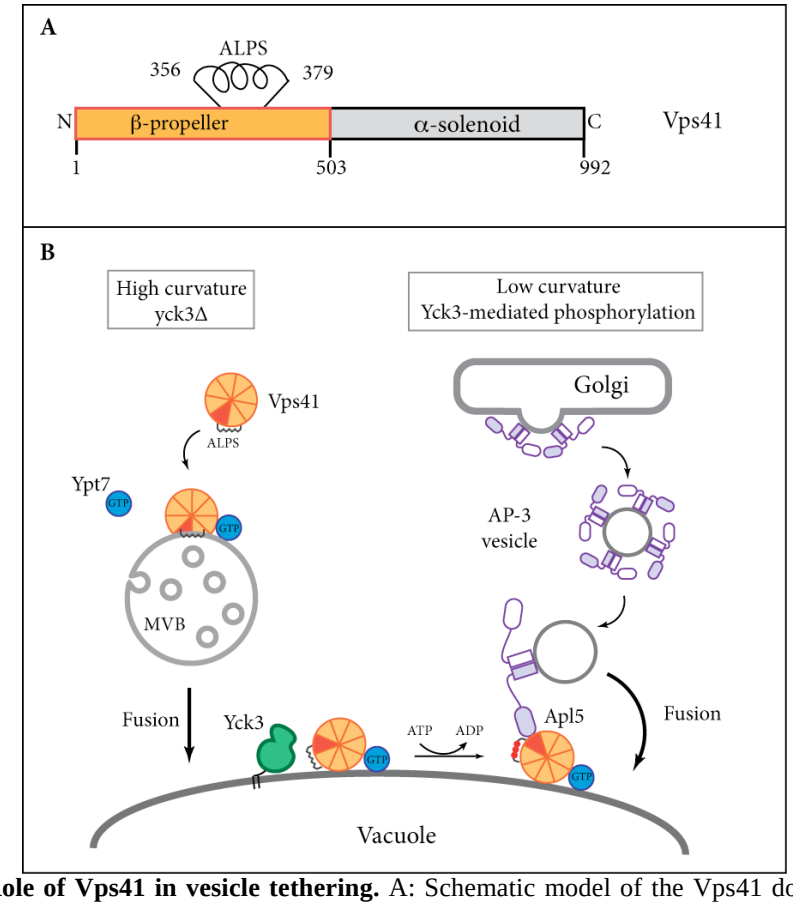

Figure 1.8: Role of Vps41 in vesicle tethering. A: Schematic model of the Vps41 domain structure based on prediction programs. B: Model of Vps41 phosphorylation-based switch mechanism for tethering different vesicles to the vacuole. Vps41's ALPS motif senses highly curved membranes and is thereby inserted into the MVB membrane. Reaching the vacuole, the ALPS can no longer bind, because the membrane of the vacuole is not highly curved. Here, Yck3 gains access to the phosphorylation sites, located within the ALPS motif. The binding site for Apl5 is therefore only accessible at the vacuole and AP-3-vesicles can fuse. At the MVB the ALPS motif is inserted into the membrane and the Apl5 binding site is blocked, preventing fusion of AP-3-vesicles with the MVBs. Figure from Cabrera et al., 2010.

1.4 Principles of SNARE-mediated fusion with the target organelle

The interaction of MTCs with SNAREs is required for fusion. After recognition of the transport vesicle by MTCs the two bilayers of opposing membranes are brought into close proximity. SNAREs from opposing membranes are now able to form a specific four-helix-bundle complex, which subsequently leads to fusion and lipid mixing of the bilayers (Jahn and Scheller, 2006). SNAREs are part of the vesicle (v- SNARE) or reside on the target organelle (t-SNARE) (Rothman, 1994). The common feature of all SNAREs is the SNARE motif, which allows the classification as Q- or R-SNARE, depending on a conserved glutamine or arginine within the SNARE motif (Fasshauer et al., 1998; Weimbs et al., 1997). Three Q-SNAREs and one R-SNARE form a four-helix-bundle, the so-called *trans*-SNARE complex, which is an irreversible step in fusion reaction (Weber et al., 1997). After fusion, all SNAREs are present in a complex on the same membrane, the so-called *cis*-SNARE complex (Figure 1.9). With the help of the AAA-ATPase Sec18 (NSF) and its cofactor Sec17 (α-SNAP) the *cis*-SNARE complex is disassembled and the SNAREs are reactivated for the next fusion (Yu et al., 1999; Rice et al., 1999; Wang et al., 2000; Littleton et al., 2001).

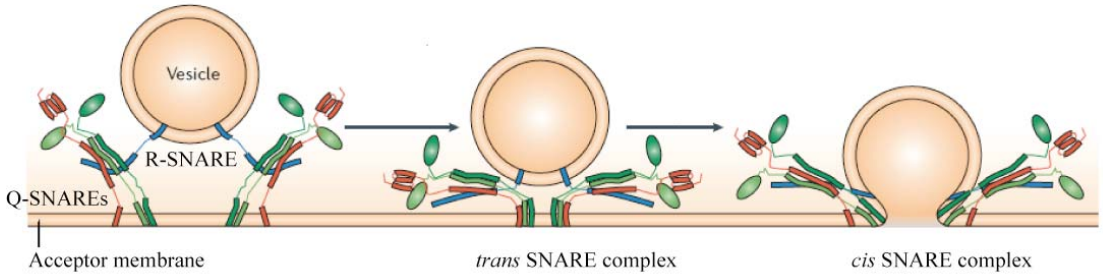

Figure 1.9: Model of SNARE-mediated vesicle fusion. During vesicle fusion three Q-SNAREs interact with one R-SNARE to form a *trans*-SNARE complex. This irreversible step leads to fusion and formation of a *cis*-SNARE complex (Picture adopted from Jahn and Scheller 2006).

Five SNAREs were identified to function in vacuole fusion: three Q-SNAREs (Vam3, Vam7, Vti1) and two R-SNAREs (Nyv1, Ykt6) (Sato et al., 1998; Ungermann et al., 1998; Ungermann et al., 1999). Vam3 and Nyv1 reach the vacuole via the AP-3 pathway. Vti1 is transported via the CPY pathway to the vacuolar membrane and Vam7 is recruited from the cytosol via its phox-homology (PX) domain, which binds to phosphoinisitide-3-phosphate (PI-3-P) to the vacuole. The interaction between tethers and SNAREs to mediate the fusion is described below.

1.4.1 Coupling of tethering and SNARE-mediated fusion*

Rab binding to MTCs is one part of the recruitment reaction for tethers. However, MTCs are also able to bind to SNAREs. This binding could be required to stabilize the MTC, or one of its subunits, on membranes or could be required to couple tethering to SNARE-mediated membrane fusion. Both cases may not be exclusive, but part of a concerted scenario of MTC function.

The Dsl1 complex, for instance, binds the amino-terminal domain of the SNAREs Use1 and Sec20 at the ER membrane (Ren et al., 2009; Tripathi et al., 2009), which presumably positions the Dsl1 complex like an antenna on the ER membrane. SNARE binding may be required for membrane association, as Dsl1 does not interact with a Rab. In addition, the complex promotes the assembly of ER SNAREs *in vitro* (Ren et al., 2009), suggesting that the Dsl1 complex combines tethering with the initiation of membrane fusion.

Similar models have been proposed for the remaining MTCs. COG interacts with the Golgi Q-SNARE Sed5 and stabilizes intra-Golgi SNAREs (Shestakova et al., 2007; Suvorova et al., 2002). GARP has several SNARE binding domains (Siniossoglou et al., 2002; Perez-Victoria et al., 2009), and the Exocyst recognizes the SNARE Sec9 via its Sec6 subunit (Sivaram et al., 2005).

Only for the HOPS complex, *in vitro* fusion assays have been developed. HOPS binds to vacuolar SNAREs (Collins et al., 2005), and strongly stimulates SNARE-mediated liposome fusion (Cabrera et al., 2010; Figure 1.10). Moreover, HOPS tethers membranes by binding to Ypt7 on one membrane and SNAREs on the other (Stroupe et al., 2009; Hickey et al., 2009), which may display a common mechanism. HOPS promotes fusion (Collins et al., 2005), but also proofreads the SNARE complex (Mima et al., 2008). HOPS may thus be a paradigm for MTC-mediated control of membrane fusion (Figure 1.10).

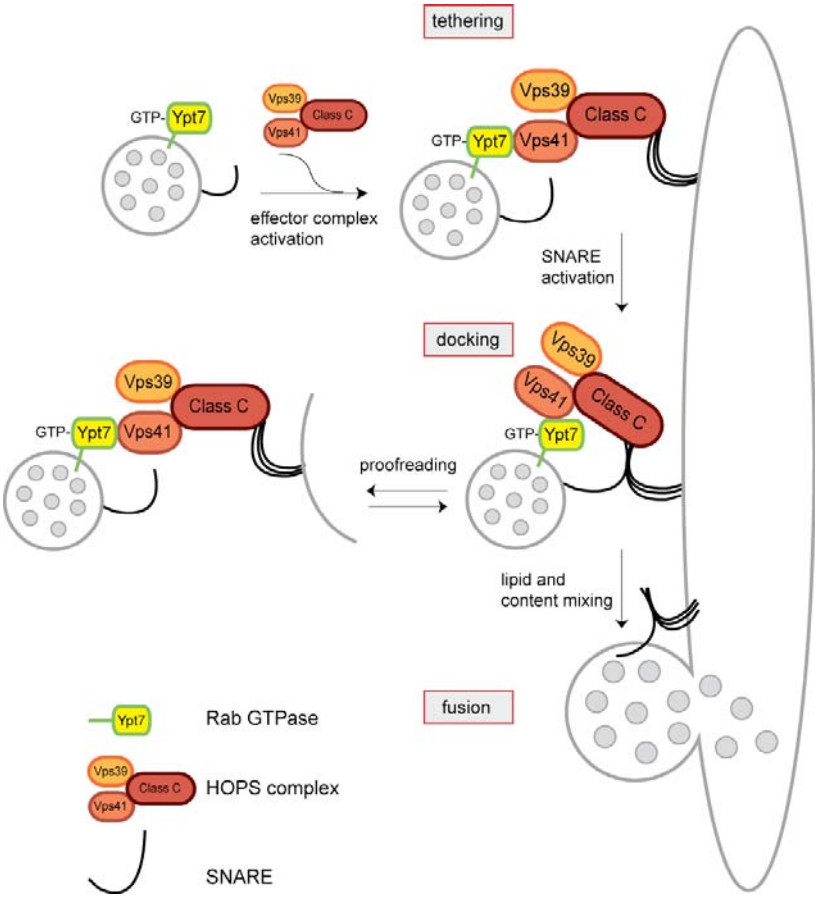

Figure 1.10: Role of the HOPS tethering complex in vacuole fusion. HOPS mediates tethering by binding the Rab Ypt7, lipids, and SNAREs. HOPS can proofread the correct assembly of *trans*-SNARE complexes. If incorrect, Sec17/18 (α-SNAP/NSF) promotes disassembly of the SNAREs. (Figure from Bröcker et al., 2010).

One of the subunits of the HOPS (and CORVET) complex that is likely involved in SNARE-mediated fusion is Vps33, a Sec1/Munc18-like protein (Peplowska et al., 2007; Starai et al., 2008; Seals et al., 2000). SM-proteins are dedicated SNARE-binding proteins that control membrane fusion (Pieren et al., 2010). Interestingly, both COG and Exocyst bind SM-proteins; COG interacts with Sly1 (Laufman et al., 2009), Exocyst with Sec1 (Wiederkehr et al., 2004). Whether the cooperation of SM-proteins with MTCs is a general feature of tethering complexes is not yet clear. It is, however, striking that only the CORVET and HOPS require Vps33 as an integral subunit of the complex.

* Text modified after Bröcker et al., 2010 Current Biology

2. Rationale

The HOPS tethering complex is the only multisubunit tethering complex, where an *in vitro* fusion assay has been established. The tethering function has further been demonstrated in an artificial system using proteoliposomes that carry SNAREs and the Rab GTPase Ypt7. These assays may mimic the *in vivo* situation, but likely do not reproduce all HOPS functions. Due to its large size, it is plausible that the HOPS complex is linked to multiple regulatory processes at the vacuole. Since the vacuole is a highly dynamic organelle, it undergoes constant remodeling and fusion of incoming vesicles different types and origins.

Within this thesis the following aspects were addressed:

To show activity of HOPS, a "semi *in vitro*" fusion system with purified vacuoles, established by Haas et al., 1995, will be used. This system measures the fusion capability of isolated vacuoles and their influence of subjected proteins towards the pre-existing fusion machinery. For this, vacuoles depleted for HOPS or incapable to fuse due to selective inhibition of the Rab GTPase might be induced for fusion by HOPS addition. For that reason, purified, active HOPS is required. The established assay would then also allow for the characterization of the identified subcomplexes and single proteins.

The role of Vps39 within the HOPS complex needs to be elucidated as the Mon1-Ccz1 complex was identified as the Ypt7 GEF. One approach involved the investigation of the intermediate complex between CORVET and HOPS (containing Vps41 and Vps3 instead of Vps39). Its activity in comparison with the HOPS complex might give hints towards the Vps39-function during tethering and fusion.

To further understand HOPS function, structural studies will be performed. For this, high protein amounts and high protein purity are a prerequisite. Such purified, active HOPS will then be analyzed by electron microscopy. Modifications of single subunits might give insights into their function within the complex. Subcomplex analysis might allow for aligning their structure with the structure of the entire complex. A three-dimensional model of the HOPS complex, even at low resolution, would be very helpful to understand the general mechanisms of multisubunit tethering complexes.

3. Results

3.1 Functional analysis of the HOPS tethering complex

3.1.1 Purification of the HOPS complex

Previous work in the lab has established a purification protocol for the hexameric HOPS complex from *Saccharomyces cerevisiae*. The method takes advantage of a carboxy-terminally tagged subunit. We selected the established TAP (tandem affinity purification) tag, which can be coupled via its protein A tag to IgG beads. The native complex is eluted after TEV-cleavage and further analyzed via gelfiltration, glycerol gradient centrifugation or functional assays (Ostrowicz, et al., 2010; see also methods). To increase the yield, a yeast strain overexpressing all six HOPS subunits with an inducible *GAL1*-promoter was generated for further studies (Ostrowicz et al., 2010). To confirm that the overexpressed proteins form a hexameric complex of 630kDa total mass, the purified, TEV-cleaved eluate was applied onto a gelfiltration column where it eluted as an apparent heterohexamer (Figure 3.1). The complex containing fraction 9 corresponded to a molecular weight of approximately 700kDa. The surplus of the bait protein, Vps41, eluted shortly after the complex in fraction 11, equivalent to a molecular weight of approximately 100 to 150kDa. A comparable peak of monomeric complex was also obtained when the HOPS eluate was added to glycerol gradient centrifugation (Figure 3.1B). The holo HOPS appeared in fractions 6 and 7, whereas single Vps41 turned up earlier in fraction 3, consistent with its lower molecular mass. This suggests a monomeric complex with a 1:1:1:1:1:1 ratio of each subunit.

Since the HOPS complex is membrane-associated but does not contain any transmembrane domains or lipid anchors, purification in the absence of detergent was possible as depicted in Figure 3.1C. In this case, the HOPS containing fraction migrated at the same molecular mass in the glycerol gradient as in the presence of detergent, but no monomeric Vps41 was observed in lower glycerol density fractions, pointing towards a function of Vps41 in membrane association of HOPS (Cabrera et al., 2009; Cabrera et al., 2010). The purification of the HOPS complex without any detergent is an important issue, since lipid binding and fusion assays are only feasible without detergent.

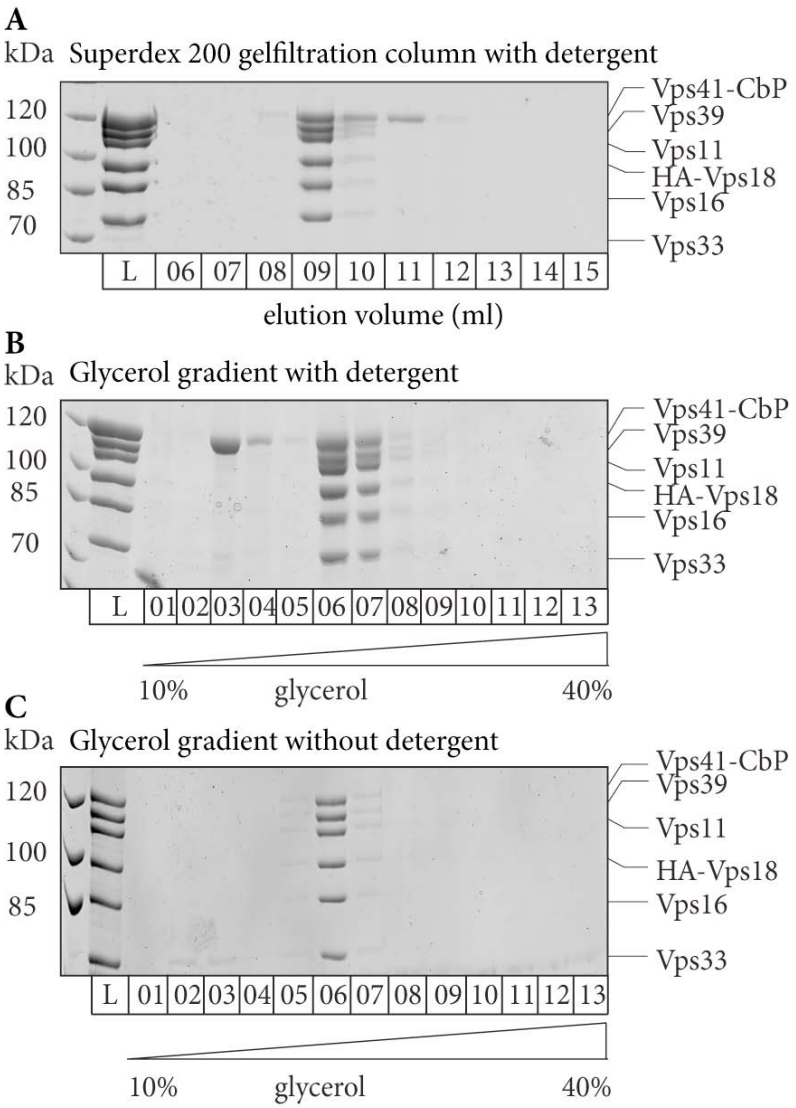

Figure 3.1: Purification of the HOPS complex. The SDS-PAGE gels loaded with HOPS from different fractions were stained with Coomassie. A: Gelfiltration (Superdex 200 column) of purified HOPS TEV-eluate in the presence of detergent. B: Glycerol gradient centrifugation of purified HOPS TEV-eluate in the presence of detergent. C: Glycerol gradient centrifugation of HOPS TEV-eluate in the absence of detergent. L: loading control, CbP: Calmodulin binding peptide, HA: Hemagglutinin tag.

3.1.2 Activity analysis of purified HOPS in the vacuole fusion assay

In order to determine biological activity of the purified HOPS eluate, an "semi *in vitro*" fusion assay according to Stroupe et al., 2006 was established. Therefore, vacuoles were isolated from two tester strains. One strain lacks a vacuolar peptidase (*pep4*Δ) required for proenzyme activation, the other one lacks the prophosphatase (*pho8*Δ). Upon fusion, the contents of different vacuoles become mixed; the phosphatase is cleaved and activated by the peptidase resulting in substrate processing. Both of these tester strains in addition contain a temperature-sensitive variant of Vps11 (*vps11-1*). Peterson and Emr identified this Vps11 mutant by

random mutagenesis. The mutation in Vps11 is located at the very carboxy-terminal RING domain (I877S, I878S, C913S). The mutant strain showed pronounced intracellular accumulation of the CPY precursor (p2CPY) and of the alkaline phosphatase Pho8 at the restricted temperature. The transport pathway between late endosome and vacuole therefore seems to be affected by this mutation, also indicating an impaired HOPS function. At the permissive temperature *vps11-1* is functional and incorporated into the HOPS complex. Also CPY maturation and Pho8 processing are normal. After a shift towards the restrictive temperature *vps11-1* becomes inactivated leading to a blocked trafficking route between late endosome and vacuole (Peterson and Emr, 2001). The vacuoles, isolated at non-permissive temperature, are unable to fuse since no active tethering complex is present on their surface. The fusion of these HOPS depleted vacuoles is only rescued in the presence of supplemented HOPS (Stroupe et al., 2006; Figure 3.2).

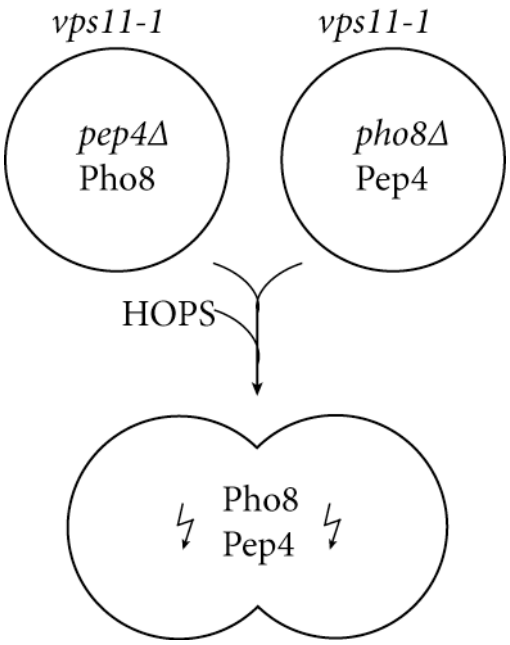

Figure 3.2: Model of HOPS-dependent fusion. Two tester strains contain a temperature-sensitive version of Vps11 (*vps11-1*). At the restrictive temperature *vps11-1* becomes inactivated and the trafficking between late endosomes and the vacuole is blocked. Fusion of theses *vps11-1* vacuoles lacking Pep4 or Pho8 can only be rescued in the presence of biological active HOPS.

HOPS was purified from an overexpression strain and the resulting eluate was titrated into the *vps11-1* vacuole fusion assay. Upon addition of HOPS, the fusion activity was rescued, indicating that my purified HOPS complex is active. Increasing amounts of HOPS raised the fusion rate up to a maximal value and afterwards decreased again, which can be explained by the concomitantly increasing volume and salt concentrations, resulting in dilution of the vacuoles and thereby inhibited fusion

(Figure 3.3). The addition of buffer or Vps41 alone as a control was not sufficient to support fusion, indicating that the entire HOPS is required for fusion and that a single HOPS-specific subunit is unable to stimulate fusion.

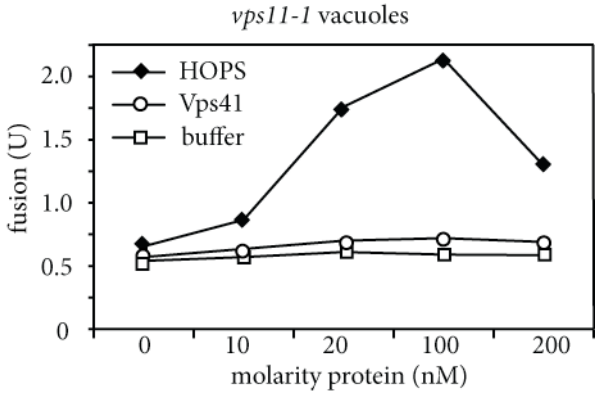

Figure 3.3: Vacuole fusion assay with *vps11-1* vacuoles. Fusion of isolated vacuoles from *vps11-1* tester strains could be rescued by addition of purified HOPS complex. Supplemented Vps41 alone or buffer did not rescue the fusion.

3.1.3 Identification and purification of stable HOPS subcomplexes

During a successive single deletion screen of HOPS subunits, several stable subcomplexes were identified (Ostrowicz et al., 2010). These subcomplexes might represent precursors during the assembly or debris from the disassembly. They might also be involved in the transition from CORVET to HOPS during endosome maturation (Peplowska et al., 2007). The four common subunits of HOPS and CORVET (Vps11, Vps16, Vps18 and Vps33) are believed to form a so-called “Class C core” complex (Rieder and Emr, 1997). To test if the identified subcomplexes and the “Class C core” proteins can be purified stoichiometrically, several diploid yeast strains overexpressing different subunits with a *GAL1*-promoter were generated (Table 8.1) and pulldown experiments performed. A carboxy-terminal TAP tag was fused to one of the overexpressed proteins. By performing small-scale purifications as described in 6.3.4.2 direct interactors of the bait protein were identified.

In none of theses pulldowns a tetrameric, stoichiometric complex could be isolated (Figure 3.4A). The only apparent stoichiometric subcomplex contained Vps16 and Vps33 in an apparently dimeric complex (Figure 3.4A lanes 2 and 4). In lane 2, the Vps16-Vps33 subcomplex additionally contained untagged Vps16. This might be due to diploid strains, which additionally contain a wild-type copy of Vps16. This was also observed with Vps33 as bait. In this diploid strain, additional endogenous Vps33 is copurified (Figure 3.4A, lane 4). This subcomplex was also isolated, when just Vps16 and Vps33 were overexpressed together (Figure 3.4B lane

2). The other identified stable subcomplexes were heterooligomers of the minimal subcomplex consisting of Vps39 and Vps11 (Figure 3.4B lane 3,4 and 5). This apparent dimeric complex was isolated alone (lane 5), or as a trimeric subcomplex, when Vps18 was additional overexpressed (lane 4). Upon additional overexpression of Vps41, it was isolated as a hetero-tetramer with Vps41 in substochiometric amounts (lane 3).

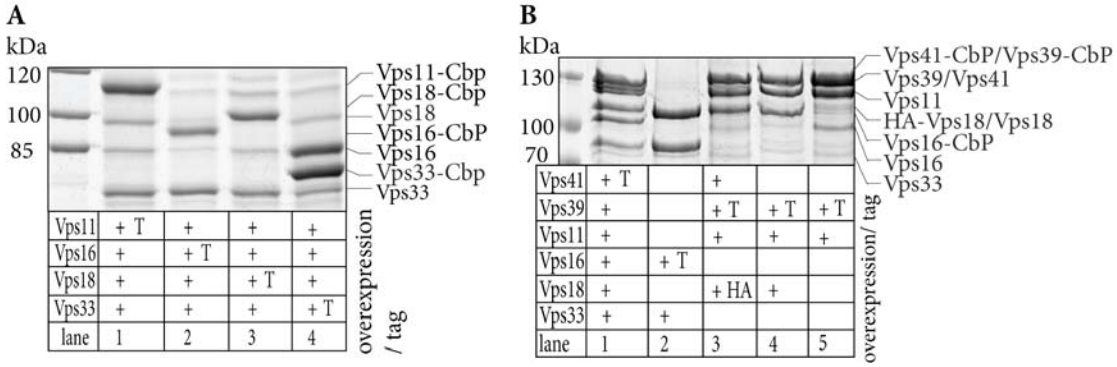

Figure 3.4: Small-scale purification of HOPS subcomplexes. A: All four "Class C core" proteins were co-overexpressed and successively tagged for pulldowns. The TEV-cleaved eluate was loaded onto a SDS-PAGE gel and stained with Coomassie. B: Identified subcomplexes from single subunit deletion screens were confirmed in overexpression strains via small-scale TAP purifications. The TEV-cleaved eluate was loaded on a SDS-PAGE gel and stained with Coomassie. CbP: Calmodulin binding peptide, HA: Hemagglutinin tag.

This analysis revealed several stable subcomplexes, which were initially identified in a deletion screen (Ostrowicz et al., 2010), but could also be isolated in the same stoichiometry when overexpressed. The function of these subcomplexes will be partially addressed in the following chapter.

3.1.4 Reconstitution of active HOPS from subcomplexes

The HOPS complex seems to contain different apparently stoichiometric subcomplexes. Their biological relevance is so far unknown. To test their activity, different subcomplexes were supplemented into the above described *vps11-1* vacuole fusion assay in order to check for possible tethering activity. As depicted in Figure 3.5, none of the subcomplexes rescued fusion on their own, indicating that they were not sufficient to increase the fusion rate on their own or were just inactive.

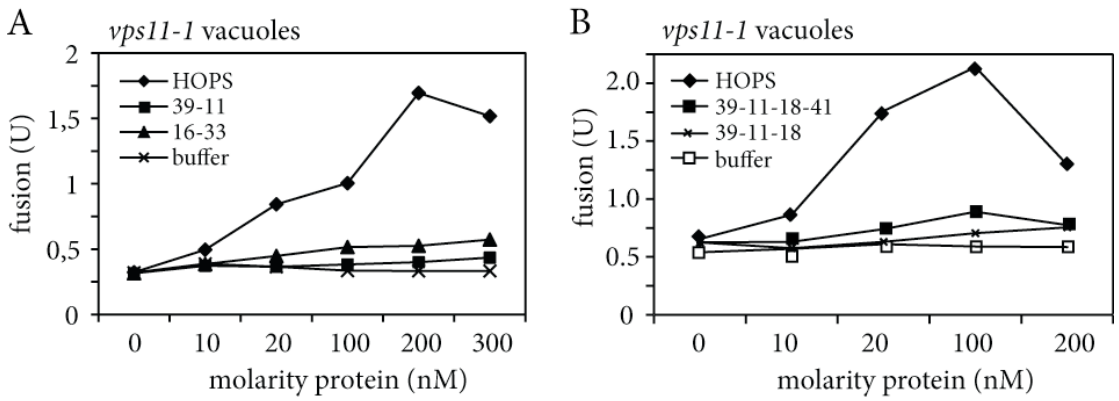

Figure 3.5: Vacuole fusion assay with *vps11-1* vacuoles. HOPS dependent vacuole fusion is not rescued upon addition of different HOPS subcomplexes. A: Titration of two different dimeric subcomplexes (Vps39-Vps11 and Vps16-Vps33) and HOPS. B: Titration of one trimeric (Vps39-Vps11-Vps18) or one tetrameric subcomplex (Vps39-Vps11-Vps18-Vps41) and HOPS.

Despite their inability to rescue fusion of HOPS depleted vacuoles, it is possible that the subcomplexes can stimulate fusion in combination. Therefore, two different subcomplexes were added to the fusion reaction. To reduce the assembly options, the dimeric Vps16-Vps33 subcomplex together with the tetrameric Vps41-Vps39-Vps11-Vps18 subcomplex was used, even though Vps41 is substoichiometric in this complex (Figure 3.6A, lane 2).

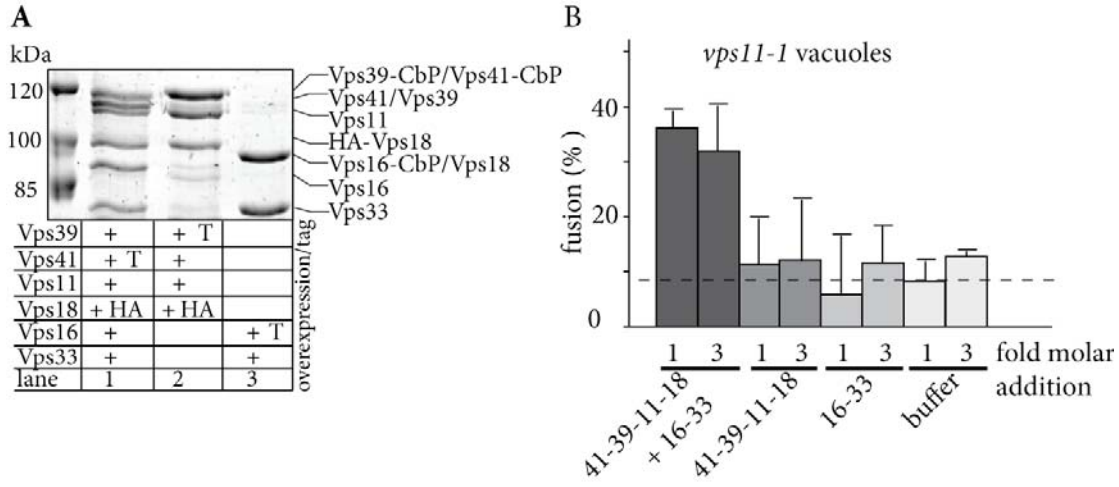

Figure 3.6: Reconstitution of active HOPS from subcomplexes. A: The SDS-PAGE gel loaded with purified holo HOPS, one tetrameric (Vps39-Vps11-Vps18-Vps41) and one dimeric (Vps16-Vps33) subcomplex was stained with Coomassie. CbP: Calmodulin binding peptide, HA: Hemagglutinin tag. B: Vps16-Vps33 subcomplex and Vps39-Vps11-Vps18-Vps41 subcomplex together and alone were incubated with *vps11-1* vacuoles. Both subcomplexes together were able to rescue fusion.

The concentration of the two subcomplexes was chosen according to the empirically identified HOPS concentration with maximal fusion rate (approximately 150nM). When the dimeric subcomplex together with the tetrameric complex was incubated with the vacuole fusion mix, resulting in 1-fold molarity or 3-fold molarity of HOPS,

fusion activity was rescued to approximately 35% in comparison with the holo complex (Figure 3.6B). The single subcomplexes again were unable to restore fusion, indicating that the complete hexamer is required for fusion activity. Two subcomplexes were reconstituted into active HOPS, but the role of any of the single subunits during fusion was not yet clear. Therefore, the HOPS-specific subunit Vps39 was analyzed in more detail.

3.1.5 Role of Vps39 as part of the HOPS complex

The HOPS complex shares four of its six proteins with the CORVET complex, namely the above-mentioned "Class C core" proteins. Vps41 as one of the HOPS specific subunits has been characterized as the HOPS effector subunit (Brett et al., 2008; Cabrera et al., 2009). The other HOPS specific subunit, Vps39, was claimed to be the GEF for the vacuolar Rab GTPase Ypt7 (Wurmser et al., 2000). Recently, it became clear that the dimeric Mon1-Ccz1 complex is the GEF for Ypt7 (Nordmann et al., 2010). Thus, the precise role of Vps39 is again unresolved.

3.1.5.1 Role of Vps39 in Rab binding specificity

In our study, we confirmed the data of Wurmser et al. (2000) that Vps39 binds to Ypt7 but does not show any nucleotide-specificity (Ostrowicz et al., 2010). The purified protein interacted with the GDP- and the GTPγS-loaded (non-hydrolysable GTP) form as well as the nucleotide-free version of Ypt7 (Figure 3.7A). In contrast, the HOPS effector subunit Vps41 bound both as isolated protein and as part of the HOPS exclusively to Ypt7-GTPγS (Figure 3.7B and C). Vps39, when incorporated into the HOPS complex did not influence HOPS binding to Ypt7-GTPγS, indicating that it became inactivated in the HOPS complex or is not accessible for Ypt7 (compare Figure 3.7A and C).

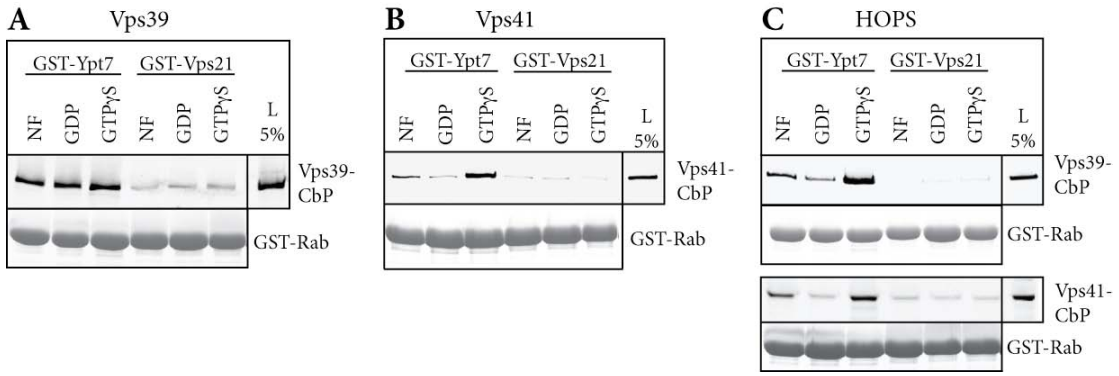

Figure 3.7: Rab binding specificity of HOPS and HOPS subunits. In the upper lanes immuno-stained Western blots are shown. In the lower lanes SDS-PAGE gels loaded with GST-Rab GTPases stained with Coomassie are shown as loading controls. A: The HOPS subunit Vps39 binds to Ypt7, but independently of the nucleotide status. B: Vps41, the HOPS effector subunit binds specifically to Ypt7-GTPγS as a single protein, as well as from within the HOPS complex (C). Figures from Ostrowicz et al., 2010; pulldowns performed by C.W. Ostrowicz. L: loading control; CbP: Calmodulin binding peptide.

To further investigate the Rab-binding specificity of Vps39 in the HOPS complex an intermediate complex (i-CORVET), which is lacking Vps39 but contains Vps3 instead, was isolated. The i-CORVET complex might represent a transitory state in the "maturation" from CORVET at the endosomes into HOPS at the vacuole via subunit exchange (Peplowska et al., 2007). I-CORVET was isolated by co-overexpression of Vps3 together with the "Class C core" proteins and Vps41 (Figure 3.9B). To show specific interactions with Rab-GTPases, pulldowns with isolated i-CORVET or cell lysates from a *vps39*Δ strain were performed.

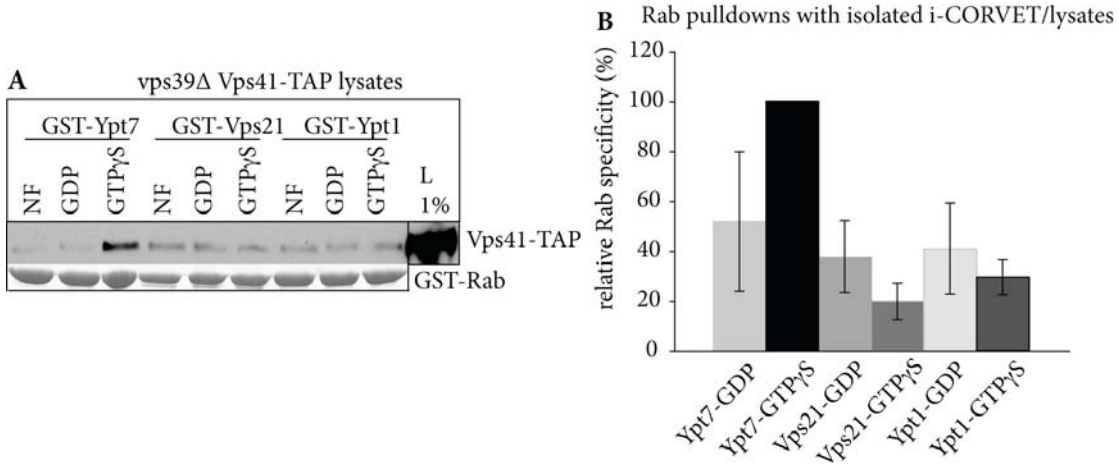

Figure 3.8: Rab binding specificity of i-CORVET. A: Upper lane: Western blot and immuno-detection of the TAP-tag. Lower panel: The SDS-PAGE gel loaded with GST-Rabs as a control was stained with Coomassie. I-CORVET interacted with Ypt7-GTPγS. B: Quantification of three independent Rab pulldowns with isolated i-CORVET or cell lysates lacking Vps39.

As shown in Figure 3.8A the i-CORVET complex interacted specifically with Ypt7. It exhibited the same specificity for Ypt7-GTPγS as observed for the HOPS. This further strengthens the notion that Vps39 does not influence the Rab binding specificity of HOPS, which is exclusively mediated by Vps41. The replacement of Vps39 by Vps3 did not change this nucleotide preference. It seems therefore likely that Vps39 is inactivated or not accessible for Ypt7, when incorporated into the HOPS, which acts as an Ypt7-GTPγS effector complex.

3.1.5.2 Role of Vps39 in vacuole tethering

HOPS is the tethering factor at the vacuolar membrane and required for fusion of isolated vacuoles (Figure 3.3). To further analyze the role of Vps39 from within the complex and during tethering and fusion, the i-CORVET was subjected to the *vps11-1* vacuole fusion assay as described above. Since supplemented HOPS could rescue fusion of isolated vacuoles, it was directly compared with the i-CORVET. This might give hints towards the function of Vps39 from within the complex.

In Figure 3.9A, the fusion rate of *vps11-1* vacuoles after titrating HOPS, i-CORVET or buffer is depicted. As a control, equal amounts of the added protein complexes were confirmed on a Coomassie stained SDS-PAGE gel (Figure 3.9B).

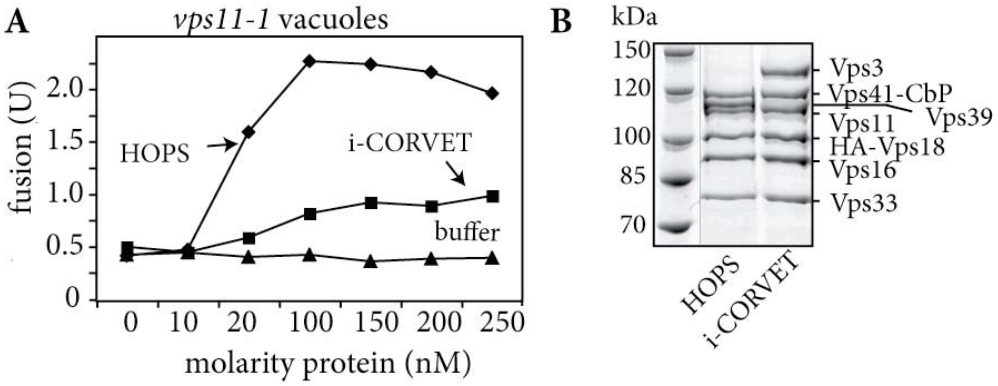

Figure 3.9: Vacuole fusion assay with supplemented i-CORVET. A: Titration of HOPS, i-CORVET or buffer to isolated *vps11-1* vacuoles. B: The SDS-PAGE gel loaded with equal volumes of HOPS and i-CORVET was stained with Coomassie. CbP: Calmodulin binding peptide, HA: Hemagglutinin tag.

HOPS and i-CORVET were isolated in the same stoichiometry but behaved differently in the fusion assay. In comparison with HOPS, the i-CORVET could only partially (up to approximately 25%) rescue fusion of *vps11-1* vacuoles. This suggests that Vps39 is required for full tethering activity of the complex and this could not be compensated for by Vps3. The activity of each tethering complex seems to be

independent of the Rab specificity, since both complexes showed binding to Ypt7-GTPγS.

To further investigate the functional relevance of Vps39 during vacuole fusion and its interaction to Ypt7, tester strains overexpressing Ypt7 were generated. Since both complexes bind Ypt7-GTPγS, they might exhibit comparable effects on the fusion activity of Ypt7-enriched vacuoles compared to wild-type vacuoles. As shown in Figure 3.10A, overproduced Ypt7 is indeed enriched at vacuolar membranes. The localization and expression of another vacuole resident protein, Vac8, was not affected. Interestingly, the fusion rate of wild-type vacuoles was not further increased by supplementation of both complexes (Figure 3.10B). Rather the fusion rate even decreased, probably due to dilution and increasing salt concentrations in the fusion reaction mix, as observed before (Figure 3.3). The fusion rate with supplemented i-CORVET did not decrease as strong as with HOPS or buffer, but both complexes did not further stimulate fusion. Possibly, the fusion rate had reached already maximal values and therefore the supplemented complexes were unable to stimulate the fusion of wild-type vacuoles even further.

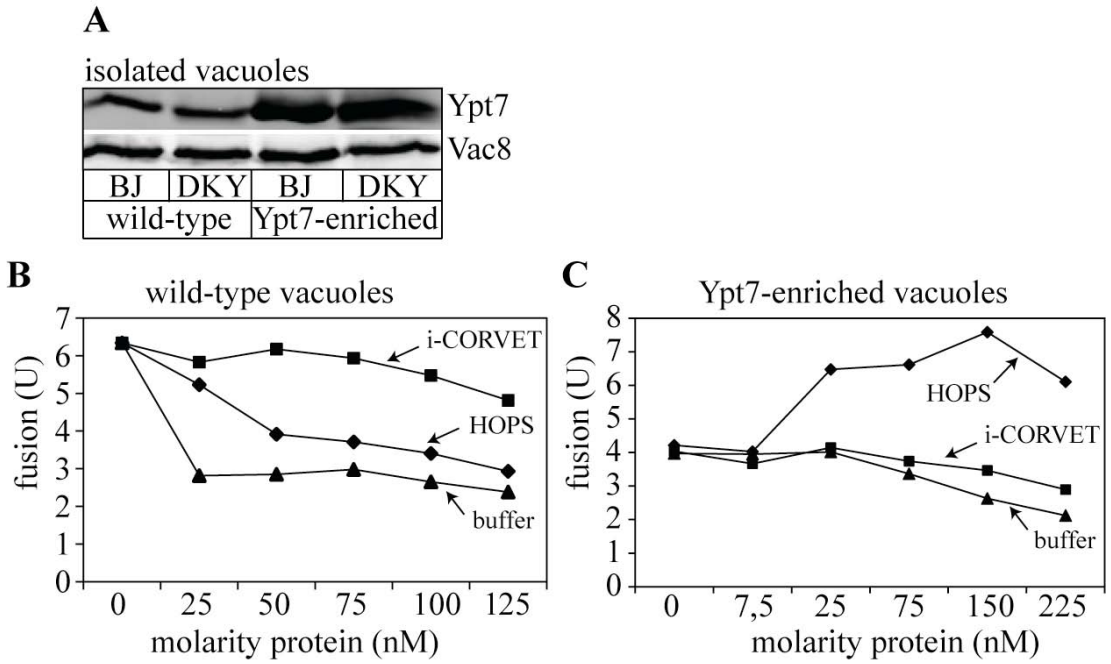

Figure 3.10: Fusion of wild-type vacuoles and Ypt7-enriched vacuoles. A: Isolated vacuoles from wild-type and Ypt7 overexpression tester strains were loaded on a SDS-PAGE gel and transferred onto a western blot membrane. Immuno-detection of Ypt7 showed that it was enriched at the vacuoles, when overproduced. The amount of the vacuolar protein Vac8 was unaffected. B: Titration of HOPS, i-CORVET or buffer to wild-type vacuoles. C: Titration of HOPS, i-CORVET or buffer to Ypt7-enriched vacuoles.

In contrast, vacuoles enriched for Ypt7 were stimulated to fuse after HOPS addition (Figure 3.10C). When i-CORVET was titrated into these Ypt7-enriched vacuoles, the fusion rate did not increase. In general, Ypt7-enriched vacuoles exhibited a reduced fusion rate compared with wild-type vacuoles. Fusion was stimulated by HOPS, but not by i-CORVET. This suggests an indispensable function of Vps39 in tethering and fusion of vacuoles, which cannot not compensated for by Vps3. The interaction (direct or indirect) between Vps39 and Ypt7 might be required for fusion of vacuoles, which leads to the model that tethering occurs via HOPS binding to Ypt7 on one membrane and SNAREs on the other membrane. The two opposing membrane might thereby get into close proximity to form *trans*-SNARE complexes.

To gain further insight into the function of Vps39 during fusion, vacuoles from tester strains overexpressing Vps39 were isolated. The overexpressed Vps39 is enriched at the isolated vacuoles (Figure 3.11A). Surprisingly, theses vacuoles fused very poorly. The fusion could not be rescued by mixing with wild-type vacuoles (Fig 3.11, B). A defect in the transport pathway of the peptidase (Pep4) or the phosphates (Pho8) to the vacuole could be excluded, because mixing with both wild-type vacuoles from either DKY or BJ background strain did not further enhance fusion. Supplementation of HOPS also was unable to stimulate the fusion (not shown).

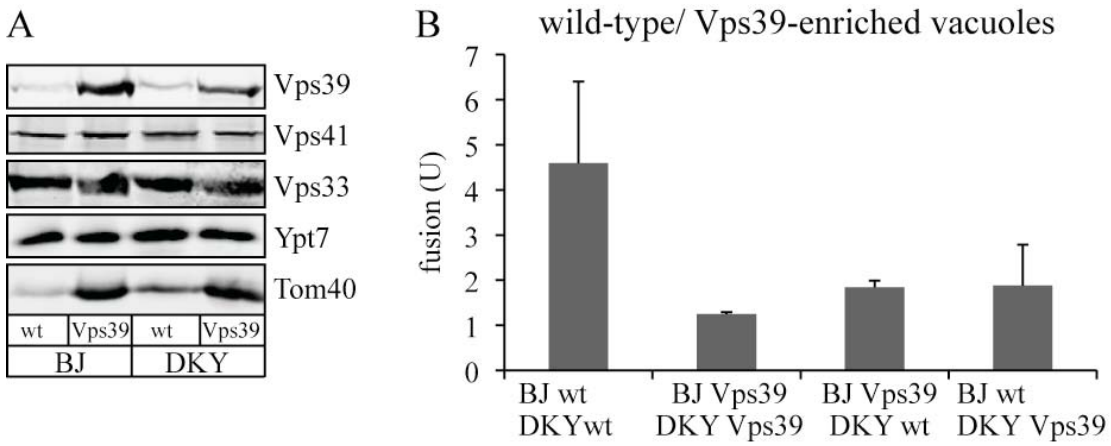

Figure 3.11: Comparison of fusion rates of wild-type and Vps39-enriched vacuoles. A: Isolated vacuoles were loaded onto a SDS-PAGE gel used for western blotting and immuno-detection. Vps39 was enriched at the vacuoles of BJ and DKY background strains overexpressing Vps39. HOPS subunits (Vps41 and Vps33) and Ypt7 localization was not effected upon Vps39 overexpression. The mitochondrial marker protein Tom40 was enriched in Vps39 BJ and DKY overexpression strains. B: The fusion rate of vacuoles enriched for Vps39 was strongly decreased compared to wild-type vacuoles. The fusion rate could not be rescued upon mixing with wild-type *pep4*Δ (BJ) or wild-type *pho8*Δ (DKY) vacuoles.

It therefore seems possible that the fusion of these Vps39-enriched vacuoles is somehow blocked. Interestingly, the isolated vacuoles showed an enrichment of the mitochondrial marker protein Tom40 (Figure 3.11A), a phenotype also observed by M. Cabrera in our lab. Here, the overexpression of Vps39 led to clustering of mitochondria to the vacuole. Therefore, the mitochondria were probably co-purified with the vacuoles during this approach, resulting in a block of the vacuole-vacuole contact sites. This might inhibit fusion and explain why supplementation of HOPS did not show any effect.

3.1.5.3 Role of Vps39 as a GEF or GDF for Ypt7

Vps39 is required in the HOPS complex to fulfill its function as a tethering complex. The interaction between Vps39 and Ypt7 might also be required for fusion. Ypt7-enriched vacuoles are stimulated to fuse upon addition of HOPS but not of i-CORVET. Vps39-enriched vacuoles did not provide any further insights into the function of Vps39 within the HOPS complex, because co-purified mitochondria likely blocked fusion. Therefore, I took advantage of isolated wild-type vacuoles. Even though fusion was not stimulated upon titration of the complexes (Figure 3.10B), it could be selectively inhibited with Gyp1-46 or with Gdi1. Gyp1-46 is a truncated version of the GAP (GTPase activating protein) protein Gyp1, which is capable to stimulate hydrolysis of GTP bound to Ypt7 to the inactive GDP-bound form and thereby counteracting the GEF (GTPase exchange factor). Gdi1 (GTPase dissociation inhibitor) extracts inactivated Ypt7 from membranes and chaperones the GDP-loaded protein in the cytosol. The Rab is then recruited back to membranes with the help of GDF (Gdi1 displacement factor) (for details see Figure 1.4). Both Gyp1-46 and Gdi1 are therefore efficient fusion inhibitors. To analyse if HOPS or i-CORVET can counteract these inhibitions, they were titrated to such vacuoles. A rescue in fusion would point towards a GDF or GEF function of Vps39 from within the holo HOPS complex.

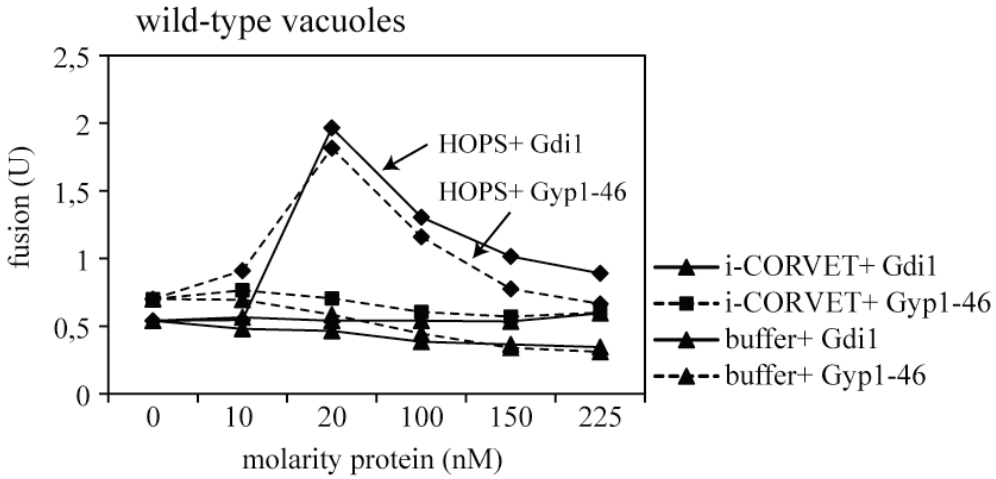

Figure 3.12: Fusion of wild-type vacuoles with HOPS. Fusion of wild-type vacuoles was inhibited with Gdi1 or Gyp1-46. HOPS could partially rescue fusion under both conditions, whereas i-CORVET or buffer was not able to rescue fusion.

Figure 3.12 shows that HOPS but not i-CORVET could partially overcome Gyp1-46 or Gdi1 inhibited vacuole fusion. Surprisingly, this rescue appeared to be independent of the kind of inhibition, such that no conclusion about GEF or GDF activity is possible. Also indirect effects might be involved here. I-CORVET was unable to rescue fusion under both conditions. The i-CORVET could not stimulate the fusion of Ypt7-enriched vacuoles and of fusion-deminished wild-type vacuoles. It is therefore obvious that Vps39, and potentially its interaction with Ypt7, is required in the complex to fulfill its function as a tethering factor. The precise role of Vps39 in the complex remains unkown.

3.1.6 Analysis of HOPS mutations

In Ostrowicz et al., 2010 we published a single subunit deletion screen to identify direct interaction partners in the HOPS complex. Different subcomplexes were identified and their localization within the complex was analyzed. It turned out that Vps41 is the HOPS effector subunit that binds to Ypt7-GTPγS (Ostrowicz et al., 2010; Figure 3.7). The localization of each subunit in the complex might give hints towards their role in the complex and about tethering function of the entire HOPS. Currently, we are lacking a high-resolution structure of holo HOPS. Within a long-term strategy to elucidate the HOPS structure, GFP-tags were added to the carboxy-termini of each of the subunits. Therefore, the tagged complexes were functionally and structurally investigated.

3.1.6.1 Purification and in vivo localization of GFP-tagged HOPS versions

The GFP-tag was fused carboxy-terminally to single HOPS subunits and the resulting complexes were purified from overexpression strains as before. Here, the GFP-tag with its molecular mass of approximately 25kDa might interfere with the HOPS assembly and/or functionality, which could provide insights into the role of each subunit in the complex. Another advantage of GFP-tags is the possibility to localize them under the electron microscope (see 3.2.3.1). To gain insights into the effect of carboxy-terminal tags upon HOPS functionality, yeast overexpression strains were analyzed by fluorescence microscopy. Diploid yeast cells were observed in the depletion situation (YPD), where just the wild-type copy of each protein is expressed, and the overexpression situation (YPG), where the concomitant expression of all six HOPS proteins is induced (Figure 3.13). Under depletion conditions, the vacuoles were fragmented in each strain, except for the HOPS-Vps39-GFP construct. One wild-type copy of each protein seemed not sufficient to drive fusion with the vacuole or to assemble into functional HOPS. Already the depletion of one “Class C” protein results in total vacuole fragmentation (not shown), which shows that the expression of these proteins is fine-tuned. Contrary, in the overexpression situation, the strains showed round (untagged HOPS, HOPS with Vps18- and Vps33-GFP) or multilobed (HOPS with Vps39- and Vps16-GFP) vacuoles, with the GFP-tagged subunit localized to the vacuolar rim. HOPS with Vps11-GFP exhibited one large round vacuole surrounded by smaller vacuoles with Vps11 localized to the rim. Cells overexpressing HOPS with Vps33-GFP showed a mixed phenotype, with either Vps33-GFP localized to the vacuolar rim or a more cytosolic localization. Nevertheless, in the overexpression situation, the transport and fusion to and with the vacuole seemed not to be completely impaired and the GFP-tag might not block HOPS localization and function completely. The overexpression of one single subunit results in a cytosolic accumulation of the respective protein (not shown), whereas the overexpression of all six HOPS subunits assemble into active HOPS at the vacuolar membrane and the subunits were only weakly detectable in the cytosol. Here, Ypt7 might serve as an assembly and recruitment platform at the vacuole. Alternatively, the complex might be bound via its interaction with vacuolar SNAREs and lipids to the membrane. The surplus of overexpressed HOPS subunits, which were not bound, then accumulates in the cytosol.

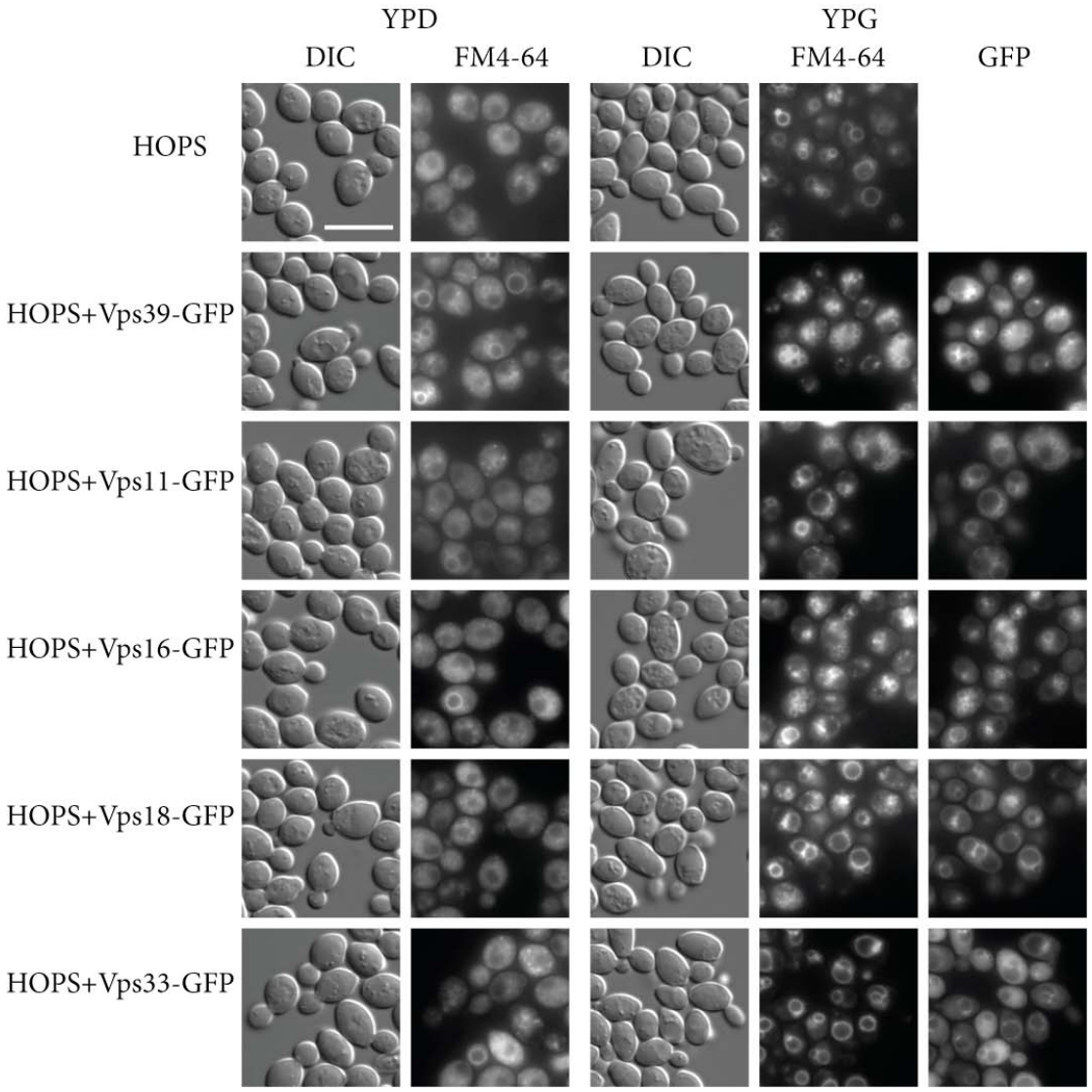

Figure 3.13: Microscopy images of HOPS overexpression strains with additional carboxy-terminal GFP-tag. All diploid cells were grown under depletion conditions (YPD, two left panels) or under overexpression conditions (YPG, three right panels). Vacuoles were stained with FM4-64 and analyzed under the fluorescence microscope using DIC, FM4-64 and GFP filters. After an exposure time of 500ms the GFP signal was detected. The expression of the GFP-fusionproteins is only induced in the presence of galactose (YPG). Scale bar: 10µm.

To analyze the stability of the different carboxy-terminal GFP-tagged HOPS versions, small-scale purifications were performed. The purification procedure is based on the TAP purification (for details see 6.3.4.2). As shown in Figure 3.14, HOPS was purified with an additional GFP-tag at each of the subunits (except for Vps41, because this is the bait protein).

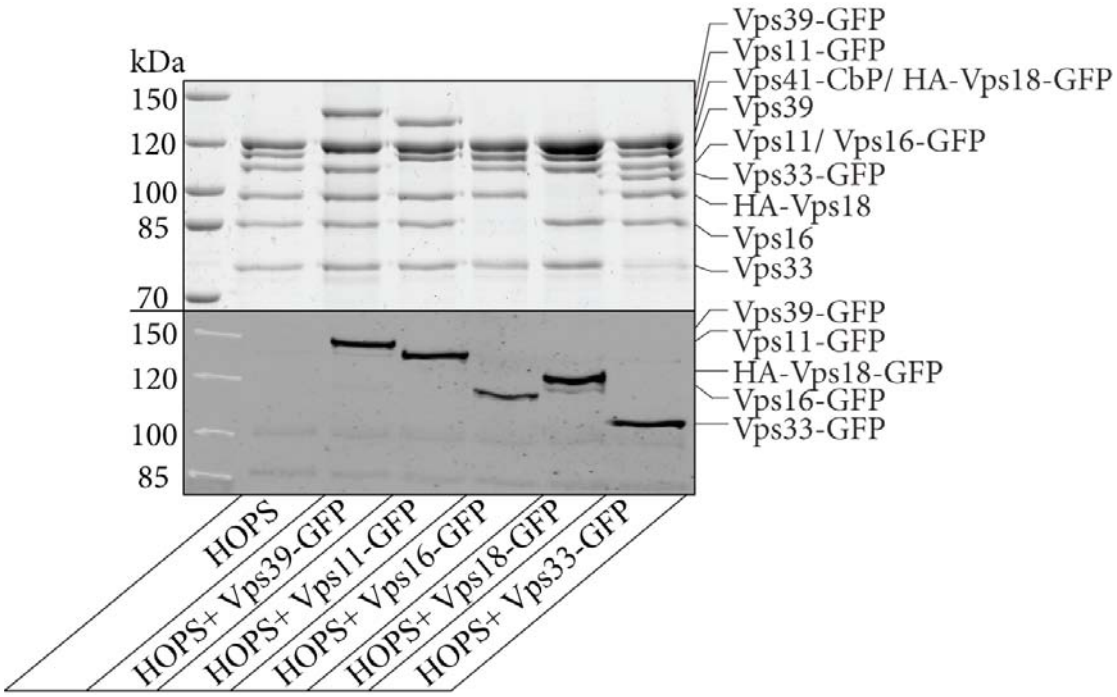

Figure 3.14: Purification of HOPS with carboxy-terminal GFP-tag. Upper panel: The SDS-PAGE gel loaded with purified wild-type HOPS or HOPS with one GFP-tagged subunit was stained with Coomassie. Lower panel: Western blot decoration against the GFP-tag. CbP: Calmodulin binding peptide, HA: Hemagglutinin tag.

The stoichiometry of each subunit in the complex appeared unaffected compared with untagged HOPS. This indicated, that the GFP-tag did not interfere with HOPS assembly. The influence on functionality of HOPS is analyzed in more detail below (see 3.1.6.3).

3.1.6.2 Purification of HOPS with deleted ALPS motif of Vps41

The second modification of the HOPS complex within the presented work was the deletion of the amphipathic lipid packing sensor of Vps41. This motif has a regulatory role for Vps41 function during tethering (Cabrera et al., 2010). It is required for the localization of Vps41 and HOPS at membranes (see 1.2.2.4.3). The deletion might therefore alter the membrane association of the entire HOPS complex and consequently influence its tethering function.

To find out about the role of the ALPS motif during fusion, two different HOPS overexpression yeast strains, lacking the complete ALPS motif or half of it were generated. Small-scale purifications of HOPS and HOPS with deleted ALPS motif or half of the ALPS motif (HOPSΔALPS, HOPSΔALPS/2) were performed (Figure 3.15).

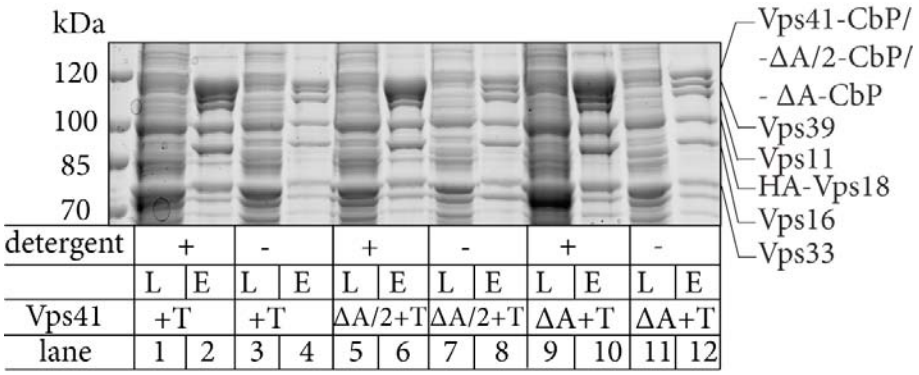

detergent	+		-		+		-		+		-	
	L	E	L	E	L	E	L	E	L	E	L	E
Vps41	+T		+T		ΔA/2+T		ΔA/2+T		ΔA+T		ΔA+T	
lane	1	2	3	4	5	6	7	8	9	10	11	12

Figure 3.15: Purification HOPS with ALPS motif deletions. The SDS-PAGE gel loaded with HOPS total lysates (L) or purified HOPS eluates (E) was stained with Coomassie. Vps41 was used in all cases as bait protein for the purification in the presence (+) or absence (-) of detergent. +T: HOPS with Vps41-TAP; ΔA/2+T (aa 366 to aa 377Δ): HOPS with Vps41-TAP lacking half of the ALPS motif; ΔA+T (aa 356 to aa 379Δ) HOPS with Vps41-TAP lacking the entire ALPS motif.

The role of the ALPS motif in membrane interaction suggests a model depicted in Figure 1.7B. Therefore, both modified HOPS constructs were purified in the presence and absence of detergent. The purification of holo HOPS was possible under all conditions (Figure 3.15 (lanes 2, 4, 6, 8 and 10)). As observed before the bait protein Vps41 with and without the ALPS deletion was more abundant when HOPS was purified in the presence of detergent than in its absence (Figure 3.1). The assembly of the complex therefore seemed unaffected by the ALPS deletion. Comparing the purifications without detergent, no significant increase in solubility was observed.

3.1.6.3 Influence of different HOPS modifications towards fusion activity

All generated HOPS modifications might alter its activity. The assembly seems unaffected, because all GFP-tagged HOPS and HOPS without ALPS motif were purified as stoichiometric hexameric complexes. The preparative yield was comparable with the wild-type complex. To characterize the various HOPS mutants, vacuole fusion assays with isolated vacuoles from *vps11-1* tester strains were performed. The activity of the different HOPS preparations was thereby directly compared with the wild-type. This analysis might point to the role of each subunit in the complex and during vacuole fusion, because the GFP-tag and the ALPS motif deletion might influence HOPS tethering function.

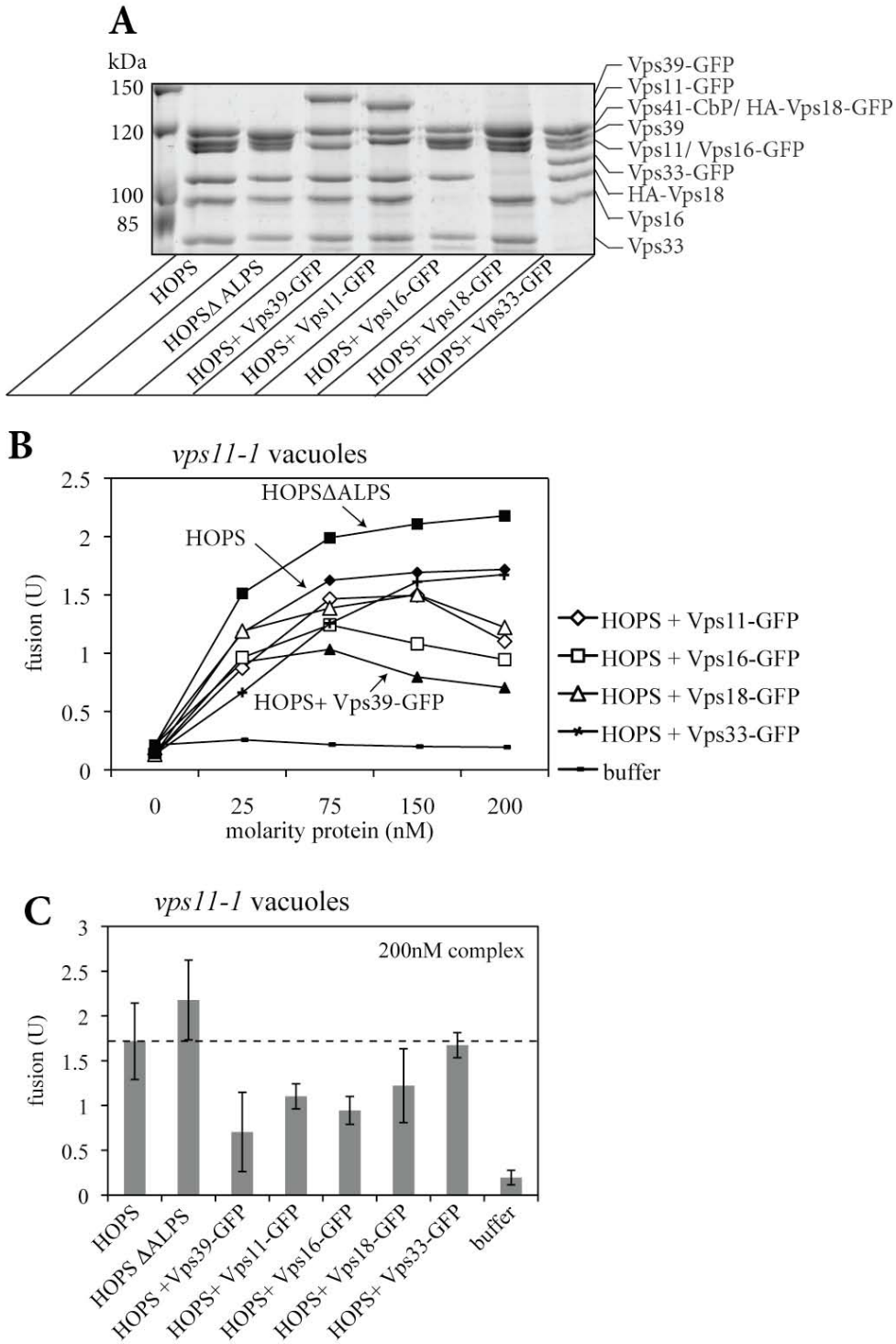

Figure 3.16: Fusion activity of HOPS mutants. A: The SDS-PAGE gel loaded with equal volumes of purified wild-type HOPS, HOPSΔALPS and different GFP-tagged HOPS versions was stained with Coomassie. B: Titration of equal amounts of wild-type HOPS, HOPSΔALPS and different GFP-tagged HOPS versions or buffer to the *vps11-1* vacuole fusion mix. Depicted are the average values of three independent experiments. C: Fusion activity of wild-type HOPS, HOPSΔALPS and GFP-tagged HOPS versions at 200nM. Depicted are the average values of three independent experiments.

Figure 3.16A shows a SDS-PAGE gel loaded with equal amounts of each purified complex to ensure comparable protein concentrations for the fusion assay. The protein concentration was additionally determined with the NanoDrop®-ND1000

spectrophotometer to confirm equal concentrations. The fusion rate of different GFP-tagged HOPS mutants and HOPSΔALPS were compared to the wild-type HOPS (Figure 3.16B). Figure 3.16C shows the fusion effectivity after addition of 200nM of each modified complex. It is obvious that the GFP-tags impaired the HOPS activity, since all of them, except for HOPS with Vps33-GFP, showed a reduced fusion rate (indicated by the dashed line in Figure 3.16C). The most severe fusion reduction occurred in HOPS with Vps39-GFP. After an increase in fusion at low complex concentrations, the rate decreased after further increasing its concentration. The carboxy-terminal GFP-tag might therefore interfere with Vps39 function, further pointing towards a crucial role of Vps39 in the HOPS complex and during fusion. All other GFP-tagged versions also exhibited a decreased fusion rate, which might be due to a reduction in flexibility due to sterical hindering of the entire complex. Surprisingly, HOPSΔALPS showed an increased fusion rate compared with wild-type HOPS. In this case, the internal ALPS deletion might led to a more flexible complex, which seemed to be more fusion-active. This modified complex with deleted ALPS motif in Vps41 might mimic the unphosphorylated form of Vps41 (Cabrera et al., 2010, Figure 1.7B), which could act independently of the phosphorylation by Yck3. One regulatory step is therefore missing under these conditions, which then results to a more fusion-competent complex.

Since the different modified HOPS complexes behaved differently in *vps11-1* vacuole fusion, the effect of the modifications on the postulated function of HOPS as a GEF or GDF was further examined. To this end, wild-type vacuoles were incubated with Gyp1-46 or Gdi1 as described before (Figure 3.12) and incubated with increasing amounts of the HOPS mutants. Equal concentrations of all complexes were analyzed on a Coomassie-stained SDS-PAGE gel and with the NanoDrop®-ND1000 spectrophotometer as before (not shown).

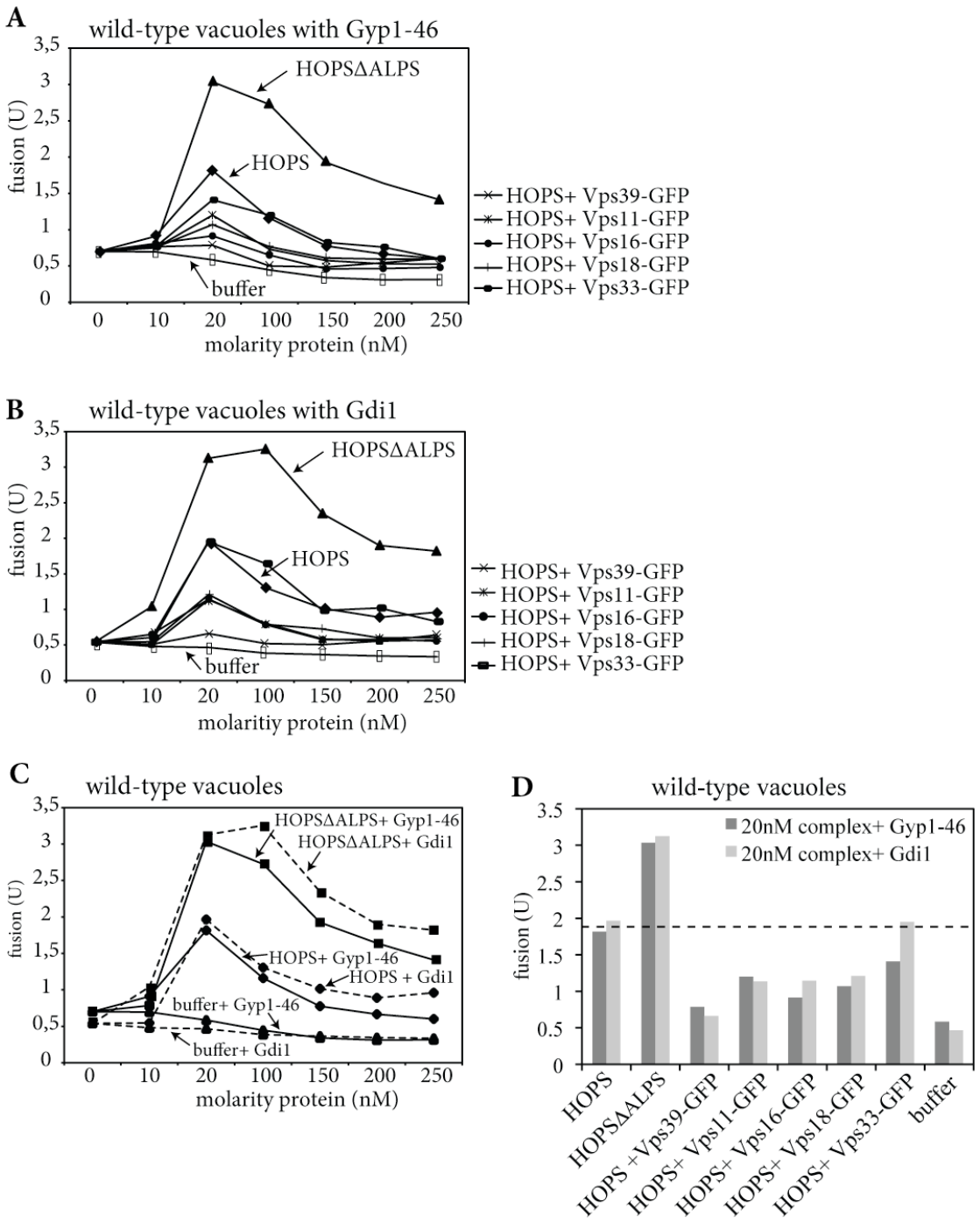

Figure 3.17: Rescue of wild-type fusion activity by different HOPS mutants. A: Wild-type vacuoles were inhibited with Gyp1-46 and incubated with wild-type HOPS, HOPSΔALPS and GFP-tagged HOPS mutants. B: Wild-type vacuoles were inhibited with Gdi1 and incubated with wild-type HOPS, HOPSΔALPS and GFP-tagged HOPS mutants. C: Comparison of fusion rates between wild-type HOPS and HOPSΔALPS of Gyp1-46 or Gdi1 inhibited vacuoles. D: Comparison of fusion rescue between all complexes at 20nM concentration (taken from C). Both kinds of inhibitions were directly compared.

The fusion rate of wild-type vacuoles inhibited with Gyp1-46 was rescued upon addition of 20nM wild-type HOPS as observed before (Figure 3.17A; Figure 3.12). All GFP-tagged HOPS mutants could also rescue fusion at this low concentration, but not to the same extend as observed for wild-type HOPS. Just HOPS with Vps33-GFP

showed a rescue comparable with the wild-type complex. Interestingly, HOPS with ALPS deletion appeared to be more active than wild-type HOPS and increased the fusion rate even further. The same scenario was observed when vacuoles were inhibited for fusion with Gdi1 (Figure 3.17B). Wild-type HOPS and HOPS with Vps33-GFP showed a comparable rescue, whereas the other GFP-tagged mutants could only partially rescue the fusion at low concentrations (20nM). HOPS with a deleted ALPS motif again stimulated the fusion stronger as the wild-type. Since the effect of fusion rescue was comparable under both inhibition conditions, no conclusion about an interference with GDF of GEF function of the complexes is possible (Figure 3.17C). Interestingly, HOPS with Vps39-GFP showed the weakest activity under both conditions. These results were consistent with the *vps11-1* fusion observed before (Figure 3.16B and C). Here, HOPS with ALPS deletion was more active and HOPS with Vps39-GFP was the least active one compared with the wild-type complex. The influence of GFP-tagged HOPS mutants on its structure is investigated in the following chapter.

3.2 Structural analysis

HOPS is involved in all fusion events at the vacuole. Hints towards the tethering mechanism can profit from structural information. A rough idea about the subunit arrangement and the direct interaction partners within the holo complex was obtained previously (Ostrowicz, et al., 2010; Plemel et al., 2011), though a three-dimensional model is still lacking. As a first step towards this goal, electron microscopy of the purified protein complex was tackled in cooperation with the group of Stefan Raunser at the Max-Planck Institute for molecular physiology, Dortmund, Germany.

3.2.1 Optimization of HOPS purification for electron microscopy

To visualize proteins under the electron microscope, pure and stable preparations are indispensable. The first step therefore was to improve yield and purity of the HOPS complex. For this purpose large-scale TAP purifications were established (for details see 6.3.4.3) and the TEV-cleaved eluate was analyzed by electron microscopy. In Figure 3.18A two Coomassie stained SDS-PAGE gels loaded with HOPS TEV-eluate are shown. The complex appeared to be highly pure, but still contained some impurities. Some low molecular mass contaminations were visible in the 7,5% SDS-PAGE gel; one below the 80kDa band of Vps33. This turned out to be a yeast

chaperone (Hsp60), which was probably up regulated due to the overexpression of the six HOPS subunits and therefore co-purified (confirmed by mass spectrometry by H.J.k.B., data not shown). Another protein of 50kDa co-eluted with HOPS, which was identified as the IgG heavy chain (Figure 3.18A left picture). When HOPS was loaded on a 12% SDS-PAGE gel to visualize smaller protein contaminations, two weak protein bands appeared between 25 and 30kDa. Theses proteins corresponded to TEV protease required for elution of the complex from IgG beads (for details see 6.3.4). The lower band corresponded to a degradation product of the upper TEV band during its purification.

This sample was then analyzed by electron microscopy. For this purpose, it was applied onto a glow-discharged copper grid and negative-stained with uranyl-formate (for details see 6.4.2). As shown in Figure 3.18B much more inhomogeneous particles as expected form the purity of the preparation showed up. The discernible particles did not show any distinct shape or size. One reason for the disordered appearance might be due to the TEV protease in the sample, even though only traces were visible in the SDS-PAGE gel. This might have caused a protein background, which hampered the clear visualization of HOPS. In addition, the complex seemed to disassemble or to form aggregates on the grid. For these reasons, the complex was subjected to size-exclusion chromatography after elution.

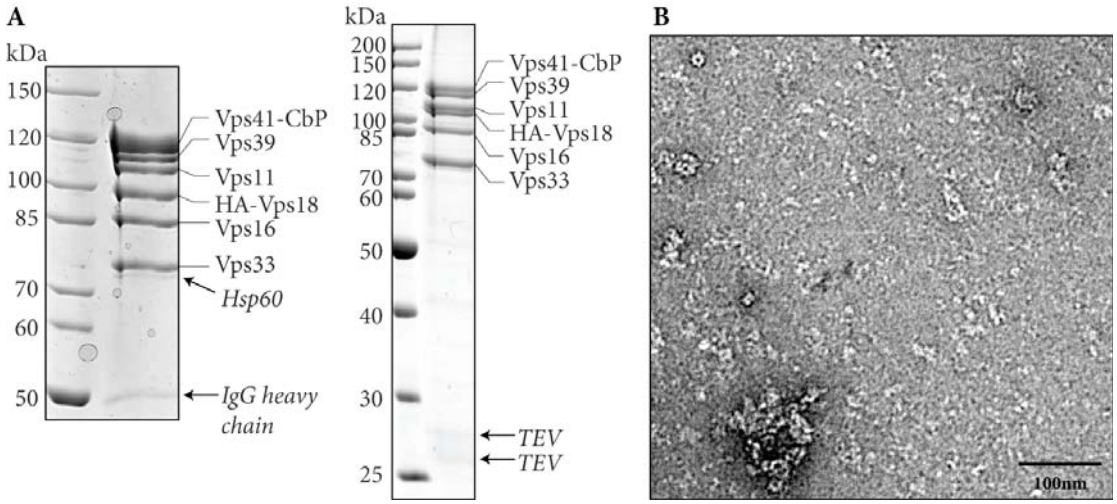

Figure 3.18: Purified HOPS TEV-eluate appeared partially denatured under the electron microscope. A: Purified HOPS TEV-eluate was loaded onto a 7,5% (left) and 12% (right) SDS-PAGE gels and stained with Coomassie. Only traces of low molecular mass proteins were visible (indicated by arrows). B: Electron microscopy picture of negative-stained HOPS TEV-eluate. Picture by S. Raunser, MPI, Dortmund, Germany.

The TEV-cleaved HOPS eluate was subjected to a Superdex 200 gelfiltration (GE Healthcare) prior to analyzing HOPS under the electron microscope. The gelfiltration

fractions were loaded onto an SDS-PAGE gel (Figure 3.19A). A clear elution peak in fraction 9 was observed; hence this fraction was further analyzed by electron microscopy (Figure 3.19B). This time, more distinct structures, but also both, smaller and larger fragments were visible. This experiments suggested that the complex is quite unstable and tends to aggregate or to disassemble during the time between preparation and electron microscopy measurement.

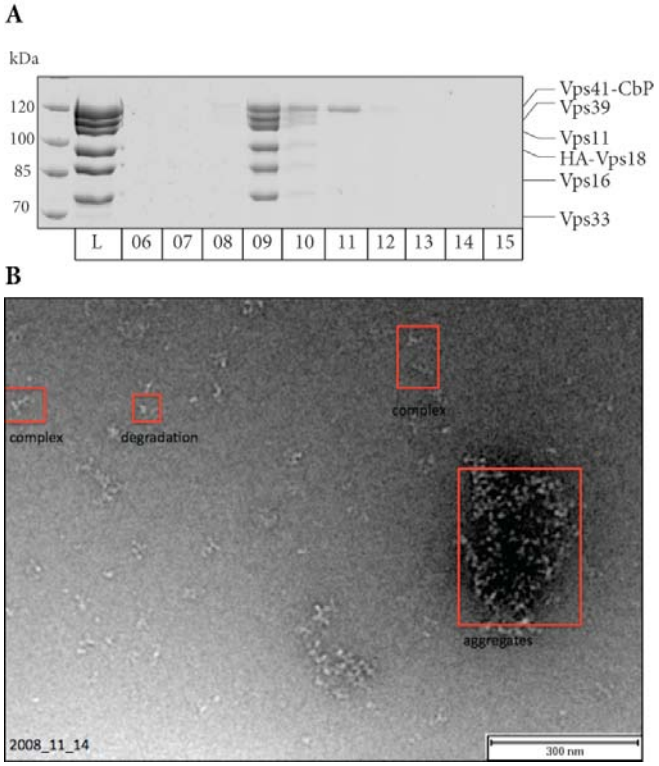

Figure 3.19: HOPS structure analysis by electron microscopy. A: TEV-cleaved eluate of HOPS was applied onto a Superdex 200 gelfiltration column. The loading control (L) and aliquots of fractions 6 to 15 were analyzed on a SDS-PAGE gel stained with Coomassie. B: Negative-stained sample of purified HOPS, eluted in fraction 9 from the gelfiltration column was visualized under the electron microscope. Picture by S. Raunser, MPI, Dortmund, Germany.

It was likely that the HOPS complex is flexible, since structural adjustments might be required for tethering and fusion. To overcome this issue, one possibility was to stabilize the putative flexible regions within the complex via cross-linking. This treatment might favor one specific conformation and thus could result in a more uniform particle distribution. The following chapters deal with optimization procedures of this issue and might therefore be skipped. The results following these optimizations continue in chapter 3.2.5.

3.2.2 Cross-linking by GraFix method

A promising protocol for cross-linking was the so-called GraFix method by Kastner et al., 2008. It is based upon a continuous glycerol gradient centrifugation in combination with cross-linking. Here, the HOPS complex was stabilized via cross-linking by glutharaldehyde (for details see 6.3.6).

A SDS-PAGE gel of a glycerol gradient centrifugation with marker proteins is depicted (Figure 3.20A). These proteins were used to calibrate the glycerol gradient, because they were migrating corresponding to their masses into the glycerol gradient (Thyroglobulin (660kDa) in fraction 8, Aldolase (68kDa) mainly in fraction 3 and Albumin (66kDa) in fraction 1 and 2).

Next, the same experiment was performed with HOPS TEV-eluate in the presence and absence of cross-linker. Fractions were loaded onto SDS-PAGE gels (Figure 3.20B and C). The glycerol gradient without cross-linker showed a clear elution peak for HOPS in fraction 6. As before, the surplus of Vps41 was separated from the complex and appeared earlier in the gradient (fractions 2 and 3). In the SDS-PAGE gel separated cross-linked fractions of HOPS were not visible (Figure 3.20C). This was not surprising, because cross-linking via glutaraldehyde is irreversible and the complex did not migrate into the SDS-PAGE gel. Smaller cross-linked fragments still migrated into the gel, as indicated by the dark smear. Figure 3.20D shows the electron microscopy image of negative-stained cross-linked HOPS from fraction 6. The complex appeared to be very pure; no large aggregates were visible. Surprisingly, smaller unstructured fragments were still observed.

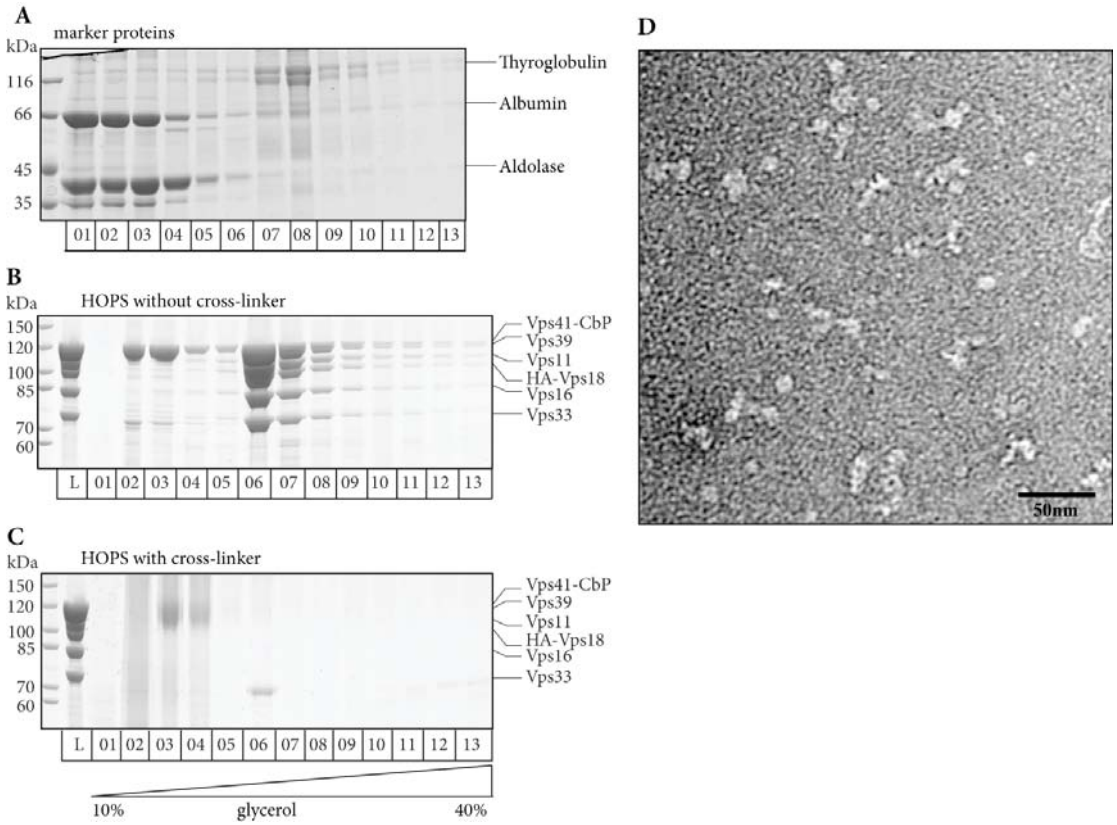

Figure 3.20: Electron microscopy of HOPS after glycerol gradient centrifugation with simultaneous cross-linking. A: The SDS-PAGE gel loaded with fractions of marker proteins from glycerol gradient centrifugation was stained with Coomassie. B: Purified HOPS from glycerol gradient centrifugation without cross-linking was loaded onto a SDS-PAGE gel stained with Coomassie. The surplus of Vps41 is visible in fractions 2 and 3. C: Fractions of HOPS from glycerol gradient centrifugation with simultaneous cross-linking was loaded onto a SDS-PAGE gel stained with Coomassie. Cross-linking is irreversible and the complex did therefore not migrate into the gel. D: Electron microscopy picture of HOPS fraction 6 after glycerol gradient centrifugation with simultaneous cross-linking. Picture by S.Raunser, MPI, Dortmund, Germany. Scale bar as indicated.

Considering the larger particles, some common features were evident as elongated dumb-bell like structures. Nevertheless, it was not clear at this point, which of the particles represented HOPS, because the complex still seemed to be very flexible and hard to distinguish from smaller fragments. It also was lacking one specific orientation. Larger aggregates were not observed, but many smaller fragments. Taken together, the glycerol gradient centrifugation with simultaneous cross-linking seemed suitable as it improved the purity and signal-to-noise ratio of the obtained electron microscopy pictures (Kastner et al., 2008).

3.2.2.1. HOPS subcomplex analysis via glycerol gradient centrifugation with cross-linking

In view of the above-described procedure, also the HOPS subcomplexes were investigated. Structural analysis of these subcomplexes might provide a first hint towards their shape and possibly might be modeled into the structure of the entire

HOPS complex. Therefore, Vps39-Vps11, Vps39-Vps11-Vps18 and Vps16-Vps33 subcomplexes were purified by the TAP protocol.

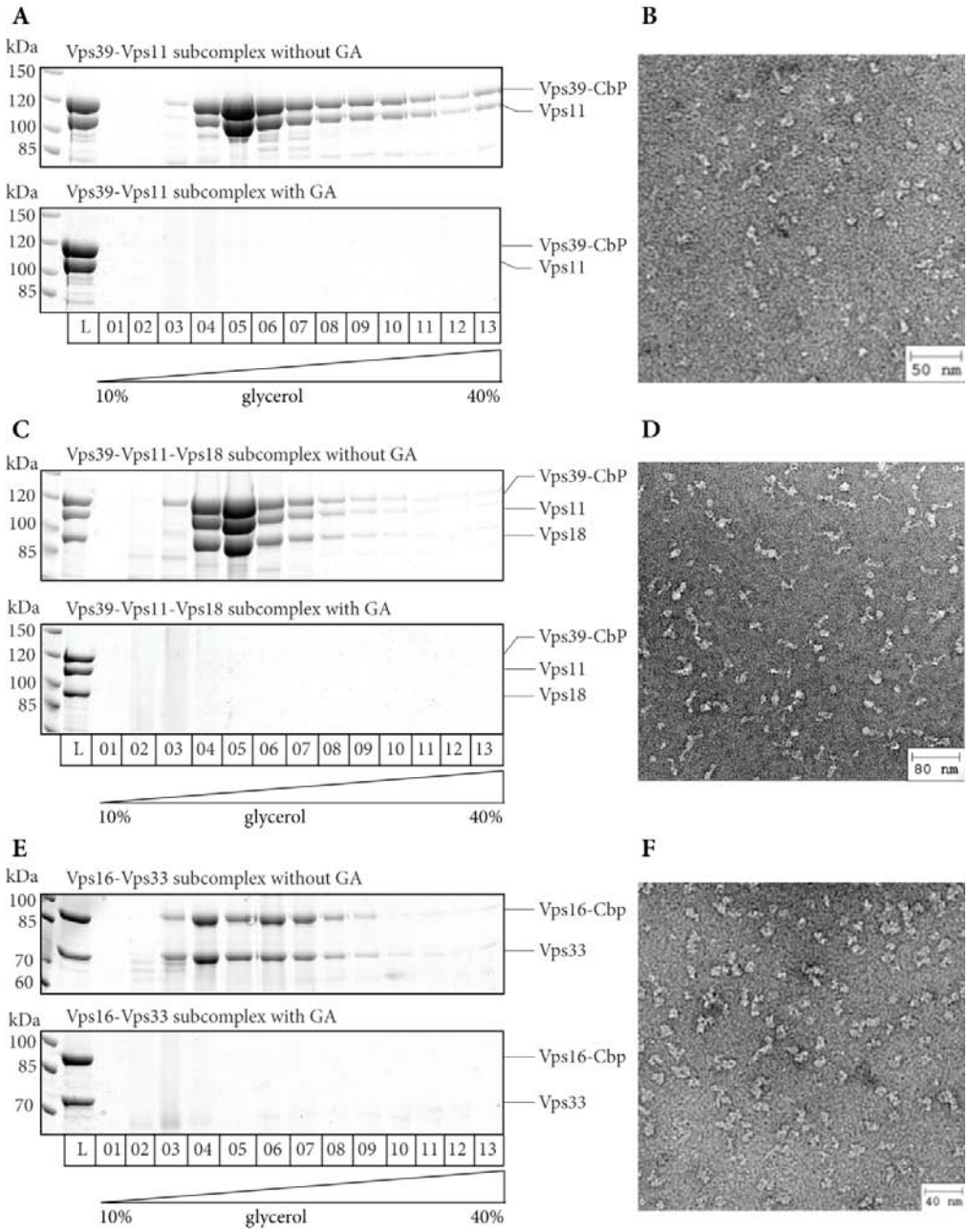

Figure 3.21: Electron microscopy analysis of HOPS subcomplexes after cross-linking. A: The SDS-PAGE gels loaded with fractions from glycerol gradient centrifugation of Vps39-Vps11 subcomplex without (upper part) and with (lower part) cross-linking were stained with Coomassie. B: Electron microscopy picture from peak fraction of glycerol gradient centrifugation with simultaneous cross-linking. C: The SDS-PAGE gels loaded with fractions from glycerol gradient centrifugation of Vps39-Vps11-Vps18 subcomplex without (upper part) and with (lower part) cross-linking were stained with Coomassie. D: Electron microscopy picture from peak fraction of glycerol gradient centrifugation with simultaneous cross-linking. E: The SDS-PAGE gels loaded with fractions from glycerol gradient centrifugation of Vps16-Vps33 subcomplex without (upper part) and with (lower part) cross-linking were stained with Coomassie. F: Electron microscopy picture from peak fraction of glycerol gradient centrifugation with simultaneous cross-linking. All electron microscopy images by S. Raunser/ A. Schwedt, MPI, Dortmund, Germany. Scale bars as indicated.

All three subcomplexes were purified in stoichiometric proportions and ran in distinct peak fractions after glycerol gradient centrifugation (Figure 3.21A, C and E (upper parts)). Vps39-Vps11 (240kDa) and Vps39-Vps11-Vps18 (347kDa) subcomplexes ran in one peak in fraction 5. Even though the molecular mass of these two subcomplexes differ by approximately 100kDa, they ran at the same glycerol density. This might be due to the low resolution of the glycerol gradient or the glycerol density might differ slightly because of the manual pouring device. Alternatively, the axial ratios of these to subcomplexes might differ, resulting in a different running behavior. The peak for the third subcomplex (Vps16-Vps33) appeared earlier in fraction 4 consistent with its lower molecular mass of 172kDa. The cross-linking protocol worked for all three subcomplexes (Figure 3.21A, C and E (lower parts)). No protein bands were observed, because the cross-linked proteins did not migrate into the SDS-PAGE gel. The corresponding peak fractions of the cross-linked subcomplexes were visualized after negative staining with by electron microscopy (Figure 3.21B, D and F) The Vps39-Vps11 subcomplex appeared unstructured in comparison to the Vps39-Vps11-Vps18 subcomplex. It seems possible, that Vps18 is stabilizing the Vps39-Vps11 subcomplex in an elongated structure. Vps16-Vps33 appeared higher concentrated and more structured as Vps39-Vps11-Vps18 subcomplex. Some unique shapes were visible. This part of the HOPS complex seemed to be the most stable one as compared with the others. Unfortunately, in all cases smaller fragments were visible, which might complicate further analysis. It seems that even the subcomplexes are flexible, as already observed before for the holo complex.

3.2.3 HOPS structure determination

All electron microscopy images shown so far gave a very broad overview of the shape of HOPS and its subcomplexes. To gain a more detailed view of the complex, a closer look at single HOPS particles was necessary. Therefore low dose mode pictures were taken at high resolution of the complexes and up to 10000 particles were manually selected. The images were computationally analyzed and sorted via overlay into different classes, the so-called class averaging with the Sparx program (Hohn et al., 2007; see 6.4.2). With this method distinct features of the averaged HOPS structure became visible.

Figure 3.22 shows the class averages of the HOPS holo complex purified via the cross-linking procedure. Different numbers of classes are depicted with varying

numbers of particles per class. Each square refers to one class. The more particles are picked, the more classes one can get and the more detailed the picture of the complex becomes. HOPS appeared as an elongated dumb-bell-like structure in almost all pictures. Apparently both ends are flexible or appear in multiple conformations, since they were often not clearly resolvable as distinct structures.

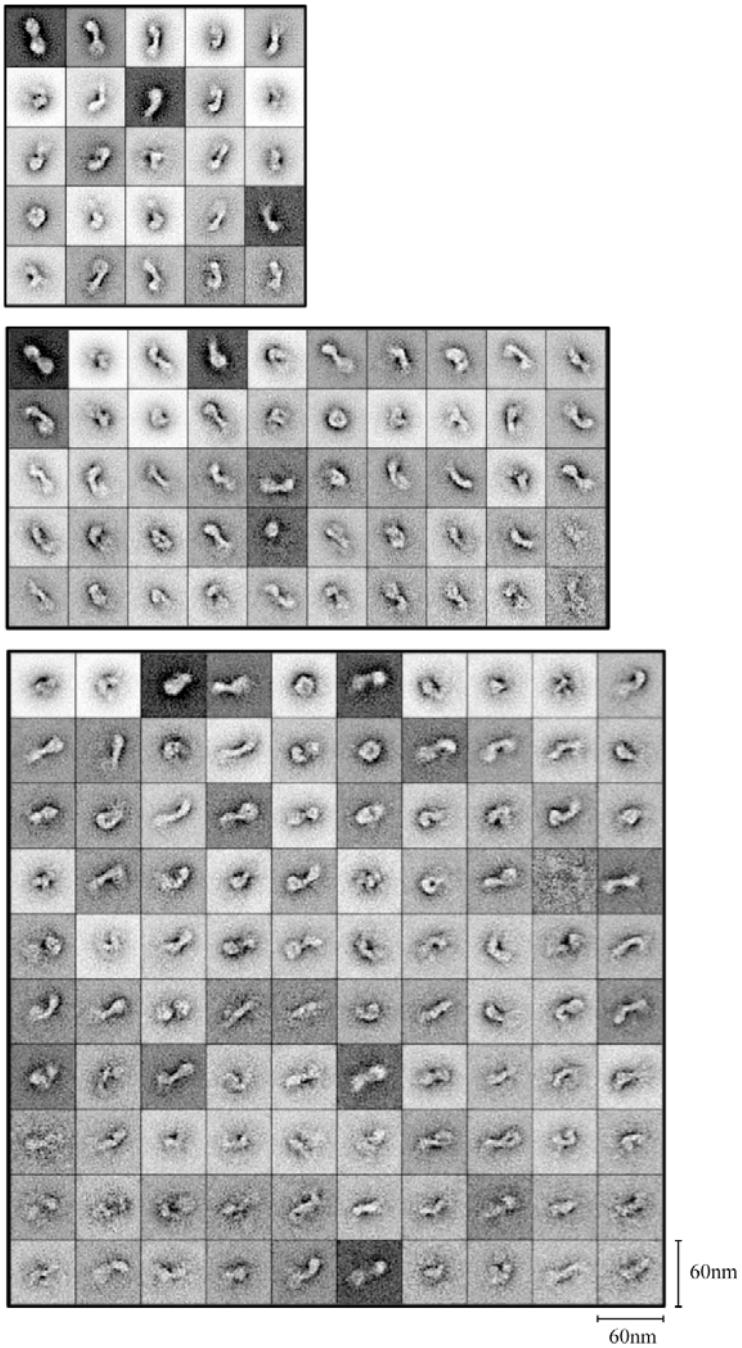

Figure 3.22: Single particle analysis of the HOPS complex. Single particles were picked from low dose mode pictures at high-resolution, aligned and sorted into classes. Class averages by S. Raunser, MPI, Dortmund, Germany. Scale bars as indicated.

To gain more information about the flexible ends of the HOPS complex, we performed the above-described single particle analysis also for the Vps16-Vps33

subcomplex. This subcomplex seemed to be the most stable one analyzed so far. Even though this subcomplex also appeared not absolutely stable under the electron microscope, single particle analysis was carried-out.

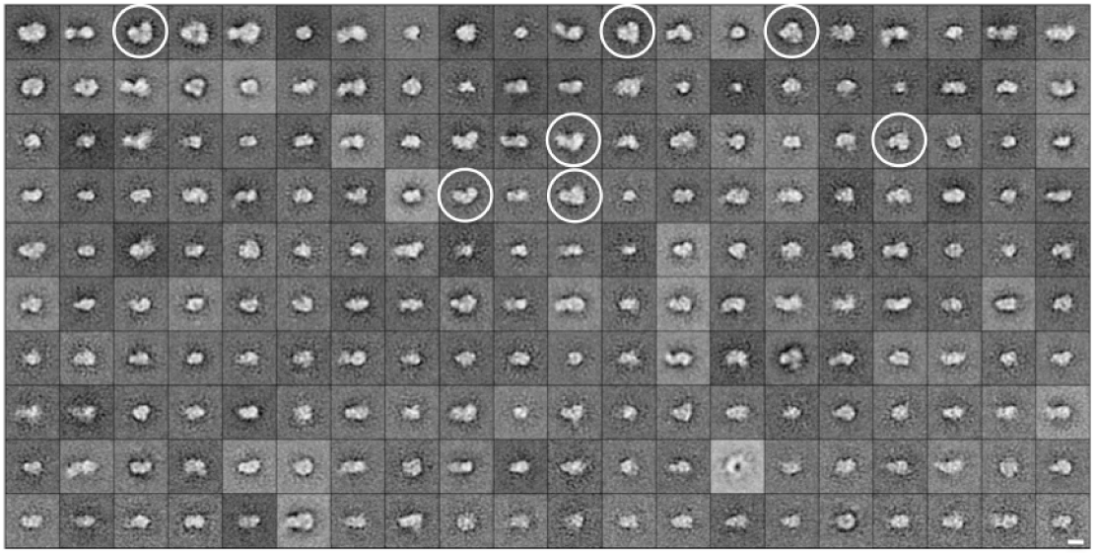

Figure 3.23: Single particle analysis of the Vps16-Vps33 subcomplex. Single particles were picked from low dose mode pictures at high resolution, aligned and sorted into classes. Class averages by S. Raunser, MPI, Dortmund, Germany. Scale bar: 20nm.

Class averages of the Vps16-Vps33 subcomplex is shown in Figure 3.23. Compared to the HOPS classes, the class averages differed much more. Nevertheless, some comparable structures were discernable, which are encircled. Vps16-Vps33 appeared as a „V-shaped“ structure and thus likely represents one end of the HOPS complex, which was not resolved in the class averages of the holo complex before.

3.2.3.1 HOPS subunit localization within the complex

At this point, both the subcomplexes of HOPS and the holo HOPS complex itself appeared to be flexible and partially unstructured under the electron microscope. An alternative approach to localize single subunits within the complex and in addition to stabilize it, was the analysis of carboxy-terminally GFP-tagged HOPS samples (see 3.1.6). Since these exhibited a reduced activity that might result from reduced flexibility, they might be stabilized by the tag and thus might orientate less randomly. Therefore, HOPS with GFP-tags at different subunits was applied to glycerol gradient centrifugation with simultaneous cross-linking, according to the GraFix protocol (Kastner et al., 2008) and afterwards analyzed by electron microscopy. After single particle analysis and class averaging the GFP-tag even might be directly visible. It therefore might be possible to localize each subunit within the complex. Figure 3.24 shows the cross-linked gradient fractions of all HOPS mutants with single GFP-tags

at one subunit. The upper parts show Coomassie stained SDS-PAGE gels loaded with fractions from the glycerol gradient centrifugation without cross-linking. Distinct peak fractions in the gradient were obtained for each GFP-tagged HOPS as observed before for the wild-type complex. After cross-linking according to the GraFix protocol (Kastner et al., 2008), no protein bands were visualized in the SDS-PAGE gel thus indicating a successful cross-linking.

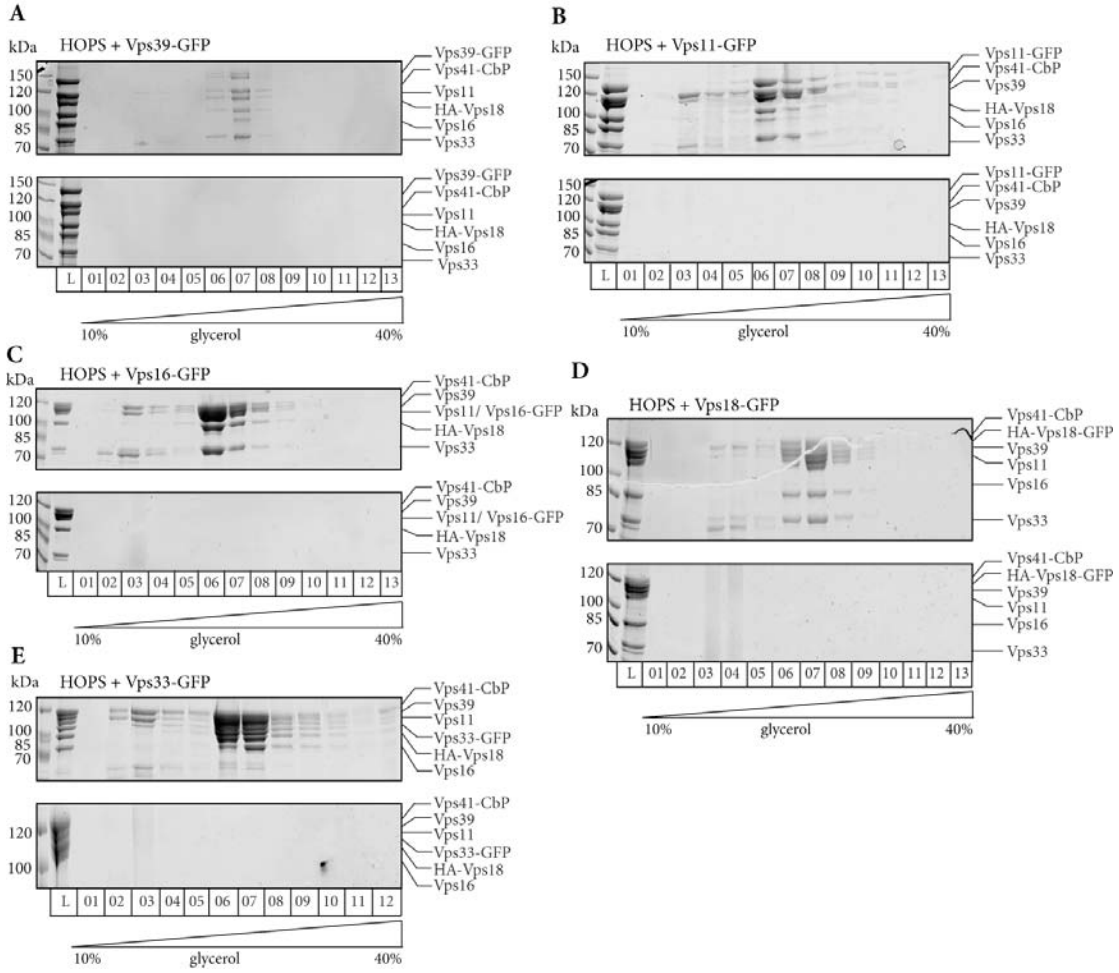

Figure 3.24: Glycerol gradient centrifugation after cross-linking of HOPS with GFP-tags. HOPS with an additional GFP-tag at one subunit was purified via TAP purification and applied onto a glycerol gradient centrifugation without (upper parts) and with (lower parts) glutaraldehyde. Fractions were loaded on SDS-PAGE gels and stained with Coomassie.

The peak of stoichiometric HOPS mutants appeared in fractions 6 and 7, consistent with their equal molecular mass. This also indicated, as mentioned before, that the GFP-tag did not influence the assembly of the HOPS complex. All peak fractions from glycerol gradient centrifugation with simultaneous cross-linking, according to the GraFix protocol (Kastner et al., 2008), were analyzed directly after negative staining with uranyl-formate under by electron microscopy.

The structure of the HOPS complex was partially influenced by the GFP-tag depending on the tagged subunit (Figure 3.25). None of the structures, however appeared to be more homogenous than the untagged HOPS. HOPS with Vps39-GFP behaved as the wild-type HOPS. The particles still seemed to be unstable and partially fragmented as observed before for wild-type complex, but some elongated structures also were observed. The same seemed true for HOPS with carboxy-terminally GFP-tagged Vps11 and Vps16. These structures resembled the elongated forms observed for HOPS but again did not favor one distinct conformation. Surprisingly, HOPS with GFP-tagged Vps18 did not exhibit an elongated structure; it rather was “curled-up”. In the image of HOPS with Vps33-GFP also some elongated particles comparable with wild-type were observed. Apparently, the GFP-tag influences both, the structure and function of HOPS, depending on its position.

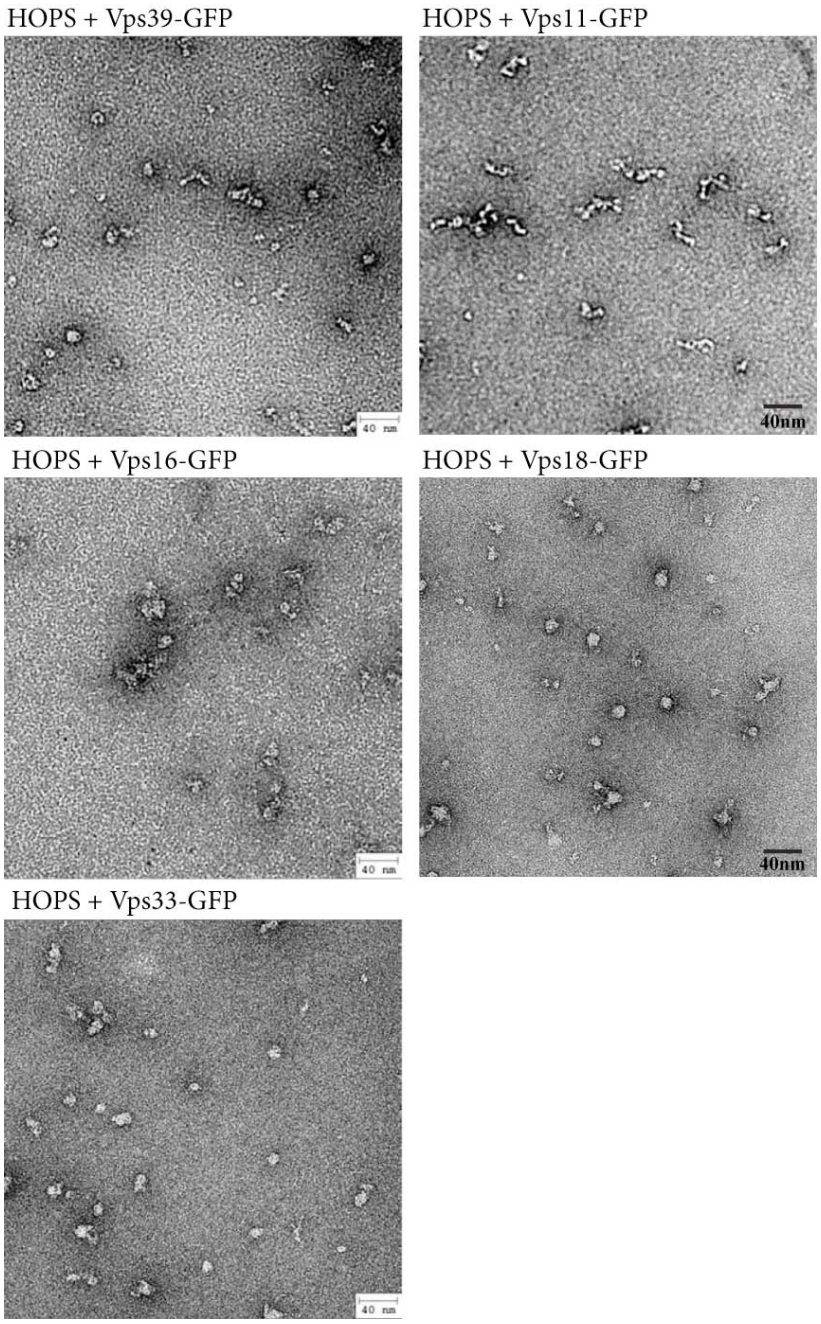

Figure 3.25: Electron microscopy of HOPS with carboxy-terminal GFP-tag. Peak fractions from glycerol gradient centrifugation with simultaneous cross-linking, according to the GraFix protocol (Kastner et al., 2008; Figure 3.24) were applied to copper grids, negative-stained with uranyl-formate and visualized with the electron microscope. Pictures by A.Schwedt, MPI, Dortmund, Germany. Scale bars as indicated.

These electron microscopy images of the HOPS complex provided a first insight into the structure. The complex appears as an elongated structure with two flexible ends. Unfortunately, the complex was still flexible under all conditions tested so far. Additional GFP-tags did not significantly improve the stability and rigidity of the complex. Possibly, one flexible part was partially resolved by analyzing the Vps16-Vps33 subcomplex.

3.2.4 Optimization of the HOPS purification

The electron images obtained so far gave an idea about an elongated dumb-bell like structure of the HOPS complex. The smaller fragments, which co-purified with the complex, might indicate that HOPS was partially disassembled. Therefore, an optimization screen for purification conditions, monitored by SDS-PAGE gel analysis was performed. Figure 3.26 shows all tested conditions varying in salt, detergent and pH. Arrows indicate the purification conditions used before. A SDS-PAGE gel analyzing the effect of increased NaCl concentrations in combination with different detergents is depicted (Figure 3.26A). In the presence of detergent the yield was generally increased, as expected. The complex was very inefficiently purified in 150mM NaCl buffer but seemed to be stable at higher salt concentrations (600mM NaCl buffer). Purification with Chaps at higher NaCl concentrations decreased the yield. To favor putative hydrophobic interactions, the salt concentration was further increased. Figure 3.26B shows that the purification in buffer with up to 1M NaCl was possible without disturbing the stoichiometry of the complex. pH of 8,5 only seemed to have minor effects. Detergent resulted again in an increased yield under all conditions, but did not interfere with complex stoichiometry. Since salt might play a critical role in the stability of the HOPS complex, different kinds of salts were tested (Figure 3.26C). The varying cations in the buffer did not affect HOPS purification; the complex again seemed to be stable in buffer with up to 1M salt. After further increasing the salt concentration to 1,5M in the buffer, the yield began to decrease (Figure 3.26D). This observation might be an indirect effect connected to the activity of the TEV protease or the binding of the complex to IgG beads.

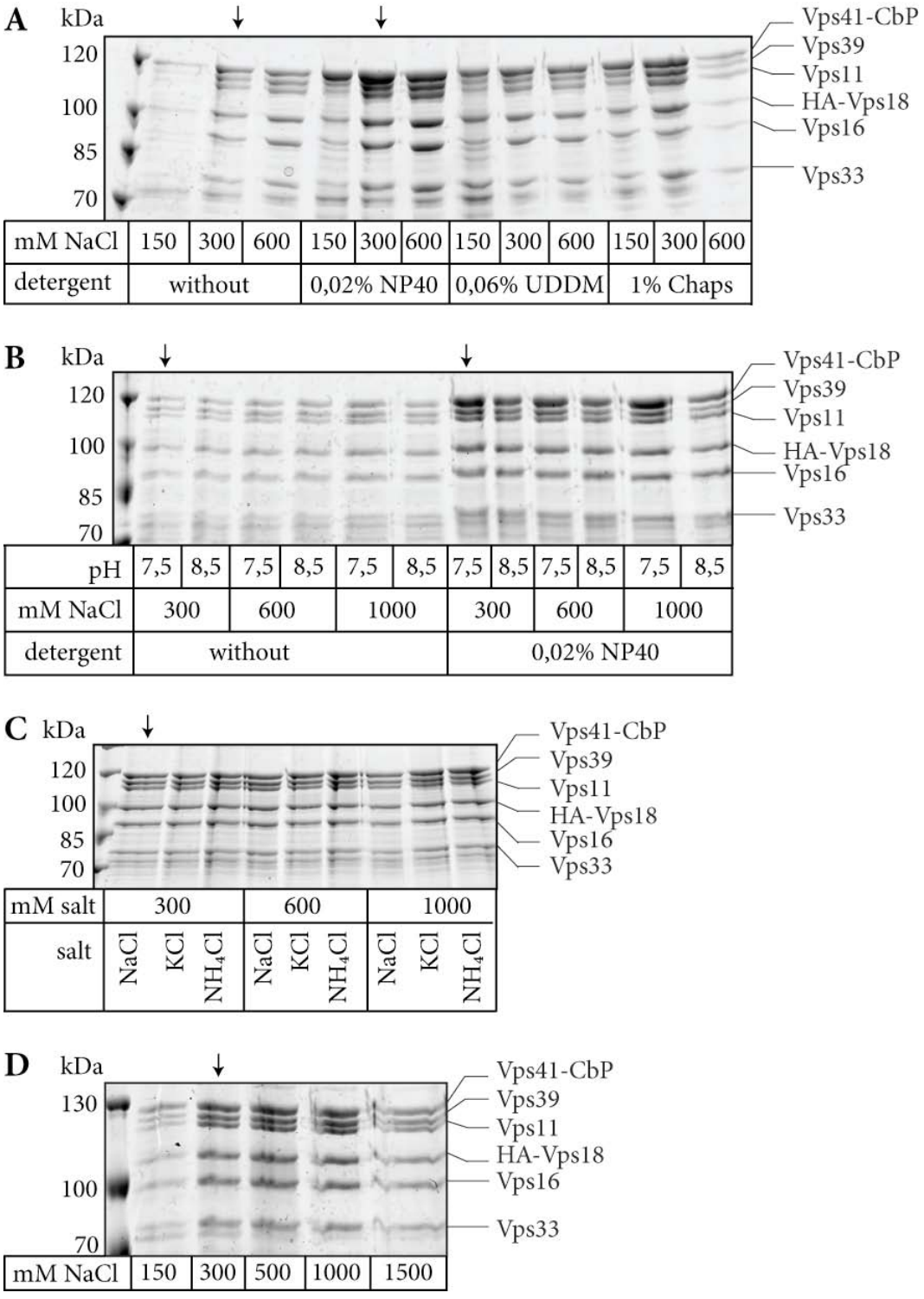

Figure 3.26: Optimization of HOPS purification conditions. A screen for optimization of HOPS purification with varying salts, detergents and pH was performed in a small-scale TAP purification. The yield of HOPS and its stoichiometry was confirmed on Coomassie-stained SDS-PAGE gels. A: HOPS was purified in buffer with varying NaCl concentrations and detergents (or without). B: HOPS purification in the presence or absence of 0,02% (v/v) NP40 in combination with different NaCl concentrations and two distinct pH-levels. C: Purification of HOPS in the presence of varying salts at three different concentrations. D: HOPS purification in higher NaCl buffers. Purifications in C, D were performed without detergent. The concentrations of the individual detergent referred to the double CMC (critical micellar concentration). Arrows indicated the "standard" conditions used so far.

The HOPS complex seemed to tolerate high salt concentrations, in accordance with hydrophobic interactions as predominant factors of intersubunit stabilization. The purity might increase, since electrostatic interactions are weakened. Still, the activity of the complex might be compromised during the purification in 1M salt buffer. Therefore activity tests were performed as described below.

3.2.5 HOPS activity analysis after glycerol gradient centrifugation

To confirm that the electron microscopically analyzed HOPS complex contained particles that are active in fusion, HOPS TEV-eluates purified in 1M NaCl and as a control under standard conditions (300mM NaCl) were applied to glycerol gradient centrifugation comparable to the GraFix protocol (Kastner et al., 2008). The cross-linker was omitted here, since no activity was expected from the cross-linked complex. Several of the harvested fractions were afterwards tested in the *vps11-1* fusion assay. In Figure 3.27B and D, aliquots of the glycerol gradient fractions loaded onto an SDS-PAGE gel are depicted. The peak fractions were clearly visible. Figure 3.27A and C shows that the HOPS-containing fractions harvested from the glycerol gradient were active in the *vps11-1* fusion assay and could rescue fusion of HOPS depleted vacuoles. The fusion activity correlated with the amount (µg) of HOPS (numbers above the error bars) in both preparations. Therefore, HOPS purified in 300mM salt buffer as well as HOPS purified in 1M salt buffer was active in fusion. In all preparations, the peak fractions of both purified HOPS centrifugations showed the highest fusion rate (Figure 3.27E). This indicates that the purified HOPS analyzed by electron microscopy was active and lead to a dumb-bell like structure. Unexpectedly, the HOPS purified in 0,3M salt buffer and 1M salt buffer differed in the peak fraction. This is probably due to the manual pouring device as observed before (Figure 3.21) and did not reflect a different behavior in the glycerol gradient centrifugation.

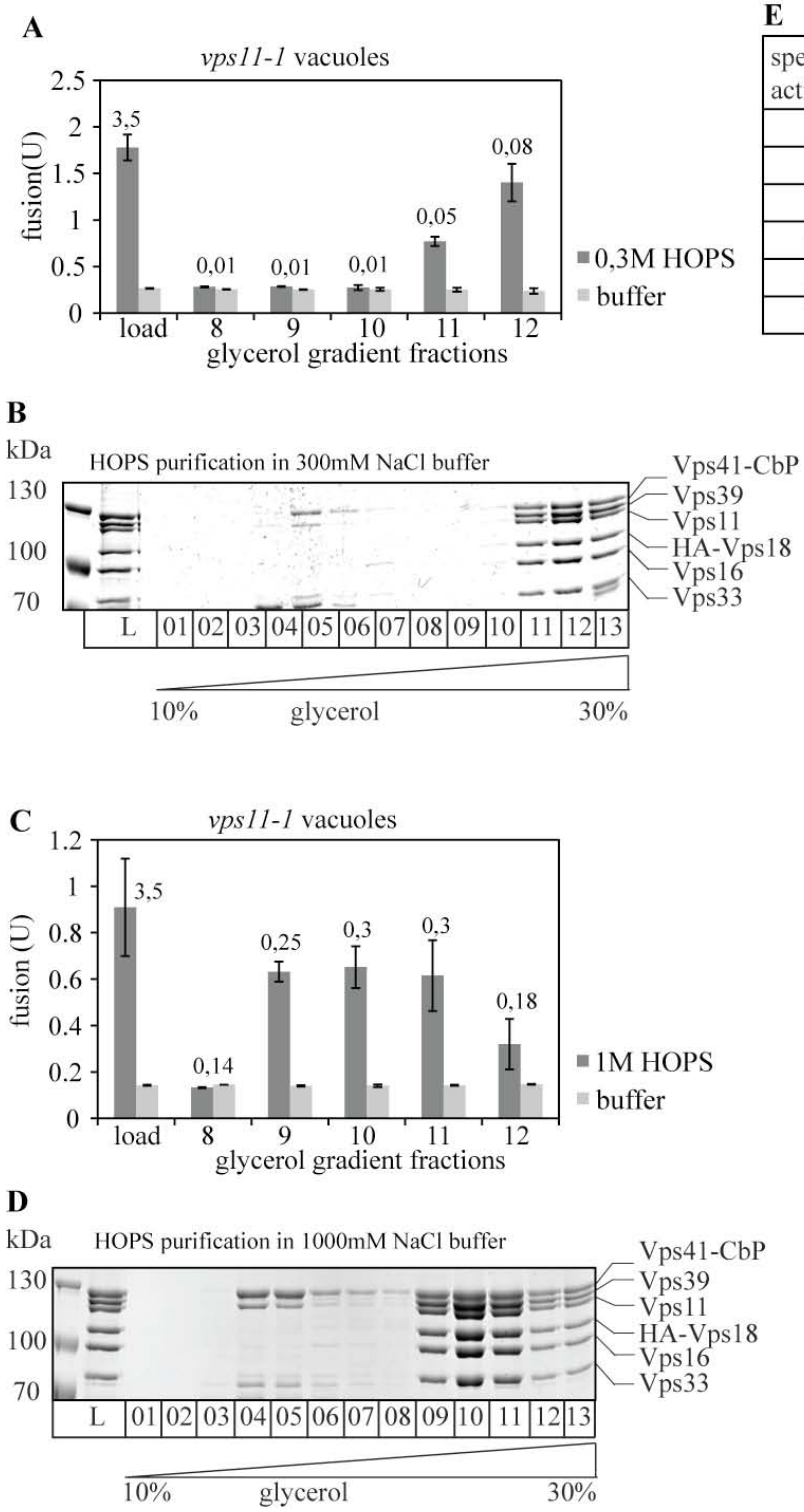

E

specific fusion activity (U/µg)	0,3M	1M
load	0,4	0,2
fraction 8	n.d.	n.d.
fraction 9	n.d.	2,0
fraction 10	n.d.	1,5
fraction 11	9,5	1,6
fraction 12	14,4	1,0

Figure 3.27: HOPS purified via glycerol gradient centrifugation and activity tests in 300mM or 1M NaCl buffer. A: Glycerol gradient fractions of HOPS purified in 300mM NaCl buffer were analyzed in *vps11-1* fusion assay. Numbers above the error bars indicate the calculated protein amount (µg) used in this fusion assay. B: The SDS-PAGE gel loaded with HOPS purified in 300mM NaCl buffer from glycerol gradient fractions was stained with Coomassie. C: Glycerol gradient fractions of HOPS purified in 1M NaCl buffer was analyzed in *vps11-1* fusion assay. Numbers above the error bars indicated the calculated protein amount (µg) used in this fusion assay. D: The SDS-PAGE gel loaded with HOPS purified in 1M NaCl buffer from glycerol gradient fractions was stained with Coomassie. E: calculated specific fusion activity of different fractions (in fusion (U)/µg HOPS), n.d.: not determined.

The protein concentration correlated with fusion activity (Figure 3.27A, C, E). Obviously, the complex was more pure after the glycerol gradient centrifugation. Therefore, the fractions with lower protein concentration, compared to the load, could rescue the fusion to almost the same extent, indicating an enrichment of active HOPS in these fractions. The specfic fusion activity was increased compared with the load (Figure 3.27E). Probably also during this purification, many smaller fragments of the HOPS were co-purified as observed for the cross-linked particles under the electron microscope. This debris, mainly present in the load, is likely not active in fusion and might even act as an inhibitor resulting in a low specific fusion rate. The HOPS purified in 1M NaCl buffer showed a lower activity compared with HOPS purified in 300mM NaCl buffer, probably because high salt concentrations were hindering the fusion. Nevertheless, under both purification conditions the increase in specific activity correlated with the increase in purity (Figure 3.27E). To examine the effect of purification in 1M NaCl buffer on the HOPS structure, electron microscopy after glycerol gradient centrifugation with cross-linking was performed.

3.2.6 HOPS electron microscopy with optimized purification conditions

HOPS is stoichiometrically stable and active in fusion in 1M NaCl buffer. To investigate the effects of these optimized conditions upon electron microscopy, purified HOPS TEV-eluate in 1M salt was applied to glycerol gradient centrifugation with simultaneous cross-linking, according to the GraFix protocol (Kastner et al., 2008). The cross-linked fractions were analyzed by electron microscopy. In Figure 3.28A, the reference glycerol gradient of purified HOPS without cross-linking is depicted. A distinct peak in fractions 8 and 9 was observed and the ratio of subunits in the holo complex was stoichiometric. These fractions were then subjected to electron microscopy. Figure 3.28B (upper image) shows an overview over the negative-stained sample. Clear and distinct structures are visible. Smaller fragments, as before, were not observed. The circle and rectangle indicate magnified structures visualized in the bottom part. An elongated dumb-bell like shape is clearly visible. Many particles resembled each other in size and shape.

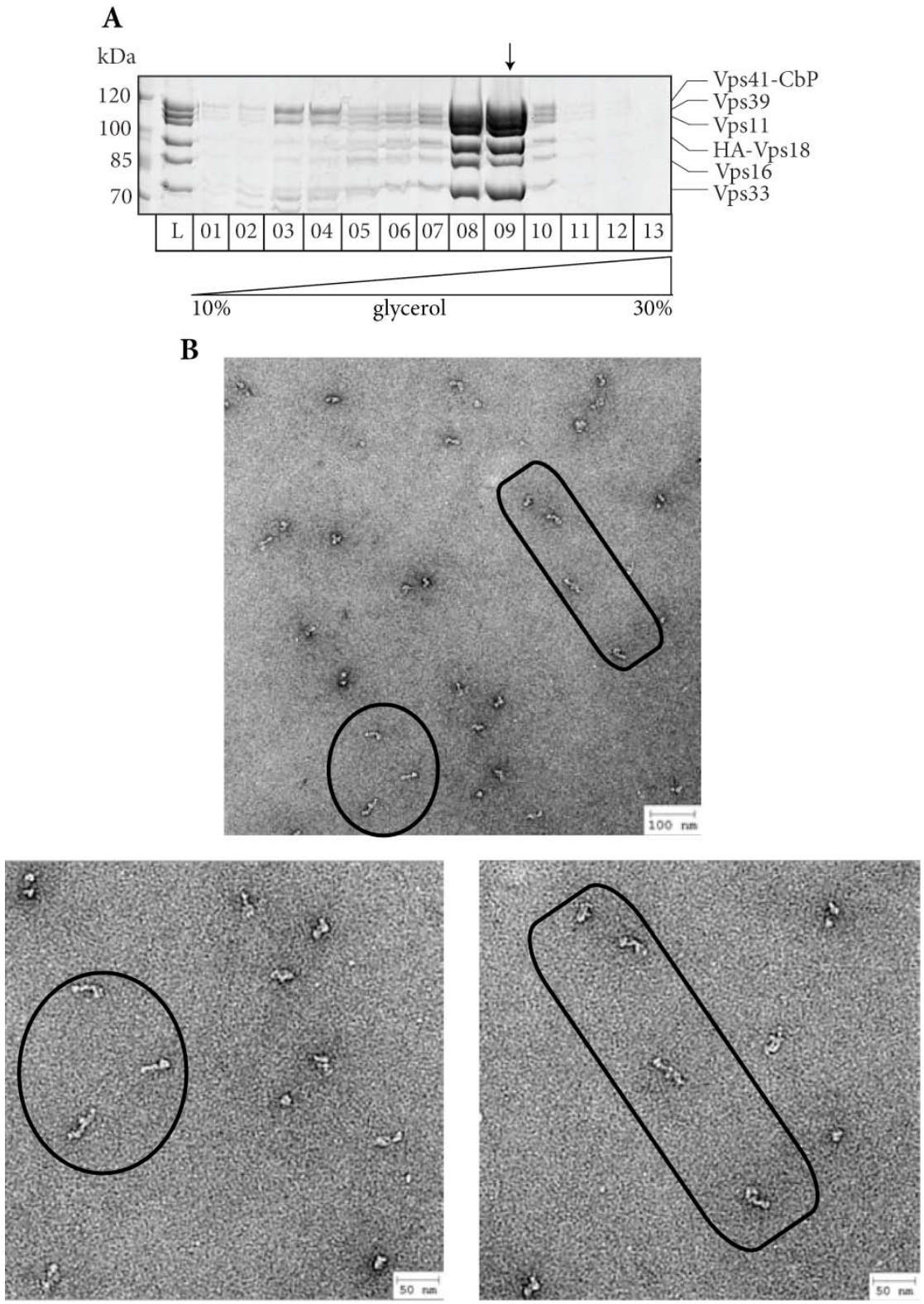

Figure 3.28: Purification and electron microscopy of HOPS in 1M NaCl buffer after glycerol gradient centrifugation with simultaneous cross-linking. A: The SDS-PAGE gel loaded with reference gradient fractions of HOPS without cross-linker was stained with Coomassie. B: negative-stained HOPS from fraction 9 of a cross-linked glycerol gradient centrifugation. The top picture gives an overview of a representative part of the grid. The circle and rectangle indicate the magnified parts in the bottom pictures. Pictures by A. Schwedt, MPI, Dortmund, Germany. Scale bars as indicated.

The protocol with optimized purification condition in combination with cross-linking treatment worked reproducibly and was further optimized to increase the total amount of single particles on the grid. Interestingly, the increase of particles did not directly correlate with an increase in protein concentration applied to the glycerol gradient. This was probably due to the fact that a portion of the holo complex was already disassembled when applied to the gradient or fragmented during centrifugation. Smaller but longer centrifugation tubes were used to optimize the length-to-width ratio and to enrich the complex in a distinct fraction.

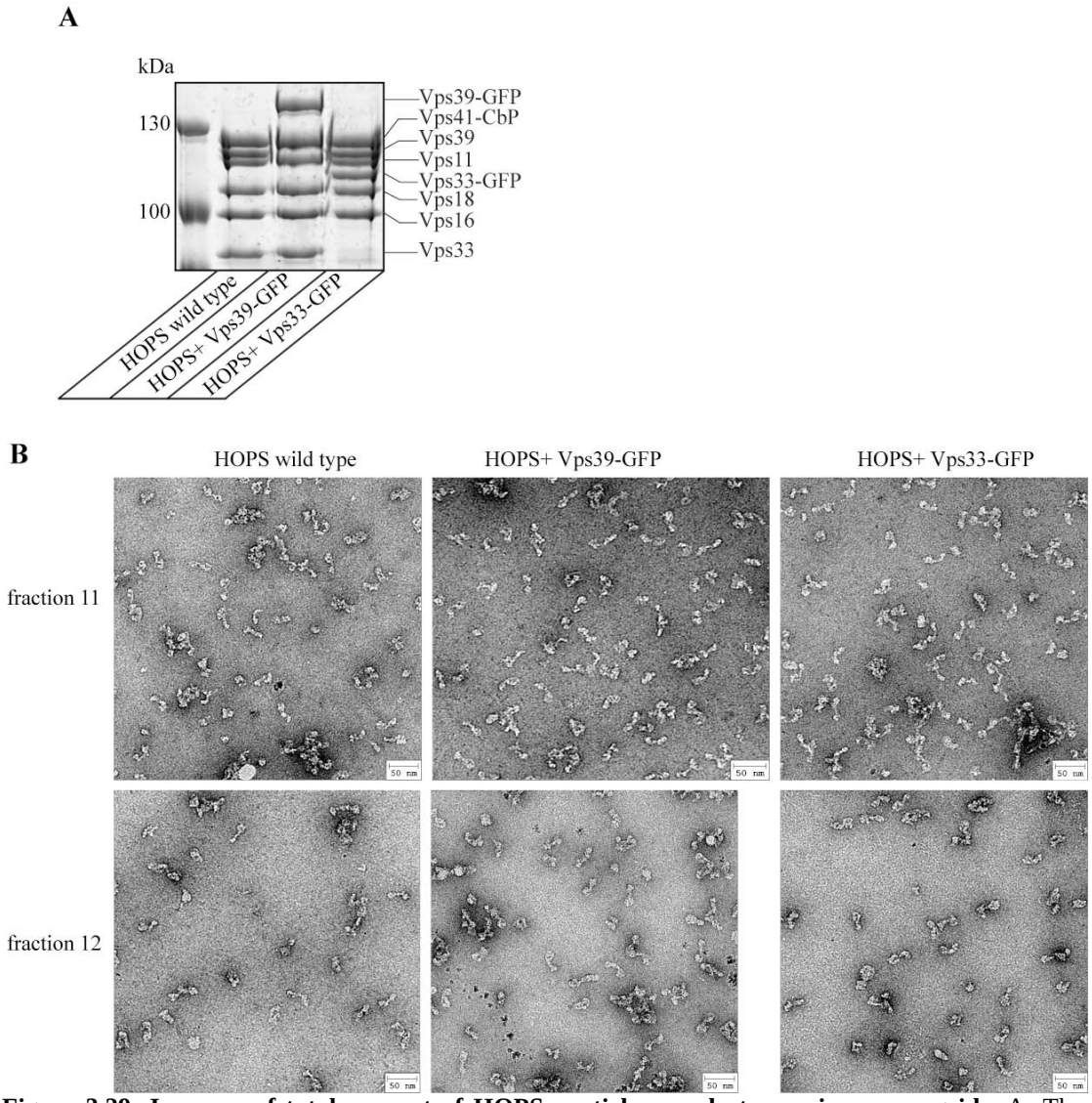

Figure 3.29: Increase of total amount of HOPS particles on electron microscopy grids. A: The SDS-PAGE gel loaded with TEV-eluates of wild-type HOPS, HOPS+ Vps39-GFP and HOPS+ Vps33-GFP was stained with Coomassie. B: Negative-stained images of wild-type HOPS, HOPS with Vps39-GFP and HOPS with Vps33-GFP from fractions 11 and 12. Pictures by A. Schwedt, MPI, Dortmund, Germany.

Figure 3.29A shows the Coomassie stained SDS-PAGE gel analysis of three HOPS purifications (wild-type, HOPS with Vps39-GFP and with Vps33-GFP) before

loading the eluates into glycerol gradient centrifugation with simultaneous cross-linking, according to the GraFix protocol (Kastner et al., 2008). The purified complexes showed the desired 1:1:1:1:1:1 stoichiometry. SDS-PAGE gels loaded with cross-linked fractions are not shown. Fractions 11 and 12 of each HOPS mutant were then further analyzed by electron microscopy, and showed an enrichment of single particles (Figure 3.29B in comparison to Figure 3.28). These particles aggregated not at all or just very rarely, but contained comparable shapes and sizes. HOPS with Vps39-GFP appeared slightly more stable as compared with wild-type HOPS and HOPS with Vps33-GFP. These two mutants seemed to be comparable stable. As a common theme, elongated dumb-bell like shapes are visible throughout. Theses particles were analyzed in more detail. To this end, more grids were generated and 500 images were taken per HOPS mutant. Afterwards, single particles were picked for class averages and two-dimensional reconstitution. Also tomographic analysis of HOPS was performed to derive a three-dimensional picture of the particles.

3.2.7 Single particle analysis of the HOPS complex

To gain more insight into the structure of HOPS, low dose mode pictures were taken at a magnification of 50.000x on negative films. For this, images of three independent purifications (each for wild-type HOPS, HOPS with Vps39-GFP and HOPS with Vps33-GFP) were developed. Since these pictures still contain some HOPS debris or aggregates, particles were manually selected for the alignment. A representative picture with wild-type HOPS is depicted (Figure 3.30A). The red boxes indicate picked particles, which were manually selected by size-exclusion. The common elongated shape once again was clearly visible. In Figure 3.30B some representative picked particles that were magnified and processed with a program called BOXER are shown (http://blake.bcm.tmc.edu/eman/eman1; Ludtke et al., 1999). A clear preference for the elongated dumb-bell like shape was observed. This dump-bell appeared in two different conformations. One structure seemed roughly rotation symmetric, whereas the other one contained one condensed lobe and one lobe, which seemed to loop-out, like a flexible arm.

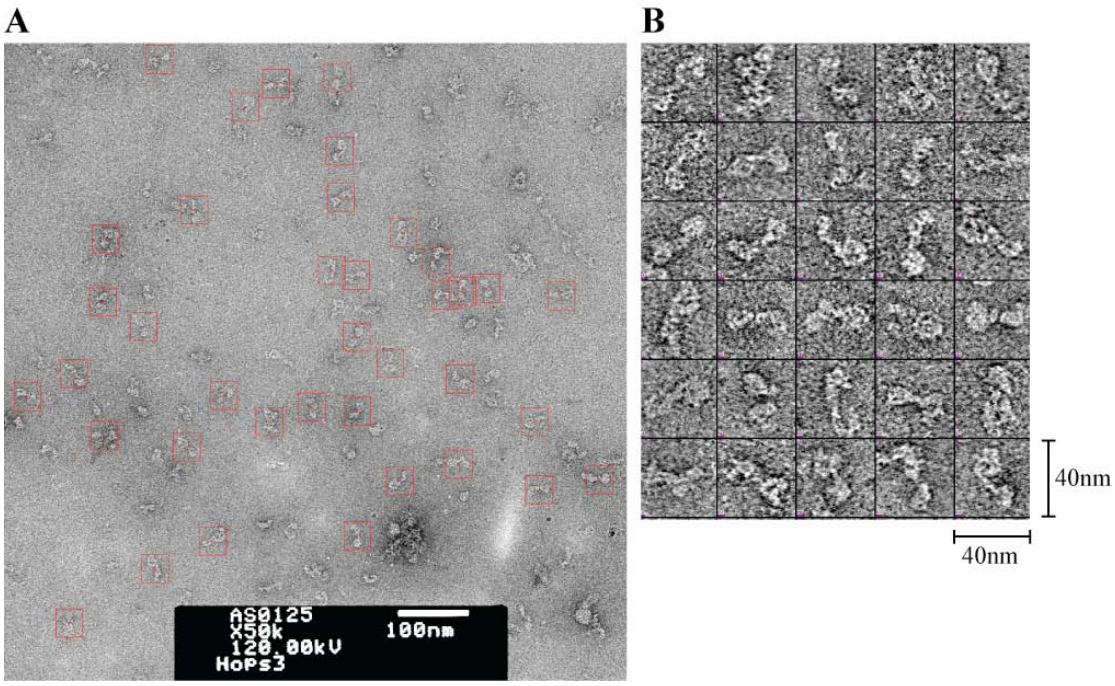

Figure 3.30: Single particle analysis of wild-type HOPS. A: A representative, low dose mode electron microscopy image of wild-type HOPS taken at 50000x magnification after negative staining with uranyl-formate. Red boxes indicate the picked particles. Image by A. Schwedt, MPI, Dortmund, Germany. B: Representative picked particles from A were magnified and processed by using a program called BOXER. Scale bars as indicated.

This analysis was performed in the same way also for HOPS-Vps39-GFP and for HOPS-Vps33-GFP (not shown). In all cases the results resembled those as for the wild-type HOPS. After alignment and class averaging the GFP-tag might become visible as dot-like structures. This might locate these two subunits inside the complex and give insights into the orientation and function of the HOPS complex. This analysis is currently still in progress.

3.2.7.1 Class averages and tomographic analysis of the HOPS complex

Alignments and class averages were performed for wild-type HOPS and HOPS with Vps39-GFP. It might then be possible to localize the GFP-tag within the complex by direct comparison with the wild-type structure. In Figure 3.31, class averages of approximately 25.000 particles from HOPS with Vps39-GFP are shown. The particles were aligned into 400 classes, of which 72 are depicted. The alignments were performed with a program called SPIDER (Frank et al., 1981; Frank et al., 1996; see also 6.4.2) in this way, to get classes with different particle orientations.

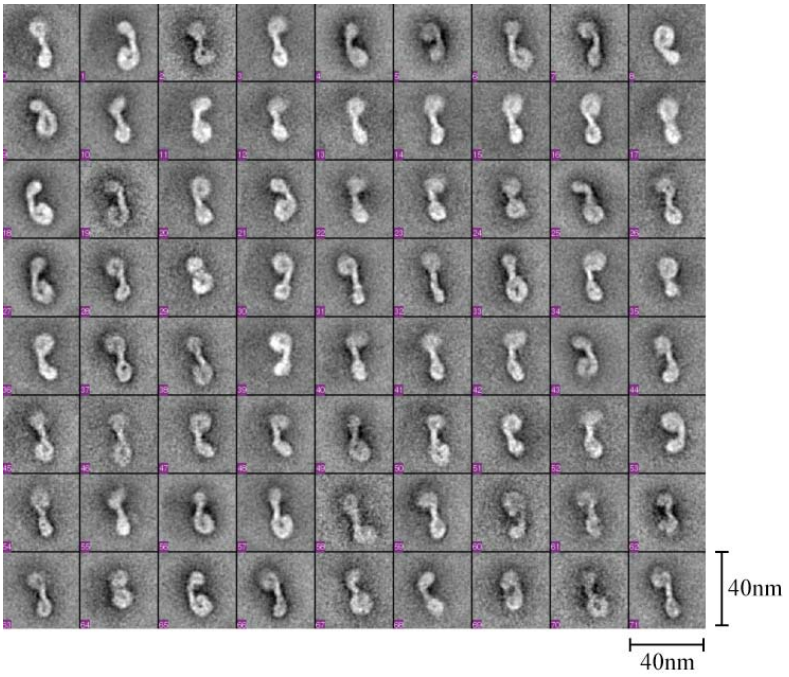

Figure 3.31: Class averages of 25.000 HOPS with Vps39-GFP particles. Class averaging was performed with a program called SPIDER. The particles were sorted into 400 classes. 72 classes are depicted. Class averages by A. Schwedt, MPI, Dortmund, Germany. Scale bar as indicated.

A dumb-bell like shape was obtained for all classes. Always one end of the complex appeared to be more flexible compared with the other one, because it was not completely resolvable. The same procedure was performed with wild-type HOPS (not shown). After optimizing the alignments procedures, they will be used to localize the GFP-tag in the structure and will be repeated with HOPS with GFP-tagged Vps33. Further analysis of the remaining GFP-tagged HOPS versions and subcomplexes are planned. This work is still in progress.

To further analyze single particles, three-dimensional images were generated. For this, the grid with negative-stained HOPS with Vps39-GFP particles was tilted stepwise in the microscope and images were taken at different angles. The resulting images of one selected particle were then assembled into a three-dimensional structure (Figure 3.32A). Figure 3.32B shows an overlay of two HOPS with GFP-tagged Vps39. One lobe of the complexes is nicely overlapping, whereas the other lopes are not co-localized at all.

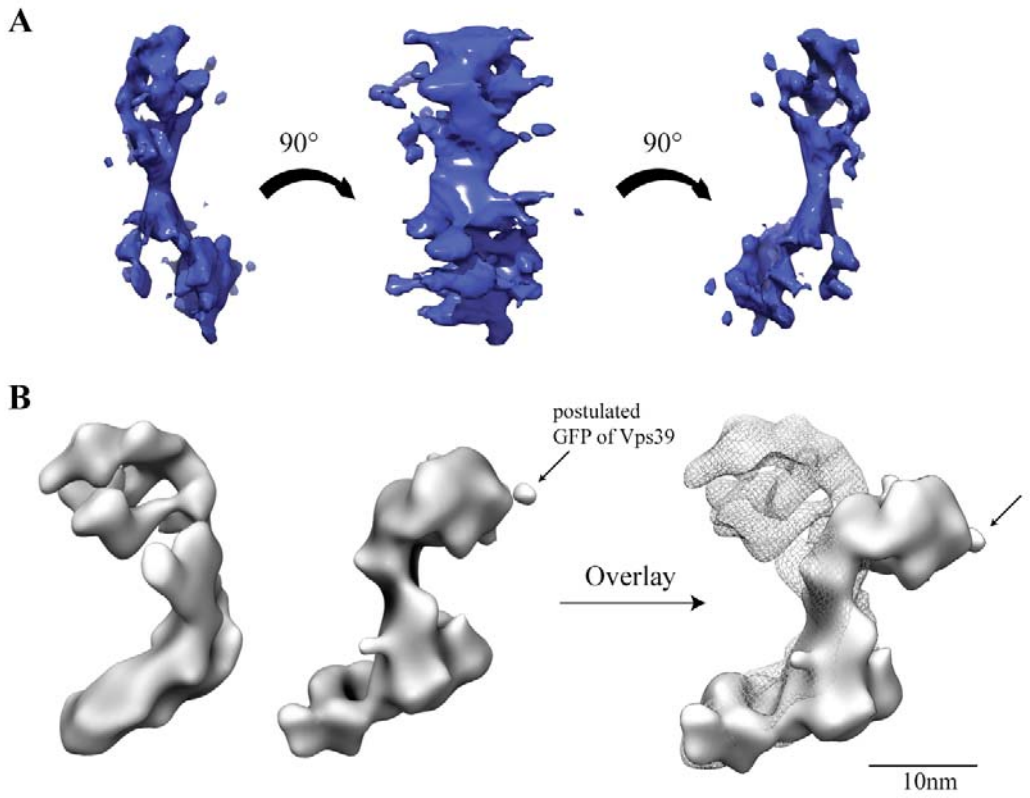

Figure 3.32: Three-dimensional structure of HOPS with Vps39-GFP. A: Tomographic analysis of one representative particle via negative-stain electron microscopy in three different orientations. A dumb-bell like shape is visible. B: Tomographs of two particles were overlaid. The postulated GFP-tag of Vps39 is indicated by the arrows. Images by A. Schwedt, MPI, Dortmund, Germany. Scale bar as indicated.

The overlapping parts might represent the static portion of the complex with a flexible hinge region in its center. The second lobe, which was not overlapping, might be the flexible arm of the complex.

In general, HOPS appears as a dumb-bell like structure, with roughly rotation symmetry. One lope appears static, whereas the other one seems to adopt multiple orientations. Both lobes might be connected by a flexible hinge region. White spaces represent highly flexible regions, which were not resolvable (Figure 3.32).

4. Discussion

4.1 Role of HOPS in fusion

The HOPS complex is the sole multisubunit tethering factor, whose tethering activity was directly shown *in vivo* and *in vitro* (Cabrera 2009; Stroupe et al., 2009; Hickey et al., 2010). Using the „semi *in vitro*" fusion assay with isolated vacuoles, HOPS activity could be directly linked to tethering and fusion activity (Stroupe et al. 2006). For this purpose, Stroupe et al. isolated HOPS from vacuoles with Vps33 as bait protein. In this study, a different approach was applied. Here, HOPS was purified directly from cell lysate of a yeast overexpression strain (Ostrowicz et al., 2010). The HOPS specific subunit Vps41 was used as a bait, because Vps33 is also part of the CORVET complex and might therefore lead to a mixed population of HOPS and CORVET. To confirm that the purified complex forms a hexamer of 630kDa with expected 1:1:1:1:1:1 ratio of the subunits, size exclusion chromatography was performed (Figure 3.1). Since the HOPS containing fraction corresponded to a molecular mass of approximately 700kDa, estimated by calibrating proteins, a dimeric complex was excluded. The purified HOPS TEV-eluate was then subjected to functional as well as structural analyses. When added to isolated *vps11-1* vacuoles, purified HOPS from the overexpression strain was active, indicated by an increased fusion rate (Figure 3.3). The *vps11-1* vacuole tester strains, used for HOPS activity tests, were identified in a random mutagenic screen for defects in the late CPY and AP-3 pathway (Peterson and Emr, 2001). The mutations in Vps11 responsible for the observed phenotype are found at its very carboxy-terminal RING domain. These mutations caused HOPS to disassemble at the non-permissive temperature; consequently the precursors of CPY (p2CPY) and Pho8 are accumulated in vesicles in the cell. The vacuoles of such cells are unable to fuse, since they are lacking one of the three crucial factors required for fusion. They still contain the Rab GTPase and the vacuolar SNAREs that are additionally required for fusion. In order to finalize fusion after tethering, theses SNAREs need to be activated in an ATP-dependent manner. This activation, mediated by Sec18 (NSF), is supported by Sec17 (α-SNAP). During activation Vam7 is released and able to associate with SNAREs of the opposing membrane to form a *trans*-SNARE complex (Boeddinghaus et al., 2002). Importantly, additional Vam7 can bypass the SNARE-activation or further support the formation

of fusion-active-*trans* complexes, if added to isolated vacuoles (Thorngren et al., 2004). This finding was also corroborated here and hence all *vps11-1* fusion assays were performed in the presence of 80nM recombinant Vam7.

HOPS is involved at the very organelle where multiple trafficking pathways converge, since MVBs, AP-3-vesicles, autophagosomes and also homotypic vacuole fusion require HOPS tethering activity (Radisky et al., 1997; Nakamura et al., 1997). Even though some of these vesicles could have been co-purified during vacuole isolation and in principal are capable to fuse with the vacuole, mainly homotypic vacuole fusion is measured. Therefore, probably not all facets of HOPS-mediated tethering were relevant for this assay. This rather would require further „full *in vitro*" assays or yet more modifications of the present fusion assay. With proteoliposomes loaded with SNAREs and Rabs, tethering and fusion has been investigated in a fully artificial system (Stroupe et al., 2009; Hickey et al., 2010). It was shown in theses studies that HOPS-dependent tethering precedes SNARE complex formation and requires GTP-loaded Ypt7. For the clustering of proteoliposomes three assembled Q-SNAREs are sufficient (Stroupe et al., 2009, Hickey at al., 2010). With this approach, the fusion of proteoliposomes could only be induced without HOPS, when SNAREs were present in excess on both membranes and random collisions of the liposomes might then be exploited by the SNAREs (Mima et al., 2008). In the presented work, I reproduced the finding that HOPS is indispensable for fusion at the vacuole. The complex was purified in an active form and in stoichiometric ratios of its subunits as one entity from an overexpression strain (Figures 3.1 and 3.3).

4.1.1 Assembly and disassembly of HOPS from and into subcomplexes

The HOPS complex consists of six subunits (Vps41-Vps39-Vps11-Vps18-Vps16-Vps33) in a 1:1:1:1:1:1 ratio and shares four of them (Vps11-Vps18-Vps16-Vps33) with the CORVET complex. A switch from CORVET to HOPS via subunit exchange would seem possible (Peplowska et al., 2007). The „Class C core" proteins (Vps11-Vps18-Vps16-Vps33) thus might serve as an assembly platform, even though they were never purified as a tetrameric complex (Figure 3.4). Vps11 binds via its carboxy-terminal region to both Vps3 (CORVET) and Vps39 (HOPS) and upon overproduction of Vps3 Vps39 is replaced by Vps3 from the complex. This points towards a competition at the Vps11 binding site (Plemel et al., 2011; Ostrowicz et al., 2010; Peplowska et al., 2007). An intermediate between HOPS and CORVET

consisting of the „Class C core“ proteins along with Vps3 and Vps41 indeed was observed (Peplowska et al., 2010) and isolated from an overexpression strain. It had fusion activity; albeit at lower extend than HOPS (Ostrowicz, et al., 2010; Figure 3.9). Whether this intermediate complex did not just results from experimental conditions, but rather represented a short-lived physiological meaningful entity, remains an open question.

Alternatively, the entire complexes exchange during endosomal maturation and along with Rab exchange. Then, they should assemble as independent complexes in the cytosol followed by recruitment to the membrane. Cytosolic assembly and subsequent recruitment to the membrane was also observed for the ESCRT-0, ESCRT-I and ESCRT-II complexes. They shuttle between membrane and cytoplasm as holo complexes (Teis et al., 2008; Wollert, et al., 2009). A third possibility would be an independent assembly of CORVET and HOPS right at the membrane.

However, several HOPS subcomplexes identified in single deletion screens, were somewhat in support of subunit interchange (Ostrowicz et al., 2010). The *in vivo* function of theses subcomplexes remains unclear, since they have no activity so far. However, the Vps16-Vps33 subcomplex together with Vps41-Vps39-Vps11-Vps18 subcomplex could be reconstituted “semi *in vitro”* into fusion-active HOPS with up to 35% of wild-type activity (Figure 3.6). This combination does not necessarily reflect the *in vivo* assembly path of HOPS. Membrane constituents or other cytosolic proteins that support assembly might be bypassed under these conditions. E.g., the two subcomplexes might assemble before binding to the vacuolar membrane or just in its presence. The failure of other available subcomplexes (Vps39-Vps11 and Vps39-Vps11-Vps18) to assemble into functional HOPS points to an elaborate mechanism, perhaps involving more factors than currently known. Alternatively, some of the subcomplexes could represent a “dead end” in assembly, either due to conformational flexibility (in accordance with the structural data; see below) or caused by a wrong order of subunits/ subcomplexes subjection in the assembly reaction. The lack of proper chaperoning could be one important issue in the assembly. The *in vivo* assembly of the entire HOPS might begin much earlier at the late endosome, and constitutively involve the proper (membrane) environment. Here, the Rab GTPase Ypt7 might be involved in HOPS assembly, which localizes to late endosomes as well as to the vacuolar membrane (Balderhaar et al., 2010). A recently published paper suggests a direct interaction between Vps39 and Vps41, which builds a Rab binding

matrix for Ypt7 (Plemel et al., 2011). This might be an initializer for the HOPS assembly, even though this dimeric was never observed within my purifications. Further more the Vps39-Vps11-Vps18-Vps41 subcomplex contained substoichiometric amounts of Vps41 (Figures 3.4 and 3.6).

Obviously, a concomitant assembly of six subunits is more than unlikely, thus calling for a consecutive order. One approach to tackle this question would be reconstitution from six single, pure, soluble and monodisperse HOPS subunits. These are however not entirely available to date.

4.1.2 The intermediate complex (i-CORVET)

The identified i-CORVET could represent a true intermediate between CORVET and HOPS during endosomal maturation (Peplowska et al., 2007). Upon overexpression of CORVET's Vps3, the HOPS- specific subunit Vps39 is replaced by Vps3, resulting in i-CORVET. This complex resembles HOPS in Rab binding specificity and fusion activity (Figures 3.9 and 3.10). It might therefore function as a transitory complex during subunit exchange from CORVET to HOPS with low tethering activity. For CORVET, no tethering function was shown so far. Interestingly, the i-CORVET was inactive under all tested fusion conditions, except fusion of HOPS-depleted vacuoles (Figures 3.9, 3.10 and 3.12). In all other fusion assays, HOPS and its corresponding Rab were present on the vacuolar membrane and might have therefore taken over the tethering function. The supplemented i-CORVET would then have been kept away from membranes. The Rab binding specificity of HOPS and i-CORVET to Ypt7-GTP might result from the affinity of Vps41 towards Ypt7-GTP (Figure 3.7 and 3.8). The HOPS-specific subunit Vp39 looses its affinity in binding to Ypt7 without any nucleotide preference upon incorporation into HOPS. Here, the holo complex is just binding to GTPγS-loaded Ypt7 (Ostrowicz et al., 2010; Figure 3.7). The same scenario might apply to Vps3 in i-CORVET. The affinity for a nucleotide-loaded (or nucleotide-free) Rab of a single subunit might therefore differ from the nucleotide-loaded Rab affinity of the entire complex. Presently, a common feature of all multisubunit tethering complexes (except for Dsl1) is their ability to bind Rabs in their GTP form (Bröcker et al., 2010). The varying nucleotide-specificity of a single protein towards a Rab GTPase might result from functions separated from their role within the complex. The *in vivo* relevance of i-CORVET, despite its "HOPS traits" is not clear at this point. Since i-CORVET was initially identified under wild-type

conditions it certainly is not an overexpression artifact (Peplowska et al., 2007). Where the assembly of i-CORVET takes place and if it has *in vivo* functions needs to be elucidated. General optimization of tethering activity from CORVET via i-CORVET to HOPS might occur, accompanying the maturation of endosomes. Experimental restrictions still prevent a clear demonstration of tethering activity for CORVET (or its non-existence) at this stage.

4.1.3 Role of Vps39 in the HOPS complex

Endosomes mature by undergoing Rab exchange: The early endosomal Rab Vps21 is replaced by Ypt7 on late endosomes/ MVBs. In this context, a comparison with the Exocyst complex is revealing. Exocytic vesicles contain the Rab Ypt31/32, which is replaced by the Rab Sec4 for recruitment of the Exocyst tethering complex. During transport from TGN to plasma membrane Ypt32-GTP recruits the GEF for Sec4. This GEF (Sec2) then generates Sec4-GTP. Next, the effector subunit in the Exocyst (Sec15) is recruited (Ortiz et al., 2002; Mizuno-Yamasaki et al., 2010). Endosomal maturation might occur along similar lines. The Rab Vps21 is activated by its GEF Vps9, which might then recruit the next GEF for Ypt7, namely Mon1-Ccz1 (Hama et al., 1999; Nordmann et al., 2010). Ypt7-GTP then recruits the HOPS effector subunit Vps41 (Figure 1.7). The assignment of Vps39 as GEF for Ypt7 is untenable (Ostrowicz et al., 2010; Nordmann et al., 2010). The role of Vps39 therefore is open again. It is required as part of HOPS, since HOPS-depleted vacuoles only fuse in the presence of the entire HOPS. The place and functional part of Vps39 can be taken over in i-CORVET by Vps3 or the remaining HOPS subunits resulting in approximately 25% fusion rescue compared with HOPS (Figure 3.9). The function of Vps39 seems to differ for isolated or HOPS-incorporated Vps39. At least, the Rab binding specificity changed from nucleotide-unspecific binding for Ypt7 to GTP-loaded Ypt7, when incorporated into HOPS. Here, Vps39 might become inactive and incapable to bind Ypt7 from within the complex. Alternatively, the Ypt7 binding site might become occupied by Vps41, which abolishes Vps39 binding to Ypt7 from within the complex (Ostrowicz et al., 2010). A recently published study suggested a Rab-binding module consisting of Vps41 and Vps39, which are both binding to Ypt7 via their amino-terminal regions (Plemel et al., 2011). An interaction between Ypt7 and Vps39 might nevertheless be required for vacuole fusion. Vacuoles enriched for Ypt7 showed a reduced fusion rate per se, maybe because the endogenous HOPS

might be blocked by the surplus of Ypt7 on the same membrane and thereby inhibiting HOPS binding to Ypt7 on the opposing membrane. This could be compensated for by the addition of HOPS, but not by i-CORVET (Figure 3.10). The surplus of vacuolar resident Ypt7 might be bound less efficiently to i-CORVET and therefore fusion could not be restored. This further strengthens the model that HOPS binds to SNAREs on the vacuolar membrane and to Ypt7-GTP on the opposing membrane (e.g. MVB or another vacuole, Figures 1.3, 1.5 (1) and 4.1). Consistent with this, AP-3 vesicles are recognized by HOPS via their coat and are tethered to the vacuole by HOPS bound to vacuolar SNAREs (Figure 1.5 (2)).

However, this assay could not be performed the other way round. Vacuoles enriched for Vps39 are unable to fuse, even in the presence of added HOPS. Fusion becomes sterically blocked by mitochondria that are clustered to vacuoles (Figure 3.11). This phenomenon was initially observed by electron microscopy in cells overexpressing Vps39 (M.C, C.O. unpublished observations). A comparable clustering of organelles was also observed between ER and mitochondria. A protein complex called ERMES (**ER-m**itochondria **e**ncounter **s**tructure) composed of both ER and mitochondrial transmembrane proteins connect the two organelles (Kornmann and Walter, 2010). The physiological role is not clear, but might be linked to several regulatory effects, like lipid exchange, protein transport into mitochondria or Ca^{2+} signaling. Whether a comparable complex of Vps39 with mitochondrial proteins exists, needs to be elucidated. But at least the Vps39-induced clustering of mitochondria to the vacuole seems to be very stable. During isolation of Vps39-enriched vacuoles, mitochondria were co-purified (Figure 3.11). These vacuoles showed an accumulation of an outer mitochondrial protein (Tom40). The fusion of theses vacuoles connected to mitochondria is almost abolished and was not rescued by incubation with wild-type vacuoles. Obviously, the co-purified mitochondria blocked the fusion of vacuoles (Figure 3.11). Therefore, it is essential to find the mitochondrial interaction partner for theses contact sites. But these clustering during vacuole isolation did not further increase the understanding of the interaction between Ypt7 and Vps39.

If not the GEF for Ypt7, Vps39 might be a GDF, the factor that displaces Gdi and therefore allows membrane recruitment of Ypt7. However, vacuoles inhibited for fusion with Gdi or with the GAP protein showed a similar rescue when HOPS was added (Figure 3.12). A GDF function for Vps39 or the entire HOPS appears rather

unlikely. The inhibition of fusion in both cases might therefore result from a blocked Ypt7 by either Gdi or the GAP. This can be partially compensated for by HOPS in low concentrations but could not be further stimulated (Figure 3.12). It was shown that GEF and GDF activities might be combined within the same protein (Schöbel et al., 2009). Whether this also holds for Mon1-Ccz1 needs to be determined.

In general, the interaction between Vps39 and Ypt7 seems indispensable for tethering and fusion and might exhibit a regulatory role for GTPase activity. Ypt7 itself seems to have multiple interaction partners at the MVB that needs to be regulated. Its activation on late endosomes might be a critical step in coordination of retromer and ESCRT function (Rojas et al., 2008; Seaman et al., 2009; Balderhaar et al., 2010). Ypt7-GTP affects retromer functionality on the one hand, and is required for ESCRT down regulation on the other hand. The retromer is required for receptor recycling and thereby counteracting the ESCRT machinery. Here, transmembrane receptors are sorted into intralumenal vesicles (ILVs) for degradation. Ypt7-GTP binds to the cargo-recognition part of the retromer and also seems to be a regulator of the ESCRT machinery (Seaman et al., 2009; Balderhaar et al., 2010). The endosomal localization of Ypt7 might be induced by Vps39, which then favors HOPS assembly and fusion with the vacuole. Due to these multiple functions of Ypt7, an up-regulation might have pleiotropic effects at different organelles.

4.1.4 Structural determinations of the HOPS complex

The crystal structure of HOPS or any of its subunits are not yet known. Secondary structure predictions showed comparable folds for all HOPS and CORVET subunits, except for the Sec1/Munc18 homologue Vps33 (www.predictprotein.org; Figure 4.1). They are predicted to contain an amino-terminal β-propeller domain followed by a carboxy-terminal α-solenoid domain.

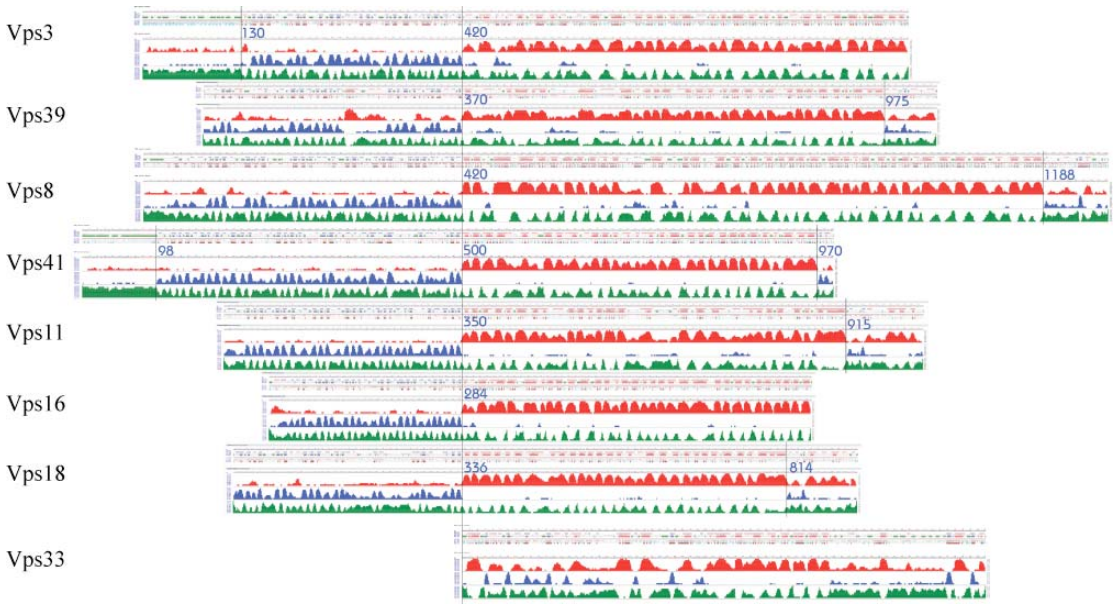

Figure 4.1 Secondary structure prediction of CORVET and HOPS proteins. The predictions are based on algorithms applied on the amino acid sequence of CORVET and HOPS proteins (www.predictprotein.org). Blue color indicates predicted β-sheets, red color indicates α-helices and green color unstructured regions. The number accounts for the respective amino acid. Image by S. Engelbrecht-Vandré (unpublished).

Due to their homology, it seems likely that the CORVET and HOPS proteins have similar folds. Amino-terminal β-propellers followed by α-solenoids were also observed in COPI and COPII coatomers as well as in proteins of the nuclear pore complexes. The authors suggested therefore a divergent evolution for coats and nuclear pore proteins, since both are required for membrane bending and stabilization (Devos et al., 2004). Whether HOPS and CORVET also fit into this group is not clear, but it seems likely, because five of the six complex proteins exhibit comparable structures (Bohawn et al., 2008, Plemel et al., 2011).

This still leaves many options for three-dimensional structures of the holo HOPS complex. Among the multisubunit tethering complexes acting along the secretory pathway (Dsl1, COG, GARP and the Exocyst) some structural similarities were recently identified. All four complexes are mainly composed of α-helices that are bundled into a compact fold, suggesting a similar function despite divergent evolution. They were therefore grouped in the so-called CATCHR (**c**omplexes **a**ssociated with **t**ethering **c**ontaining **h**elical **r**ods) family (Hughson et al., 2010). Indeed, the crystal structures of the GARP subunits Vps53 and Vps54 (Vasan et al., 2010; Perez-Victoria et al., 2010) resemble structures of subunits of the Dsl1 (Dsl1), COG (Cog4) and Exocyst (Sec6) (Richardson et al., 2009; Ren et al., 2009; Sivaram et al., 2006). Despite theses similarities among single subunits, the overall structure of

multisubunit tethering complexes might be much more diverse. Recent data for the TRAPPII complex, which is probably not a tethering factor but rather a multisubunit GEF, showed a diamond-shaped structure (Yip et al., 2010). An other multisubunit tethering complex, COG, appears as an elongated „Y“-shaped structure (Lees et al., 2010). This elongated flexible structure was also observed for another member of the CATCHR group, Dsl1. It seems to be composed of an elongated stable rod connected to a flexible arm (Tripathi et al., 2009; Ren et al, 2009). The HOPS structure also revealed an elongated flexible shape (Figures 3.30 and 3.31). Flexibility is nevertheless not unexpected for tethering complexes in view of their function (Figures 3.20 and 3.29). Both its flexibility and dynamic may account for the instability of the holo HOPS complex, resulting in a pronounced tendency for fragmentation. Even irreversible cross-linking did not completely stabilize the complex (Figure 3.29). GFP-tagging of single subunits only partially increased its stability (Figures 3.25 and 3.29). HOPS with Vps39-GFP appeared more stable, since more complete particles were observed per image (Figure 3.29). The GFP-tag might be visible as one dot-like structure with the flexible arm of the complex (Figure 3.32B). GFP-tagged Vps33 did not further stabilize the complex and the number of particles per image was comparable to untagged HOPS. Nevertheless, it might be possible to localize each subunit within the complex if the GFP-tags are detectable after class averaging (Figure 3.30 and 3.31). By tilting the grid inside the microscope, it is possible to analyze one single particle at different angles (Figure 3.32). This resulting three-dimensional model correlates with the structures observed after the class averages (Figures 3.31 and 3.32).

The flexible behavior was not just observed within the entire HOPS but also within the subcomplexes (Figure 3.21). Vps16-Vps33 turned out to be the most stable one, consistent with the current model of Vps33 stably binding to SNAREs (Dulubova et al., 2001). Vps16 might bind via its carboxy-terminal portion to Vps33 (Plemel et al., 2011). The Vps39-Vps11 subcomplex, which is probably interconnected via both carboxy-terminal regions, was completely fragmented, when analyzed by electron microscopy. It was partially stabilized by Vps18 that might interact with its carboxy-terminal region with the carboxy-terminal part of Vps11 and with the amino-terminal part of Vps39 (Plemel et al., 2011; Figure 3.21). This subcomplex might therefore be localized to the flexible arm of the dumb-bell, which

is connected by Vps18 with the other end of the dump-bell consisting of Vps16-Vps33 (Figure 3.32; Figure 4.2).

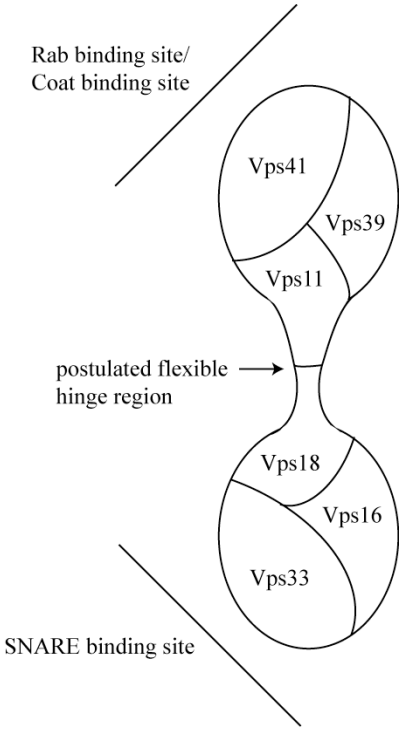

Figure 4.2: Two-dimensional model of subunit arrangement within the HOPS structure. One lobe of the complex might represent the Rab-binding site, the other one the SNARE-binding site.

It might be therefore possible that the flexible portion of the complex is required for Rab binding on the vesicular membrane, the more rigid one for SNARE binding on the vacuolar membrane (Figure 1.5 (1)). Vps41, Vps39 and Vps11 might therefore be localized to the flexible portion and Vps16, Vps33 and Vps18 to the rigid one (Figures 3.32 and 4.2). According to the two-dimensionality of the model in Figure 4.2 direct interactions, e.g. between Vps41 and Vps39, might occur, even though never observed *in vivo* (Ostrowicz et al., 2010). The direct interaction between Vp41 and Vps39, in contrast to the data presented here, was identified by Plemel et al. (2011).

The internal deletion of the Vps41 ALPS motif might influence the membrane association of the complex. This amphipathic helix was first discovered in the ArfGAP1 (GTPase-activating protein for Arf1; Bigay et al., 2003). It acts as a sensor for highly curved membranes. A comparable motif was also identified in Vps41. It inserts into highly curved membranes to anchor Vps41 to the MVB and also to hide the Apl5 binding site (Cabrera et al., 2010). The fusion of AP-3 vesicles with MVB is inhibited via this mechanism. Reaching the vacuole, HOPS can now also tether AP-3 vesicles by binding to the AP-3 coat on the one hand and to vacuolar SNAREs on the

other hand (Figure 1.5 (2)). Here, the Vps41 ALPS motif is now unable to insert into the low-curved vacuolar membrane and the casein kinase Yck3 gains access to the phosphorylation sites localized inside the ALPS motif. The Apl5 binding site is now accessible and can bind to AP-3 vesicles (Figure 1.8). The internal deletion of the ALPS motif partially affects the *in vivo* localization of HOPS (Cabrera et al., 2010) but did not disassemble the complex (Figure 3.15). The remaining amino-terminal portion of Vps41 therefore still binds to HOPS. The interaction between Ypt7 and Vps41 might not be sufficient to target Vps41 to the endosomal membrane (Cabrera et al., 2010). The ALPS deletion was thought to exhibit the following effect on HOPS: Vps41 membrane binding is weakened, and therefore the yield of HOPS purified without detergent might increase. This was not observed, however, probably because the membrane association of HOPS is generally not strong enough such that the ALPS deletion could not further weaken it (Figure 3.15). Unfortunately, also no difference in the electron microscopy images was observed (not shown).

4.1.5 Functional effects of mutations in the HOPS complex

The mutations generated within HOPS only partially stabilized the complex. Nevertheless, they influenced its activity. All GFP-tagged mutants showed a reduced fusion activity, with Vps33-GFP as the only exception. This reduction in activity was observed under all analyzed conditions, which suggest similar effects of the tag (Figures 3.16 and 3.17). Interestingly, the vacuole morphology and therefore the *in vivo* function of the different HOPS mutants appeared to be not dramatically impaired (Figure 3.13). In general, fusion of HOPS-depleted vacuoles was rescued with all GFP-tagged HOPS version, indicating a reduced but not totally abolished tethering function (Figure 3.16). The strongest influence on HOPS activity was observed with Vps39-GFP (approximately 50% fusion reduction). Here, the GFP-tag might hamper flexible regions within Vps39 required for fusion and therefore block HOPS functionality. This HOPS mutant might act comparably to i-CORVET, since both are lacking functional Vps39 in the complex (Figures 3.9 and 3.16). Both complexes showed no fusion activity towards wild-type vacuoles, pointing to an inactive or blocked Vps39 (Figure 3.12 and 3.17). By investigating HOPS with Vps39-GFP under the electron microscope, it appeared to be slightly more stable compared to the wild-type (Figure 3.29). An additional observation that fits to these findings is the high flexibility of the Vps39-Vps11 subcomplex (Figure 3.21). No distinct structures

were observed unless Vps18 was copurified. Alternatively, an increase in rigidity might be achieved by adding a GFP-tag to Vps39 within the Vps39-Vps11 subcomplex. In general, the additional GFP-tag so far decreases the fusion activity and might thereby also increase HOPS stability during tethering.

HOPS with an internal Vps41 ALPS deletion was also analyzed for activity. Surprisingly, this HOPS version was even more active as compared with the wild-type. This phenomenon was observed under all tested conditions (Figures 3.16 and 3.17). The ALPS deletion mimics the unphosphorylated version of Vps41, whereby Vps41 membrane interaction is weakened or partially compensated for by the interaction to Ypt7-GTP (Hickey et al., 2009; Cabrera et al., 2010). The Apl5 binding site within Vps41 might therefore be constantly available such that AP-3 vesicles can fuse with MVBs, which might already influence the Pho8 transport to the vacuole. This does not fully explain the increased fusion rate towards wild-type HOPS, but points towards the loss of one regulatory step (phosphorylation of Vps41 at the vacuole). Therefore, Vps41 and HOPS are immediately active for vesicle tethering. Maybe, the deleted APLS motif increases in addition the flexibility of the complex, which further facilitates tethering and fusion. Surprisingly, even though this HOPS mutant was more active in fusion assays, an increase in flexibility under the electron microscope was not observed.

4.1.6 Optimization of HOPS purification conditions

The various HOPS modifications differed in activity but not in stability as revealed by our structural analysis. Therefore, different purification conditions had to be screened. It turned out that HOPS tolerates high salt concentrations (Figure 3.26). Even though far from physiological concentrations, the holo HOPS was purified in 1M salt. The selected cation did not influence the HOPS stoichiometry, probably because high salt concentrations in general favor HOPS stability. Theses high salt concentrations strengthen hydrophobic interactions, which likely keep the complex together. Detergent is not obligatory for the purification, because HOPS is not directly anchored to membranes via transmembrane domains or lipid anchors, and the Vps41 ALPS motif is not sufficient to anchor HOPS to the membrane. The increased yield of HOPS that is purified in the presence of detergent results from membrane solubilization and therefore more efficient HOPS extraction.

With the described optimization of the purification procedure fewer fragments were observed under the electron microscope (Figure 3.28). It seems that HOPS is stabilized under this condition and single particles were therefore further analyzed (Figures 3.30, 3.31 and 3.32). The complex purified in 1M salt was still active in fusion, when subjected to isolated *vps11-1* vacuoles. The restoration of fusion was shown with the TEV-cleaved eluate and also with HOPS purified via glycerol gradient centrifugation (Figure 3.27). Here, the fusion activity correlates with the amount of HOPS applied to the reaction. HOPS analyzed with the electron microscope was treated the same way as HOPS used in the fusion assay, just the cross-linker was omitted because no fusion activity was to be expected (Figures 3.27 and 3.30).

4.2 The connection between shape and function of the HOPS

To analyze single HOPS particles they were computationally aligned. To this end, approximately 50.000 particles for each wild-type HOPS, HOPS with Vps39-GFP and HOPS with Vps33-GFP were manually selected after size exclusion and class averaging was performed (Figures 3.30 and 3.31). It seems that the HOPS complex appears as an elongated dumb-bell like structure with two different lobes at each end (Figure 3.32A). One of the lobes was always observed, whereas the other one appeared more flexible and seems to loop-out of the complex (Figures 3.30, 3.31, 3.32, B). This flexible portion might consist of Vps41, Vps39 and Vps11. A flexible hinge region might be located in the center of the complex between the two lobes. The total length is about 30nm; the width is 10nm for each of the two lobes. The hinge region between both lobes is very thin (approximately 2nm in diameter). The flexible portion, which is able to loop-out, might be slightly wider (Figure 3.32B). The more rigid portion of the complex might be composed of Vps16 and Vps33, connected via Vps18 to the flexible portion of Vps11, Vps39 and Vps41. The hinge region might be composed of the α-solenoid part of Vps18 or Vps11 (or both) since the diameter of a β-propellar is probably larger (3 to 4nm) (Figure 4.2). Comparable dimensions were observed for the COG (Lees et al., 2010) and for the Dsl1 complex (Ren et al., 2009). Here, flexible arms are probably required to catch the vesicles. The subunit Dsl1 together with Tip20 could loop out from the Dsl3/Sec39 root, comparable to the flexible HOPS arm.

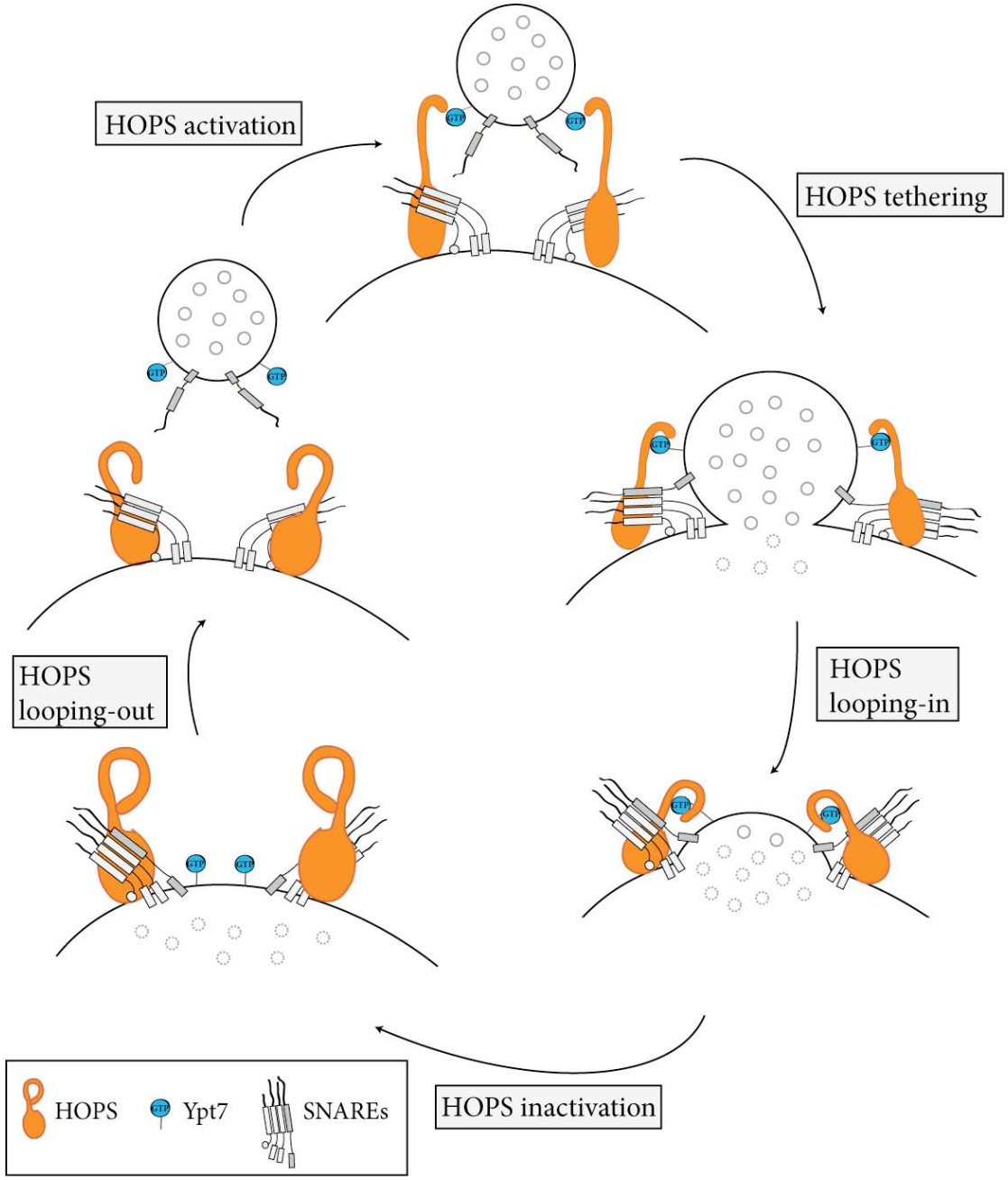

Figure 4.3: Model of HOPS-mediated tethering. The "inactive" HOPS localized to the vacuole via SNARE interaction. The flexible arm is looping-out to catch Ypt7-GTP on incoming vesicles ("active state"). For tethering, the flexible HOPS arm is looping-in again to bring the SNAREs in close proximity to drive *trans*-SNARE complex formation. During further inwards looping the vesicle is consumed and the cargo is released into the vacuolar lumen. The HOPS is then in the "inactive" state again and ready to loop-out for further activation.

Regarding the structure of the HOPS subcomplexes, one would position the Vps39-Vps11 subcomplex together with Vps41 to this flexible region. This portion might also be the interaction site for Ypt7 (Figure 4.2). A direct interaction between Vps41 and Ypt7 supported by Vps39 is therefore located to one end of the complex. A binding platform for Ypt7, composed of both β-propellars of Vps41 and Vps39 is also possible in this context (Plemel et al., 2011). The flexibility might be required to

capture incoming vesicles. Vps16-Vps33 subcomplex would be localized to the other lobe of the complex (Figure 4.2). This region seems to be more rigid and might be required for interaction with the vacuolar SNAREs. Vps33 is described as a direct interaction partner of the vacuolar SNARE Vam3 (Dulubova et al., 2001) and might therefore together with Vps16 exhibit a more rigid portion of the HOPS. Vps18 seems to connect the two lobes by interacting with the Vps11-Vps39 subcomplex together with Vps41 at one end and with Vps16-Vps33 subcomplex at the other one. It might therefore be localized to the center of the complex, whereby carboxy-terminal GFP-tagging leads to a "curled-up" structure, probably as a result of bending and the two lobes flip together (Figure 3.25). In general, the HOPS overall shape shows a dumb-bell like shape with two lobes dedicated to Rab binding at one portion and to SNARE binding at the other portion (Figure 3.32). One lobe seems to have the probability to loop-out and might therefore contain different orientations (Figure 3.32B).

I postulate the following model for HOPS-mediated tethering (Figure 4.3). The "inactive" complex is localized to the vacuolar membrane via interaction with the SNAREs, lipids and Ypt7 (Hichey et al., 2010). The flexible arm of HOPS, observed by electron microscopy (Figures 3.30, 3.31 and 3.32B), then starts to loop-out, whereby HOPS is "activated" as the flexible arm catches Ypt7-GTP on an incoming vesicle/ MVB. This binding leads to tethering by bridging Ypt7-GTP on one membrane and SNAREs on the other membrane (Figure 1.5 (1)). The following fusion is mediated by *trans*-SNARE complex formation and stabilized by HOPS (Hickey et al., 2010). Therefore, the flexible HOPS arm loops-in again to bring the SNAREs in close proximity. This looping-in further continues until the vesicle/ MVB is consumed at the vacuole and the cargo is released into the lumen. HOPS is afterwards in an "inactive" state and ready to loop-out to catch the next vesicle. Comparable tethering also seems to be possible for AP-3 vesicles. They are recognized by Vps41 and therefore tethered via the interaction between Vps41 and the AP-3 coat subunit Apl5 on the one hand and Vps33 and vacuolar SNAREs on the other hand to the vacuole (Figure 1.5 (2)).

It is possible that two different HOPS conformations exist: 1.) the "two-lobed conformation" as the "inactive" or closed one after fusion and 2.) the "one-lobe-one-arm-conformation" as an "active" or open conformation, which is ready to capture vesicles. The "inactive" state appears more condensed and more stable. This state might have been therefore more abundant in the preparation than the "active" state,

but this does not necessarily correspond to the *in vivo* situation. The partially stabilized HOPS with Vps39-GFP might therefore favor the “inactive” conformation. This HOPS mutant appeared less active and more stable, supporting again the hypothesis that the flexible part consists of Vps39, Vps11 and Vps41 (Figures 3.16, 3.29, 3.32). However, the assembly and recruitment of HOPS is not fully explained with this model, and does not completely explain the *in vivo* situation for assembly and recruitment. The role of the interaction with Ypt7, whether on the same or on opposing membrane, is not clear at this point. It might serve as an assembly platform for HOPS or is required for recognition of MVBs. Fusion of proteoliposomes is induced in the presence of HOPS, Ypt7 and SNAREs, but does not necessarily require Ypt7. The interaction with lipids might be sufficient for HOPS binding (Hickey et al., 2010). This might be one possible explanation for the recognition of autophagosomes and Cvt vesicles by HOPS, which are probably lacking Ypt7.

5. Conclusion and Outlook

The here presented data gave a more detailed view on tethering complexes. The HOPS tethering mechanism might combine some general features suitable for all multisubunit tethering complexes. I showed that Vps39 as part of the HOPS complex is required for efficient tethering and fusion. The specificity towards Rab binding differs for Vps39 as a single protein and from within the HOPS complex. This suggests additional functions for Vps39 unrelated to HOPS. Since Vps39 is not the GEF for Ypt7, its role in HOPS, even though indispensable for activity, remains unclear. I could exclude a proposed GDF function for Vps39 as part of the complex.

The intermediate complex between HOPS and CORVET (i-CORVET) can act as a tethering complex *in vitro*, also pointing towards an *in vivo* relevance. The lack of Vps39 in this complex results in reduced tethering activity, which is partially compensated for by Vps3 or the remaining subunits. The mechanism of this fusion rescue is unclear and needs to be further elucidated.

HOPS fusion activity was restored from two subcomplexes Vps41-Vps39-Vps11-Vps18 together with Vps16-Vps33. This *in vitro* assembly of HOPS gave insights into the *in vivo* assembly options. Furthermore, this reconstitution is the sole functional connection to the subcomplexes so far. Their *in vivo* relevance is nevertheless still under debate and needs to be further determined.

The electron microscopy pictures of HOPS and two tagged mutants gave insights into the shape and the function. HOPS appeared as a dumb-bell like structure with one flexible arm. The high flexibility of the entire complex and the subcomplexes could reflect a general feature of tethering complexes. One flexible arm in HOPS was observed, which might be involved in Rab binding and vesicle catching. The more static part of HOPS might bind to SNAREs and thereby anchor the complex to the membrane. The further reduction in flexibility is one aim for future structural studies. This might be achieved by analyzing HOPS together with an interaction partner. SNAREs, Ypt7 or different lipids are possible candidates.

With the help of the GFP-tagged mutants it will be possible to localize every subunit inside the complex, also the stability did only partially increase. We started already analyzing HOPS with Vps39-GFP and HOPS with Vps33-GFP. These two versions might assign both ends of the complex. Another approach in this regard is

labeling with antibodies, if GFP-tags are not detectable. With this approach the GFP-tags as well was the Calmodulin peptide, which is carboxy-terminal fused to Vps41, might be localized within the HOPS complex.

With the help of Class averages, we were able to get a two-dimensional image of HOPS. By further analyzing the HOPS tomography we could reconstitute also the three-dimensional structure. This is the first structural analysis of HOPS performed so far and constitutes a starting point for further measurements of i-CORVET, CORVET and Mon1-Ccz1. It will uncover more details of the mechanism of multisubunit tethering complexes in the endomembrane system.

6. Materials and Methods

6.1 Media

The following media were utilized for *S. cerevisiae* and *E.coli* cultures:

6.1.1 Complete media

Yeast Extract Peptone Galactose (YPG) media was used for yeast culture of *GAL1*-promoter overexpression strains. For 1l medium, 10g yeast extract, 20g peptone and 20g D-galactose were dissolved in ultrapure water and the pH was adjusted to 5.5 using 1M HCl.

Yeast Extract Peptone Dextrose (D-glucose) (YPD) media was used for all wild-type strains and strains, which did not contain a *GAL1*-promoter. For 1l medium, 10g yeast extract, 20g peptone and 20g D-glucose were dissolved in ultrapure water and adjusted to pH 5,5 using 1M HCl.

Antibiotics were added to the media after autoclaving, as indicated in table 6.1.

0,2x YPD was used during vacuole preparation. For 1l medium, 10g yeast extract, 20g peptone and 2g D-glucose were dissolved in ultrapure water and the pH was adjusted to 5,5 using 1M HCl.

For the production of plates, 20g Agar were added per liter medium before autoclaving.

For *E.coli* cultures, Luria-Bertani (LB) medium was used, supplemented with different antibiotics (Table 6.1). For 1l medium, 5g yeast extract, 10g tryptone and 10g NaCl were dissolved in ultrapure water and adjusted to a pH of 7 using 1M HCl.

For the production of plates, 15g Agar were added per liter medium before autoclaving.

6.1.2 Selective media

Synthetic Dextrose Complete dropout medium (SDC-X) was used for selecting strains harboring a genomically encoded auxotrophy marker (e.g. after transformation) or for strains containing a non-integrative plasmid. For 1l medium, 6,75g yeast nitrogen base w/o amino acids, 20g D-glucose and ca. 0,75g complete medium lacking the specific marker metabolite (CSM, exact amount depends on the drop-out medium used) were dissolved in ultrapure water and adjusted to a pH of 5,5 using 1M NaOH.

Table 6.1: Antibiotics used for *S.cerevisiae* or *E.coli* cultures.

Antibiotic	End concentration
Ampicillin	100µg/ml
Chloramphenicol	35µg/ml
Geneticin (G418)	200µg/ml
Hygromycin	300µg/ml
Kanamycin	35µg/ml
Nourseothricin (ClonNat)	100µg/ml

6.1.3 Cell culture

Yeast and bacteria liquid cultures were incubated at 30°C or 37°C, respectively. In both cases, the cultivation flasks or tubes were put in an Innova shaker (New Brunswick Scientific, Edison, NJ, U.S.A.) with a rotation of 180rpm over night. The HOPS overexpression yeast strains were incubated for 2 days in YPG. 1% D-galactose was added additionally after 1 day of incubation. For cultures up to 2ml volume, a bench top Thermo-Shaker (Eppendorf, Hamburg, Germany) was utilized over night.

6.1.4 *S.cerevisiae* and *E.coli* strains

All yeast strains used in this study are summarized in table 8.1.

E.coli strains:

The *E.coli* strain DH5α was used for all cloning purposes. Competent cells were made by A. Perz or K. Auffarth (Department of biochemistry, University of Osnabrück, Germany)

Genotype: F- Φ80*lac*ZΔM15 Δ(*lac*ZYA-*arg*F) U169 *deo*R *rec*A1 *end*A1 *hsd*R17(rk-, mk+) *pho*A *sup*E44 *thi*-1 *gyr*A96 *rel*A1 λ-.

The *E.coli* strain BL21 (DE3) rosetta was used for heterologous expression of yeast proteins. This strain carries an additional plasmid, which offers yeast tRNAs rarely used by *E.coli*, which would otherwise limit protein biosynthesis.

Genotype: F- *ompT hsdS*B(rB- mB-) *gal dcm* (DE3) pRARE (CamR)

All newly cloned *S.cerevisiae* and *E.coli* strains were stored in 15% glycerol at -80°C for back up.

6.2 Molecular biology

All enzymes and buffers used for molecular biology were taken from Fermentas (St. Leon-Rot, Germany). For all molecular works ddH_2O was utilized.

6.2.1 Polymerase-chain reaction (PCR)

For DNA amplification two different types of PCR reactions were used. To amplify open reading frames from genomic DNA and for cloning the PCR product into vectors, *Pfu* polymerase and their conditions were used. For amplifications of promoters and tags, which were afterwards inserted into the yeast genome, the Knop-PCR with the respective conditions was used.

6.2.1.1 Pfu-PCR

Isolated yeast DNA was used as a template for *Pfu*-PCR. The primers for amplification were designed in the way that they bind directly before and after the amplifying sequence and additionally contain a specific restriction site for cloning into a vector.

Table 6.2: PCR program for *Pfu*-PCR.

PCR step	Temperature	Time	Repeat
Denaturation	95°C	2min	1x
Denaturation Annealing Extension	95°C 50°C 70°C	30sec 30sec 0,5kb/min	35x
Final Extension	70°C	10min	1x
Storage	4°C	forever	

Table 6.3: Diagram for PCR reaction mix.

Reagent	Volume
genomic DNA	1µl
10x buffer without $MgSO_4$	5µl
5’ primer (10µM)	1,25µl
3’ primer (10µM)	1,25µl
dNTP Mix (10mM)	1µl
DMSO	3,5µl
$MgSO_4$	7µl
Pfu polymerase (2,5U/µl)	0,8µl
H_20	ad 50µl

6.2.1.2 Knop-PCR

This PCR program is based on Janke et al., 2004 to amplify tags and promoters from pYM (Janke et al., 2004), pRS (Rigaut et al., 1999) and pFA6a (Longtine et al., 1998) plasmids. The amplified PCR product was used for homologous recombination into *S.cerevisiae* strains (Puig et al., 1998).

Table 6.4: PCR program for Knop-PCR.

PCR step	Temperature	Time	Repeat
Denaturation	95°C	4min	1x
Denaturation Annealing Extension	95°C 54°C 68°C	30sec 30sec 2min 40sec	10x
Denaturation Annealing Extension	95°C 54°C 68°C	30sec 30sec 2min 40sec + 20sec/cycle	20x
Storage	4°C	Forever	

Table 6.5: Diagram for PCR reaction mix.

Reagent	Volume
Plasmid DNA	1µl
10x buffer	5µl
5' primer (10µM)	3,2µl
3' primer (10µM)	3,2µl
dNTP-Mix (10mM)	1,75µl
Taq polymerase (recombinant) (5U/µl)	0,4µl
Vent polymerase (2U/µl)	0,2µl
H_2O	ad 50µl

6.2.2 Preparative and analytical restriction digest

For cloning 1000ng plasmid DNA or 25µl PCR product were digested with 1µl FastDigest® restriction enzyme for 2h at 37°C. After this incubation the entire mix was loaded onto an agarose gel.

Table 6.6: Preparative restriction digest.

Reagent	Volume/ weight
10x FastDigest® buffer	5µl
FastDigest® enzyme	1µl
Plasmid DNA/ PCR product	1000ng/ 25µl
H_2O	ad 50µl

For analytical purposes of newly cloned plasmids, control digests were performed. The isolated plasmid was incubated for 1h with 0,5µl of the same restriction enzyme used for cloning and loaded onto an agarose gel.

Table 6.7: Analytical restriction digest.

Reagent	Volume
Plasmid DNA	5µl
Restriction enzyme (10U/µl)	1µl
10x buffer	1µl
H_2O	ad 10µl

6.2.3 Agarose gel electrophoresis

The digested DNA fragments were separated during agarose gel electrophoresis. Therefore 1% (w/v) agarose was dissolved in 1x TAE buffer (40mM Tris pH 8,3, 20mM acidic acid, 2mM EDTA) by heating in the microwave. 4µl ethidiumbromide (1% (w/v), Applichem, Darmstadt, Germany) per 50ml agarose solution was subjected to the dissolved solution. The DNA was separated during a 120V run for 30min. If required, the DNA was afterwards isolated from agarose gel pieces with the „Nucleospin Extract II“ kit (Macherey-Nagel, Düren, Germany) according to the manufactor's protocol.

6.2.4 Ligation and generation of plasmids

For 20µl ligation mix, 10ng vector and 5 times the molarity of the insert were incubated over night at 4°C with T4-DNA ligase. As a control, the plasmid was incubated the same way without insert.

Table 6.8: Diagram for ligation reaction mix.

Reagent	Ligation mix	Control ligation
Plasmid	10ng	10ng
Insert	5x molarity of plasmid	---
10x T4-DNA ligase buffer	2µl	2µl
T4-DNA ligase (5U/µl)	0,5µl	0,5µl
H_2O	ad 20µl	ad 20µl

Two integrative plasmids for *S.cerevisiae* were generated as described above and after linearization by digestion with AgeI (see 6.2.2) inserted into the yeast genome.

Table 6.9: Generated integrative plasmids.

Plasmid	Genotype	Origin
pRS406	*GAL1*pr-VPS41 aa 356-379Δ	This study
pRS406	*GAL1*pr-VPS41 aa 366- 377Δ	This study

6.2.5 Transformation

Ligation mixes or purified plasmids were transformed into *E.coli* DH5α for amplification or into BL21 (DE3) rosetta for heterologous protein expression, respectively. Both transformations were performed in the same way. Tags, promoters amplified with the Knop PCR or linearized integrative plasmids were transformed into *S.cerevisiae* strains. They were inserted into the yeast genome by homologous recombination (Puig et al., 1998).

6.2.5.1 E.coli transformation

50µl of competent *E.coli* cells were thawed on ice and 10µl of the ligation mix or 1µl isolated plasmid was added and incubated for 20min on ice. After a heat shock for 40sec at 42°C, 800µl LB medium was added and further incubated for 1h at 37°C. They were centrifuged for 5min at 5000rpm, plated onto antibiotics containing LB plates and incubated over night at 37°C.

6.2.5.2 S.cerevisiae transformation

Yeast strains were transformed with PCR products or linearized plasmids by using the lithium acetate method (Gietz et al., 1995). Therefore, an over night preculture (wild-type strains were incubated in YPD, strains containing *GAL1*-promoters were incubated in YPG) was diluted to an OD_{600nm} of $0{,}5ml^{-1}$ in YPD and grown for 4h. The cells were harvested and washed in H_2O, before resuspending them in 1ml 0,1M lithium acetate. The cells were centrifuged for 2min at 4000rpm and dissolved in 350µl 0,1M lithium acetate. A 50µl aliquot of competent cells was used for one transformation with 25µl Knop PCR product or H_2O as control.

Table 6.10: Diagram for *S.cerevisiae* transformation mix.

Reagent	Transformation mix	Control transformation
Competent yeast cells	50µl	50µl
Knop PCR product/ integrative plasmid	25µl 1,5µg	--- (25µl H_2O) --- (H_20)
Carrier DNA (2mg/ml)	25µl	25µl
Lithium acetate (1M)	36µl	36µl
50% (w/v) PEG 4000	240µl	240µl

After mixing the transformation setup, it was incubated for 45min at 42°C and plated onto selective media plates or YPD plates for over night incubation at 30°C. YPD-plates strains were replica plated onto antibiotic containing YPD plates the next day.

6.2.6 Plasmid isolation and sequencing

For isolation of plasmids from *E.coli* DH5α cells, a 5ml over night culture was used. The isolation was performed with the „GeneJET™ Plasmid Miniprep“ kit (Fermentas, St. Leon-Roth, Germany) according to the manufactor's protocol. Plasmids were sent to GATC (Konstanz, Germany) for sequencing according to their instructions.

6.2.7 Photometric DNA determination

To measure the DNA concentration and purity of a plasmid solution, the NanoDrop®-ND1000 spectrophotometer (Peqlab, Erlangen, Germany) was loaded with 2µl of this solution. After measuring a spectrum between 200nm and 400nm according to the manufactor's protocol, the concentration from the absorption at 260nm was determined. The ratio of the absorption of 260nm and 280nm displays the purity of the DNA and lies ideally between 1,8 and 2,0.

6.3. Biochemical assays

6.3.1 Total protein extraction from yeast and TCA precipitation

For qualitative and quantitative analysis of yeast proteins, cells equivalent to OD_{600nm} of $1ml^{-1}$ were harvested and resuspended in 500µl ddH_2O. For alkaline lysis 75µl of lysis solution (0,25M NaOH, 140mM β-Mercaptoethanol, 3mM PMSF) was added, mixed and incubated for 10min on ice. A TCA precipitation was attached afterwards.

TCA precipitation:

For denaturing protein precipitation, samples were supplemented with 100% (w/v) TCA solution to a final concentration of 13% (v/v), mixed and incubated for 10min on ice. Samples containing no detergent (except total protein extracts) were supplemented with 0,1% NP40 beforehand. After 10min incubation on ice, samples were centrifuged for 10min at 20,000xg at 4°C. The TCA-containing supernatant was discarded and the pellet was washed once with 1ml 100% Acetone at -20°C. After additional centrifugation at 20,000g for 10min, the pellet was dried at 55°C for several minutes. SDS-sample buffer (2 % (w/v) SDS; 62,5mM Tris pH 8,0; 10 % (v/v) Glycerin, 0,005 % (w/v) Bromphenolblue; Laemmli et al., 1970) was added after drying and pellets were resolved by shaking.

6.3.2 SDS-PAGE and Coomassie staining

The protein-separation according to their molecular weight was performed by using sodium-dodecylsulfate-polyacrylamide gel electrophoresis (SDS-PAGE). I used separation gels with 7,5% (v/v) or 12% (v/v) acrylamide referring to the molecular weight of the proteins. The gels were run in 192mM glycine, 25mM Tris, 0,1 % (w/v) SDS running buffer at 200V. Afterwards, the gels were used for western blotting or stained with Coomassie brilliant Blue R-250 (0,4% (w/v) Coomassie Brilliant Blue R-

250 (Serva, Heidelberg, Germany); 500ml methanol; 100ml acetic acid; 400ml H_2O) by heating in the microwave. Destaining was performed with 30% (v/v) acetone, 10% (v/v) acetic acid and tissue.

6.3.3 Western blotting and immuno detection

For detection of proteins or tags by antibody decoration, the separated proteins were transferred from the SDS-PAGE gel onto a nitrocellulose membrane (GE Healthcare, Munich, Germany). The blotting chamber for tank blotting was filled with western transfer buffer (192mM glycine, 25mM Tris, 0,025 % (w/v) SDS, 20 % (v/v) methanol) and proteins were transferred for 1,5h and 20V onto the nitrocellulose membrane.

Afterwards the membrane was blocked with 5% (w/v) milk powder in PBS (1,5mM KH_2PO_4; 8mM Na_2HPO_4; 3mM KCl; 140mM NaCl) for 30min before subjecting the first antibody for 1h. The first antibody was diluted in 5% (w/v) milk powder in PBS. The membrane was washed 3 times with TBS-Tween20 (10mM Tris, pH 7,4; 155mM NaCl; 0,5% (v/v) Tween20) before the secondary antibody (DylightTM800, Pierce; 1:10000 diluted in 5% (w/v) milk powder in PBS) was subjected for 30min. After 3 times washing in TBS-Tween20 and 1 time in PBS the signals were developed with the Odyssey-Scanner (LI-COR Biosciences, Bad Homburg, Germany).

6.3.4 Tandem affinity purification (TAP)

The tandem affinity purification of native proteins is based on Puig et al., 2001. The principle of this method was used in three different scales, depending on the amount of cells.

6.3.4.1 Standard TAP

For the standard purification amount 1l of stationary grown cells (or 2 to 4l of log-phase grown cells) were harvested, washed once in ddH_2O and TAP buffer (50mM HEPES pH 7,5; 300mM NaCl) with 1x protease inhibitor mix FY (Serva, Heidelberg, Germany) and 2mM PMSF. The pellet was frozen in liquid nitrogen and stored at -80°C. For protein purification a 10 to 15ml cell pellet was thawed and resuspended in TAP buffer (50mM HEPES pH 7,5; 300mM or 1M NaCl as indicated in results) with protease inhibitors and 1mM DTT to reach a total volume of 25ml. Cells were lysed with 25ml glass beads (Sartorius, Göttingen, Germany) in a Fritsch pulverisette (Idar-

Oberstein, Germany) for 3x 4min at 500rpm with 1min break in the cold-room. After separating the glass beads from cell suspension by pushing the lysate through a 50ml syringe, it was centrifuged at 4000xg for 10min at 4°C (Eppendorf, Germany) to remove unlysed cells and cell debris. The supernatant was applied to an ultracentrifugation tube and spun for 1h at 100.000xg at 4°C. After removal of the fatty top phase and addition of 10% (v/v) glycerol, the supernatant was incubated for 2h at 4°C with 300µl of washed IgG sepharose bead slurry (GE Healthcare, Munich, Germany) on a nutator. The IgG beads with the bound protein were centrifuged at 800xg for 1min and the supernatant was removed, except for 1ml. To transfer the IgG beads into a small MoBiCol column (MoBiTec, Göttingen, Germany), they were resuspended in the remaining supernatant and washed with 15ml TAP buffer with 0,5mM DTT and 10% (v/v) glycerol without protease inhibitors. Shortly before the beads went dry, the MoBiCol was closed from the bottom and 150µl TAP buffer (as before) and 10µl TEV protease (2mg/ml) were added. After 1h incubation on a turning wheel at 16°C, the protein was eluted by a short spin. This TEV-eluate was now ready to use or aliquoted, frozen in liquid nitrogen and stored at -80°C for later usage.

6.3.4.2 Small-scale TAP purification

The MiniTAP protocol is based on the standard TAP protocol in smaller scale. 250ml cell culture with an OD_{600nm} of $2ml^{-1}$ (refers to 500 OD_{600nm} units) was harvested and washed with ddH_2O. The pellet was frozen in liquid nitrogen and stored at -80°C for further use. After thawing, the pellet was washed in 10ml TAP buffer (50mM HEPES pH 7,5 varying NaCl concentrations and different or no detergent) with 1x protease inhibitor mix FY, 2mM PMSF and 1mM DTT and resuspended in 500µl of the same buffer. After addition of 1ml glass beads, cells were lysed for 3x 10min with 5min break at 4°C in a disrupter genie (Scientific industries, Bohemia, N.Y., USA). After a 20000xg spin and a 100.000xg spin the supernatant was applied to 30µl of washed IgG bead slurry and incubated for 1h at 4°C. After washing (4 times with 1ml TAP buffer with 0,5mM DTT) and removal of the supernatant except for 100µl, 5µl TEV protease was added and further incubated for 1h at 16°C. The eluate was applied on a SDS-PAGE gel, used for Coomassie staining or western blotting (see 6.3.2).

6.3.4.3 Large-scale TAP purification

The MegaTAP protocol is based on the standard TAP protocol in larger scale. 2l of stationary grown cells (or 4 to 6l of log-phase grown cells) were harvested and washed once in ddH_2O and TAP buffer (50mM HEPES pH 7,5; 300mM NaCl). The pellets were frozen in liquid nitrogen and stored at – 80°C for further usage. After thawing, 100 to 150ml cell pellet was resuspended in TAP buffer (50mM HEPES pH 7,5, varying NaCl concentrations, with or without detergent as indicated in results) to a final volume of 250ml.

Cells were lysed with 250ml glass beads in a Fritsch pulverisette and the glass beads were separated from cell suspension by pushing the lysate through five 50ml syringes. After centrifugation at 4000xg and 100.000xg, 10% (v/v) glycerol was added to the supernatant and incubated for 2h at 4°C with 3ml of washed IgG sepharose bead slurry on a nutator. After removal of the supernatant by centrifugation, the IgG beads were transferred to five MoBiCols and each was washed with 15ml TAP buffer containing 0,5mM DTT and 10% (v/v) glycerol. Shortly before the beads went dry, the MoBiCols were closed from the bottom and 150µl TAP buffer (as before) and 10µl TEV protease was added. After 1h of incubation on a turning wheel at 16°C, the protein was eluted by a short spin. This TEV-eluate was now ready to use or aliquoted, frozen in liquid nitrogen and stored at -80°C for later usage.

6.3.4.4 Protein determination

To determine the protein concentration, I used two different methods. One is based on a colorimetric measurement of cationic and apolar side chains of the protein, and the other one is measuring the absorption of the protein's aromatic residues.

The colorimetric protein estimation was performed after Bradford (1976). Therefore an aliquot of the protein sample (up to 10µl) was mixed with 1ml 1:5 diluted Roti-Quant (Roth, Karlsruhe, Germany) and incubated for 5min at room temperature. The sample was measured against a blank at 595nm. After calibrating with 1µg/µl to 10µg/µl bovine serum albumin (BSA), the protein content in the sample was determined.

The second measurement is based on the aromatic residues in the protein, which absorb at 280nm. Therefore, 2µl of the sample were applied on the NanoDrop®-ND1000 spectrophotometer (Peqlab, Erlangen, Germany) and measured against the reference buffer.

6.3.5 Gelfiltration

For the separation of proteins or protein complexes dependent on their molecular weight and for purifying complexes from low molecular weight proteins, size exclusion gelfiltration was employed. A Superdex 200 10/300 GL column (GE Healthcare, Munich, Germany) with a volume of 24ml was used for this procedure. The column was attached to an ÄKTA FPLC system, which was operated from a PC using the Unicorn 5.01 software (both GE Healthcare). The flow rate during the gelfiltration run was 0,3ml/min and up to 0,5ml/min for washing and equilibration. Since TEV-eluate from a TAP experiment was applied to the column, TAP buffer (see 6.3.4) containing 4mM DTT was used for the elution of the sample from the gelfiltration matrix. Buffers were filtered through a 0,22µm filter and subsequently degassed. All samples were centrifuged at 20,000xg for 10min prior to loading into the sample loop to pellet insoluble material. 1ml fractions were collected for 0,9 column volumes i.e. for approx. 21,6ml. Afterwards, collected fractions were TCA precipitated and analyzed by SDS-PAGE (see 6.3.1 and 6.3.2).

6.3.6 GraFix method and Glycerol gradient centrifugation

The GraFix method is based on Kastner et al., 2008 and relies on a glycerol gradient centrifugation with simultaneous cross-linking of the proteins. 2,2ml of two glycerol solutions (10% (v/v) and 30% (v/v)/ 40% (v/v) in TAP buffer (used for protein purification, see 6.3.4) were subjected to the gradient pouring device (Minipuls 3, Gilson, Middleton, WI, USA) and a continuous gradient into 13ml/ 4,5ml ultracentrifugation tubes (Beckman, Krefeld, Germany) was poured (flow rate for 13ml/ 4,5ml tubes: 2,5/ 1,25ml/min). For cross-linking during centrifugation 0,025% (v/v) glutaraldehyde was added to the high percentage glycerol solution. The purified protein/ protein complex (up to 10% (v/v) of the total gradient volume) was added on top of the gradient. After centrifugation for 18h at 4°C in SW40 rotor (Beckman, Krefeld, Germany) at 40.000rpm, fractions were harvested from the top. For the 13ml tubes 1ml fractions were collected and for the 4,5ml tubes fractions á 340µl were collected. As controls a reference gradient with marker protein and a reference gradient without glutaraldehyde was treated the same way. Aliquots of each fraction were stored on ice, frozen in liquid nitrogen for storage at -80°C or TCA precipitated for further analysis on SDS-PAGE gels.

6.3.7 Heterologous protein purification

One colony of freshly transformed BL21 (DE3) rosetta was inoculated in 1l LB media supplemented with antibiotics and grown at 37°C until an OD_{600nm} of 0,4ml^{-1}. After cooling down to 16°C, 0,5mM IPTG was subjected and the culture was further incubated over night at 16°C. After harvesting cells, they were washed in 100ml wash buffer (50mM Tris pH 7,4; 150mM NaCl) and centrifuged at 6.000rpm for 10min in JLA8.1000 rotor in the Avanti J26 XP centrifuge (Beckman, Krefeld, Germany). The pellet was resuspended in wash buffer containing 1mM PMSF and 0,05x PIC before lysing in the mircofluidizer M-110L (Microfluids, Lampertheim, Germany). The resulting suspension was spun for 20min at 20.000rpm in JA 25-50 rotor to remove unlysed cells and cell debris. The clear supernatant was applied onto washed Ni-NTA-Agarose (Qiagen, Hilden, Germany) and incubated for 1,5h at 4°C on a nutator. The protein bound to the Ni-NTA matrix was divided from the supernatant by passing through a filter-column. After washing the Ni-NTA with bound proteins in 25ml wash buffer containing 50mM imidazol, the protein was eluted from the Ni-NTA with wash buffer supplemented with 300mM imidazol in 1ml fractions. Protein content in each fraction was estimated via Biorad measurement (see 6.3.4.4) and 2,5ml of protein-containing fractions were rebuffered with PD10 desalting columns (GE Healthcare, Munich, Germany) according to the manufactor's protocol, if required. Aliquots of the protein were analyzed on SDS-PAGE gel after staining with Coomassie (see 6.3.2) and aliquots were frozen in liquid nitrogen for storage at -80°C for further usage.

6.3.8 Rab pulldown

GST-Rab fusion proteins (150µg per sample) were incubated in 500µl nucleotide loading buffer containing 20mM Hepes/NaOH (pH 7,4), 20mM EDTA and 1mM GDP, GTPγS or no nucleotide for 15min at 30°C. The GDP and GTPγS samples were adjusted to 25mM $MgCl_2$, and loaded onto 50µl of washed GSH-sepharose, whereas the nucleotide free sample was loaded onto the same amount of GSH-sepharose. After incubation for 1h at 4°C on a turning wheel, the GSH-bound nucleotide free form was washed once with 20mM Hepes/NaOH (pH 7,4), 20mM EDTA and the matrix was then resuspended in 200µl buffer containing 20mM Hepes/NaOH (pH 7,4) 100mM NaCl and 1mM $MgCl_2$. The GDP and GTPγS loaded samples were resuspended in 200µl of the same buffer containing additional 2,5mM GDP or GTPγS, respectively.

These nucleotide loaded Rab GTPases bound to GSH-sepharose were then immediately used for pull-down experiments. Cell lysates to be applied to Rab GTPase pull-down where prepared in parallel using the Mini-TAP protocol (see 6.3.4.2) until the 100.000xg spin or frozen TEV-eluates from standard TAP purifications (see 6.3.4.1) were directly applied to the immobilized GST-Rab proteins and the bead suspension was incubated for 1h at 4°C on a turning wheel. After the binding reaction, the beads were carefully pelleted by centrifugation and washed three times with 1ml ice-cold buffer (20mM Hepes/NaOH (pH 7,4), 100mM NaCl, 1mM $MgCl_2$ and 0.1% NP40). Bound proteins were then eluted by incubation with 600µl elution buffer containing 20mM Hepes/NaOH (pH 7,4), 20mM EDTA, 200mM NaCl, 1mM $MgCl_2$ and 0.1% NP40 for 20min at room temperature on a turning wheel. A second elution step was performed with 300µl elution buffer for 10min to elute residual protein. Eluates were then pooled, TCA precipitated and analyzed by SDS-PAGE and Western blotting (see 6.3.2 and 6.3.3).

6.3.9 Vacuole isolation from *S.cerevisiae* (Haas et al., 1995)

Precultures of the two yeast tester strains were inoculated in the morning in YPD and grown at 30°C over day. The *vps11-1* tester strain preculture was incubated over night in SDC-URA at 30°C. 0,6 OD_{600nm}-units of the DKY strain and 2,5 OD_{600nm}-units of the BJ strain were inoculated in 1l YPD and incubated over night at 30°C. The *vps11-1* tester strains were inoculated with 20 OD_{600nm}-units for the *pep4*Δ strain and 25 OD_{600nm}-units for the *pho8*Δ strain and grown for 20h at 25°C. Cells were harvested in JLA8.1000 rotor with 5000rpm for 3min, resuspended in 0,1M Tris pH 9,4, 10mM DTT and incubated for 10min at 30°C. After centrifugation as before, the cells were resuspended in 10ml spheroblasting buffer (40ml 0,2x YPD, 7,5ml 4M sorbitol, 2,5ml KP_i pH 7,4) and applied to JA25.50 tubes filled with 5ml spheroblasting buffer with appropriate amounts of lyticase for 20min incubation at 30°C. After centrifuging the cells for 3min at 3500rpm and 4°C in JA25.50 rotor (Beckman, Krefeld, Germany) the supernatant was carefully discarded and the pellet was resuspended in 2,5ml 15% (w/v) Ficoll buffer (15% (w/v) Ficoll (GE Healthcare, Munich, Germany), 10mM PIPES/KOH pH 6,8, 0,2M sorbitol). 200µl DEAE-Dextran (0,4mg/ml) was subjected for further incubation on ice for 3min and heat shocked at 30°C for 1,5min. After transferring the suspension into SW40/41 ultracentrifugation tubes (Beckman, Krefeld, Germany) stepwise gradients were poured. The 15% (w/v) Ficoll containing

suspension was overlaid with 8% (w/v) Ficoll buffer, 4% (w/v) Ficoll buffer and filled up with 0% Ficoll buffer. After centrifuging for 1,5h at 30.000rpm and 4°C in SW40/41 rotor, vacuoles were harvested at the 0% to 4% (w/v) Ficoll buffer interface. The vacuole/ protein concentration was measured via Biorad (see 6.3.4.4) and vacuoles were diluted to 0,3mg/ml for fusion. For immunostaining 20µg of isolated vacuoles were loaded onto an SDS-PAGE gel for western blotting.

6.3.10 Vacuole fusion assay

The isolated vacuoles were mixed (*pep4*Δ strain with *pho8*Δ strain) and goodies were added to stimulate fusion.

Table 6.11: Diagram for the vacuole fusion mix.

Component	Volume
10x fusion buffer *	3µl
10x ATP regenerating system **	3µl
Coenzyme A (2,5mM, Applichem, Darmstadt, Germany)	0,12µl
Sec18 (1mg/ml 1:100 diluted in 0% Ficoll)	1µl
BJ vacuoles (0,3mg/ml) /BY vacuoles *vps11-1* (0,3mg/ml)	10µl
DKY vacuoles (0,3mg/ml)/ BY vacuoles *vps11-1* (0,3mg/ml)	10µl
For *vps11-1* fusions: 1mg/ml Vam7	1µl
0% Ficoll buffer	ad 30µl

*1,25M KCl; 50mM $MgCl_2$; 0,2M Sorbitol; 10mM PIPES/KOH pH 6,8

** ATP regenerating system: 5mM ATP (pH buffered); 1mg/ml Creatine Kinase (Roche, Mannheim, Germany); 400mM Creatine Phosphatase (Applichem, Darmstadt, Germany); 10mM PIPES/KOH pH 6,8; 0,2M Sorbitol

Increasing concentrations of protein complex with or without inhibitor (20µg inhibitor/fusion reaction) or buffer (as indicated in results) were proposed and afterwards the complete vacuole fusion mix was subjected. The vacuole fusion mix was incubated for 1,5h at 26°C. One sample without protein complex or buffer was kept on ice as a negative control. After addition of 470µl developer (10mM $MgCl_2$; 0,25M Tris pH 8,5; 0,4% (v/v) Triton X-100; 1,5mM p-nitrophenol-phosphate (pNPP)) and an incubation for 5min at 30°C (*vps11-1* fusion mixes were incubated for 10min), the reaction was stopped with 500µl 1M glycine pH 11,5. The absorption was measured at 400nm against a blank sample consisting of 500µl developer and 500µl 1M glycine pH 11,5. Fusion units correspond to the OD_{400nm}*5 for 5min development or OD_{400nm}* 2,5 for 10min development. One fusion unit (U) correspond to 1µmol of product (p-nitrophenol) min^{-1} μg^{-1} of the enzyme (alkaline phosphatase, Pho8)

6.4 Microscopy

6.4.1 Fluorescence microscopy

For fluorescence microscopy of yeast cells carrying GFP-tagged proteins, they were grown to logarithmic phase in 5ml complete medium, dependent on the strain background. The cells were harvested by centrifugation, washed once with 1ml SDC+ all medium and resuspended in 10-30µl SDC+ all medium or stained with FM4-64 (see 6.4.1.1). Images were acquired using a Leica DM5500 microscope (Leica, Wetzlar, Germany) and a SPOT Pursuit-XS camera (Visitron, Puchheim, Germany) with filters for GFP and FM4-64. The pictures were processed using Adobe Photoshop CS3.

6.4.1.1 FM4-64 staining

To visualize the yeast vacuole for fluorescence microscopy analysis, the lipophilic dye FM4-64 (N- (3-triethylammoniumpropyl)-4-(6-(4-(diethylamino) phenyl) hexatrienyl) pyridinium dibromide; Invitrogen, Karlsruhe, Germany) was employed. Yeast cells were grown in an overnight culture and diluted in the morning with fresh complete medium to an OD_{600nm} of $0{,}25ml^{-1}$. These cultures were then grown 3 to 4 hours to an OD_{600nm} of 0,5 to $1ml^{-1}$. The cells were pelleted by centrifugation at 3000xg for 2min and resuspended in 50µl of fresh medium. 4µl of a 0,3mM FM4-64 solution was added and the cell suspension was incubated in the dark for 30min at 30°C while shaking in a tabletop thermo-shaker (Eppendorf, Hamburg, Germany) (“pulse”). 1ml medium was added for washing the cells and briefly centrifuged for pelleting and discarding the supernatant. The cells where then resuspended in 500µl of fresh medium and incubated for 90min in the dark at 30°C while shaking (“chase”). Afterwards, the cells were pelleted again, washed once with 1ml SDC+ all medium and were finally resuspended in 10-30µl of SDC+ all medium for microscopy.

6.4.2 Electron microscopy

Electron microscopy was performed at the MPI in Dortmund, Germany in cooperation with the group of S. Raunser. Images were obtained with negative-stained samples of wild-type HOPS, HOPS-GFP versions or HOPS subcomplexes. Pictures were taken at room temperature using a Joel-1400 electron microscope running at 120kV with a LaB6 electron source and 15.000x or 40.000x magnification. For single

particle analysis, images were taken in low dose mode at a magnification of 50.000x on negative films (Kodak, electron image film S0-163). Single particles were picked with the BOXER program (http://blake.bcm.tmc.edu/eman/eman1; Ludtke et al. 1999) and overlaid for class averaging with Sparx or SPIDER (Hohn et al. 2007; Frank et al., 1981; Frank et al., 1996). In all other cases images were detected with a 2,000 x 2,000 14μm-per-pixel FastScan-F214 CCD camera (TVIPS) and 1sec exposure time.

6.4.2.1 Negative staining

To visualize protein complexes with the electron microscope, 6μl of the sample from glycerol gradient centrifugation with simultaneous cross-linking, according to the GraFix protocol (Kastner et al., 2008), was absorbed for 1 h at 4°C and 100% humidity to a freshly glow-discharged copper grid (AGAR scientific, G2400C), covered by a thin, continues carbon film (according to Ohi et al. 2004). Excess sample was blotted using filter paper (Whatman No.4). After 3 times washing with ddH_2O and staining with 0,75% uranyl-formate (SPI Supplies/Structure Probe, Inc.) for 1min, the grid was air-dried and is ready to use.

7. References

Abenza, J.F., Galindo, A., Pantazopoulou, A., Gil, C., de Los Rios, V., and Penalva, M.A. (2010). Aspergillus RabBRab5 Integrates Acquisition of Degradative Identity with the Long Distance Movement of Early Endosomes. Mol. Biol. Cell 21, 2756-2769.

Angers, C.G., and Merz, A.J. (2009). HOPS Interacts with Apl5 at the Vacuole Membrane and Is Required for Consumption of AP-3 Transport Vesicles. Mol. Biol. Cell 29, 4563-4574.

Angers, C.G., and Merz, A.J. (2011). New links between vesicle coats and Rab-mediated vesicle targeting. Semin. Cell Dev. Biol., 22(1):18-26.

Arghi, C.N., Hartnell., L.M., Aguilar, R.C., Haft, C.R. Bonifacino, J.S. (2004). Role of the mammalian retromer in sorting of the cation-independent mannose 6-phosphate receptor. J. Cell Biol. 165(1):123-33.

Baek, K., Knodler, A., Lee, S.H., Zhang, X., Orlando, K., Zhang, J., Foskett, T.J., Guo, W., and Dominguez, R. (2010). Structure-function study of the N-terminal domain of exocyst subunit Sec3. J. Biol. Chem. 285, 10424-10433.

Balderhaar H.J.k., Arlt, H.,Ostrowicz, C.W., Bröcker, C. Sündermann, F., Brandt, R., Babst, M., Ungermann, C. (2010). The Rab GTPase Ypt7 is linked to retromer-mediated receptor recycling and fusion at the yeast late endosome. J. Cell. Sci. 123(23):4085-94.

Barr, F., Lambright, D.G. (2010). Rab GEFs and GAPs. Curr Opin Cell Biol. 22(4):461-70.

Behnia, R., and Munro, S. (2005). Organelle identity and the signposts for membrane traffic. Nature 438, 597-604.

Bigay, J., Casella, J.F., Drin, G., Mesmin, B., Antonny, B. (2005). ArfGAP1 responds to membrane curvature through the folding of a lipid packing sensor motif. EMBO J. 24(13):2244-53.

Bigay, J., Gounon, P., Robineau, S., Antonny, B. (2003). Lipid packing sensed by ArfGAP1 couples COPI coat disassembly to membrane bilayer curvature. Nature. 426(6966):563-6.

Boeddinghaus, C. Merz, A.J., Laage, R., Ungermann, C. (2002). A cycle of Vam7p from and PtdIns 3-P-dependent re binding to the yeast vacuole is required for homotypic vacuole fusion. J. Cell. Biol. 157(1):79-89.

Bonifacino, J.S., Hurley J.H. (2008) Retromer. Curr. Opin. Cell Biol. 20(4):427-36.

Bos, J.L., Rehmann, H., Wittinghofer, A. (2007). GEFs and GAPs: critical elements in the control of small G proteins. Cell. 129:865-877.

Boyd, C., Hughes, T., Pypaert, M., and Novick, P. (2004). Vesicles carry most exocyst subunits to exocytic sites marked by the remaining two subunits, Sec3p and Exo70p. J. Cell Biol. 167, 889-901.

Brett, C.L., Plemel, R.L., Lobinger, B.T., Vignali, M., Fields, S., and Merz, A.J. (2008). Efficient termination of vacuolar Rab GTPase signaling requires coordinated action by a GAP and a protein kinase. J. Cell Biol. 182, 1141-1151.

Bröcker, C. Engelbrecht-Vandré, S., Ungermann, C. (2010). Multisubunit tethering complexes and their role in membrane fusion. Curr. Biol. 20(21):R943-52.

Brohawn, S.G., Leksa, N.C., Spear, E.D., Rajashankar, K.R., and Schwartz, T.U. (2008). Structural evidence for common ancestry of the nuclear pore complex and vesicle coats. Science 322, 1369-1373.

Cabrera, M., Ostrowicz, C.W., Mari, M., LaGrassa, T.J., Reggiori, F., and Ungermann, C. (2009). Vps41 phosphorylation and the Rab Ypt7 control the targeting of the HOPS complex to endosome-vacuole fusion sites. Mol. Biol. Cell 20, 1937-1948.

Cabrera, M.,Langemeyer, L., Mari, M., Orban, I., Perz, A., Bröcker C., Griffith, G., Klose, D., Steinhoff, H.J., Ungermann, C. (2010). Phosphorylation of a membrane curvature-sensing motif switches function of the HOPS subunit Vps41 in membrane tethering. J.Cell Biol.191(4):845-59.

Cai, H., Reinisch, K., and Ferro-Novick, S. (2007). Coats, Tethers, Rabs, and SNAREs Work Together to Mediate the Intracellular Destination of a Transport Vesicle. Dev. Cell 12, 671-682.

Carlton, J., Bujny, M., Peter, B.J., Oorschot, V.M., Rutherford, A., Mellor, H., Klumperman, J., McMohan, H.T., Cullen, P.J. (2004). Sorting nexin-1 mediates tubular endosome-to-TGN transport through coincidence sensing of high-curvature membranes and 3-phosphoinositides. Curr. Biol. 14(20):1791-800.

Chen, Y.J., and Stevens, T.H. (1996). The VPS8 gene is required for localization and trafficking of the CPY sorting receptor in Saccharomyces cerevisiae. Eur. J. Cell Biol. 70, 289-297.

Christoforidis, S., McBride, H.M., Burgoyne, R.D., and Zerial, M. (1999). The Rab5 effector EEA1 is a core component of endosome docking. Nature 397, 621-625.

Collins, K.M., Thorngren, N.L., Fratti, R.A., and Wickner, W.T. (2005). Sec17p and HOPS, in distinct SNARE complexes, mediate SNARE complex disruption or assembly for fusion. EMBO J. 24, 1775-1786.

Conradt, B., Shaw, C., Vida, T., Emr, S., Wickner, W. (1992). In vitro reactions of vacuole inheritance in Saccharomyces cerevisiae. J. Cell. Biol. 119:1469-79.

Darsow, T., Burd, C.G., Emr, S.D. (1998). Acidic di-leucine motif essential for AP-3-dependent sorting and restriction of the functional specificity of the Vam3p vacuolar t-SNARE. J. Cell Biol. 142:913-22.

Darsow, T., Katzmann, D.J., Cowles, C.R., and Emr, S.D. (2001). Vps41p Function in the Alkaline Phosphatase Pathway Requires Homo-oligomerization and Interaction with AP-3 through Two Distinct Domains. Mol. Biol. Cell 12, 37-51.

Devos, D., Dokudovskaya, S., Alber, F., Williams, R., Chait, B.T., Sali, A., Rout, M.P. (2004). Components of the coated vesicles and nuclear pore complexes share a common molecular architecture. PLoS Biol. 2(12):380.

Drin, G., Casella, J.F., Gautier, R., Boehmer, T., Schwartz, T.U., and Antonny, B. (2007). A general amphipathic alpha-helical motif for sensing membrane curvature. Nat. Struct. Mol. Biol. 14, 138-146.

Drin, G., Morello, V., Casella, J.F., Gounon, P., and Antonny, B. (2008). Asymmetric tethering of flat and curved lipid membranes by a golgin. Science 320, 670-673.

Dulubova, I., Yamaguchi, T., Wang, Y., Südhof, T.C., Rizo, J. (2001). Vam3p structure reveals conserved and divergent properties of syntaxins. Nat. Struct. Mol. Biol. 8(3):258-64.

Fasshauer, D., Sutton, R.B., Brunger, A.T., Jahn, R. (1998). Conserved structural features of the synaptic fusion complex: SNARE proteins reclassified as Q- and R-SNAREs. Proc. Natl. Acad. Sci. USA. 95:559-71.

Frank, J., Shimkin, B., Dowse, H. (1981). SPIDER-a modular software system for electron image processing. Ultramicroscopy 6, 343-358.

Frank, J., Radermacher, M., Penczek, P., Zhu, J., Li, Y., Ladjadj, M., Leith, A. (1996). SPIDER and WEB: processing and visualization of images in 3D electron microscopy and related fields. J. Struct. Biol. 116(1):190-9.

Gallop, J.L., McMohan, H.T. (2005) BAR domains and membrane curvature: bringing your curves to the BAR. Biochem. Soc. Symp. 72:223-31.

Gietz, R.D., Schiestl, R.H., Willems, A.R., Woods, R.A. (1995). Studies on the transformation of intact yeast cells by LiAc/SS-DNA/PEG procedure. Yeast. 11(4):355-60.

Gillingham, A.K., and Munro, S. (2003). Long coiled-coil proteins and membrane traffic. Biochem. Biophys. Acta 1641, 71-85.

Gillingham, A.K., Pfeifer, A.C., and Munro, S. (2002). CASP, the Alternatively Spliced Product of the Gene Encoding the CCAAT-Displacement Protein Transcription Factor, Is a Golgi Membrane Protein Related to Giantin. Mol. Biol. Cell 13, 3761-3774.

Guo, W., Roth, D., Walch-Solimena, C., and Novick, P. (1999). The exocyst is an effector for Sec4p, targeting secretory vesicles to sites of exocytosis. EMBO J. 18, 1071-1080.

Haas, A., Scheglmann, P., Lazar, T., Gallwitz, D., Wickner, W. (1995). The GTPase Ypt7p of Saccharomyces cerevisiae is required on both partner vacuoles for the homotypic fusion step of vacuole inheritance. EMBO J. 14(21):5258-70.

Haas, A. (1995). A quantitative assay to measure homotypic vacuole fusion in vitro. Meth. Cell. Sci. 17:283-294.

Hamburger, Z.A., Hamburger, A.E., West, A.P., Jr., and Weis, W.I. (2006). Crystal structure of the S.cerevisiae exocyst component Exo70p. J. Mol. Biol. 356, 9-21.

Hayes, G.L., Brown, F.C., Haas, A.K., Nottingham, R.M., Barr, F.A., and Pfeffer, S.R. (2009). Multiple Rab GTPase binding sites in GCC185 suggest a model for vesicle tethering at the trans-Golgi. Mol. Biol. Cell 20, 209-217.

He, B., Xi, F., Zhang, J., TerBush, D., Zhang, X., and Guo, W. (2007). Exo70p mediates the secretion of specific exocytic vesicles at early stages of the cell cycle for polarized cell growth. J. Cell Biol. 176, 771-777.

Hickey, C.M., and Wickner, W. (2010). HOPS initiates vacuole docking by tethering membranes before trans-SNARE complex assembly. Mol. Biol. Cell 21, 2297-2305.

Hickey, C.M., Stroupe, C., and Wickner, W. (2009). The major role of the Rab Ypt7p in vacuole fusion is supporting HOPS membrane association. J. Biol. Chem. 284, 16118-16125.

Hierro, A., Rojas, A.L., Murthy, N., Effantin, G., Kajava, A.V., Steven, A.C., Bonifacino, J.S., Hurley, J.H. (2007) Functional architecture of the retromer cargo-recognition complex. Nature. 449(7165):1063-7.

Hohn, M., Tang, G., Goodyear, G., Baldwin, P.R., Huang, Z., Penczek, P.A., Yang, C., Glaesser, R.M., Adams, P.D., Ludtke, S.J. (2007). SPARX, a new environment for Cryo-EM image processing. J. Struct. Biol. 157(1):47-55.

Horazdovsky, B.F., Crowles, C.R., Mustol, P., Holmes, M., Emr, S.D. (1996). A novel RING finger protein, Vps8p, functionally interacts with the small GTPase, Vps21p, to facilitate soluble vacuolar protein localization.

Horazdovsky, B.F., Davies, B.A., Seaman, M.N., McLaughlin, S.A., Yoon, S., Emr, S.D. (1997). A sorting nexin-1 homologue, Vps5p, forms a complex with Vps17p and is required for recycling the vacuolar protein-sorting receptor. Mol. Biol. Cell. 8:1529-41.

Hughson, F.M., and Reinisch, K.M. (2010). Structure and mechanism in membrane trafficking. Curr. Opin. Cell Biol. 22, 454-460.

Hurley and Emr, S. (2006). The ESCRT complexes: structure and mechanism of a membrane-trafficking network. Annu. Rev. Biophys. Biomol. Struct. 35:277-98.

Jahn, R., and Scheller, R.H. (2006). SNAREs - engines for membrane fusion. Nat. Rev. Mol. Cell Biol. 7, 631-643.

Janke, C., Magiera, M.M., Rathfelder, N., Taxis, C., Reber, S., Maekawa, H., Moreno-Borchart, A., Doenges, G., Schwob, E., Schiebel, E., Knop, M. (2004). A versatile toolbox for PCR-based tagging of yeast genes: new fluorescence proteins, more markers and promoter substitution cassettes. Yeast. 21(11):947-62.

Kastner, B., Fischer, N., Golas, M.M., Sander, B., Dube, P., Boehringer, D., Hartmuth, K., Deckert, J., Hauer, F., Wolf, E., Uchtenhagen, H., Urlaub, H., Herzog, F., Peters, J.M., Poerschke, D., Lührmann, R., Stark, H. (2008). GraFix: sample preparation for single-particle electron cryomicroscopy. Nat. Methods. 5(1):53-5.

Kinchen, J.M., and Ravichandran, K.S. (2010). Identification of two evolutionarily conserved genes regulating processing of engulfed apoptotic cells. Nature 464, 778-782.
Klionski, D. (2005) The molecular machinery of autophagy: unanswered questions. J. Cell Sci. 118:7-18.

Klionski, D., Cueva, R., Yaver, D.S. (1992). Aminopeptidase I of Saccharomyces cerevisiae is localized to the vacuole independent of the secretory pathway. J. Cell Biol. 119:287-99.

Kornmann, B., Walter, P. (2010). ERMES-mediated ER-mitochondria contacts: molecular hubs for the regulation of mitochondrial biology. J. Cell Sci. 123(9):1389-93.

Koumandou, V.L., Dacks, J.B., Coulson, R.M., and Field, M.C. (2007). Control systems for membrane fusion in the ancestral eukaryote; evolution of tethering complexes and SM proteins. BMC Evol. Biol. 7, 29.

Kraynack, B.A., Chan, A., Rosenthal, E., Essid, M., Umansky, B., Waters, M.G., and Schmitt, H.D. (2005). Dsl1p, Tip20p, and the novel Dsl3(Sec39) protein are required for the stability of the Q/t-SNARE complex at the endoplasmic reticulum in yeast. Mol. Biol. Cell 16, 3963-3977.

Laemmli, U.K. (1970) Cleavage of structural proteins during the assembly of the head bacteriophage T4. Nature. 227:680-5.

LaGrassa, T.J., and Ungermann, C. (2005). The vacuolar kinase Yck3 maintains organelle fragmentation by regulating the HOPS tethering complex. J. Cell Biol. 168, 401-414.

Lata, S., Schoehn, G., Jain, A., Pires, R., Piehler, J. Gottlinger, H.G., Weissenhorn, W. (2008). Helical structures of ESCRT-III are disassembled by VPS4. Science. 321(5894):1354-7.

Laufman, O., Kedan, A., Hong, W., and Lev, S. (2009). Direct interaction between the COG complex and the SM protein, Sly1, is required for Golgi SNARE pairing. EMBO J. 28, 2006-2017.

Lees, J.A., Yip, C.K., Walz, T., Hughson, F.M. (2010). Molecular organization of the COG vesicle tethering complex. Nat. Struct. Mol. Biol. 17(11):1292-7.

Littleton, J.T., Barnard, R.J., Titus, S.A., Slind, J., Chapman, E.R., Ganetzky, B. (2001). SNARE-complex disassembly by NSF follows synaptic-vesicle fusion. Proc. Natl. Acad. Sci. USA. 98(21):12233-8.

Liu, J., Zuo, X., Yue, P., and Guo, W. (2007). Phosphatidylinositol 4,5-bisphosphate mediates the targeting of the exocyst to the plasma membrane for exocytosis in mammalian cells. Mol. Biol. Cell 18, 4483-4492.

Longtine, M.S., McKenzie, A., Demarini, D.J., Shah, N.G., Wach, A., Brachat, A., Philippsen, P., Pringle, J.R. (1998). Additional modules for versatile and economical PCR-based gene deletion and modification in *Saccharomyces cerevisiae*. Yeast. 14:953-61.

Ludtke, S.J., Baldwin, P.R., Chiu, W. (1999). EMAN: semiautomated software for high resolution single-particle reconstructions. J Struct. Biol. 128(1):82-97.

Marcusson, E.G., Horadovsky, B.F., Cereghino, J.L., Gharakhanian, E., Emr, S.D. (1994). The sorting receptor for the yeast vacuolar carboxypeptidase Y is encoded by the VPS10 gene. Cell. 77:579-86.

Markgraf, D.F., Ahnert, F., Arlt, H., Mari, M., Peplowska, K., Epp, N., Griffith, J., Reggiori, F., and Ungermann, C. (2009). The CORVET Subunit Vps8 Cooperates with the Rab5 Homolog Vps21 to Induce Clustering of Late Endosomal Compartments. Mol. Biol. Cell 20, 5276-5289.

Mima, J., Hickey, C.M., Xu, H., Jun, Y., and Wickner, W. (2008). Reconstituted membrane fusion requires regulatory lipids, SNAREs and synergistic SNARE chaperones. EMBO J. 27, 2031-2042.

Mizuno-Yamasaki, E., Medkova, M., Coleman, J., and Novick, P. (2010). Phosphatidylinositol 4-phosphate controls both membrane recruitment and a regulatory switch of the Rab GEF Sec2p. Dev. Cell 18, 828-840.

Munson, M., and Novick, P. (2006). The exocyst defrocked, a framework of rods revealed. Nat. Struct. Mol. Biol. 13, 577-581.

Nakada-Tsukui, K., Saito-Nakano, Y., Ali, V., Nozaki, T. (2005). A retromerlike complex is a novel Rab7 effector that is involved in the transport of the virulence factor cysteine protease in the enteric protozoan parasite Entomoeba histolytica. Mol. Biol. Cell. 16(11):5294-303.

Nakamura, N., Hirata, A., Ohsumi, Y., and Wada, Y. (1997). Vam2/Vps41p and Vam6/Vps39p are components of a protein complex on the vacuolar membranes and involved in the vacuolar assembly in the yeast Saccharomyces cerevisiae. J. Biol. Chem 272, 11344-11349.

Nickerson, D.P., Brett, C.L., and Merz, A.J. (2009). Vps-C complexes: gatekeepers of endolysosomal traffic. Curr. Opin. Cell Biol. 21, 543-551.

Niemes, S., Langhans, M., Viotti, C., Scheuring, D., San Wan Yan, M., Jiang, L., Hillmer, S., Robinson, D.G., and Pimpl, P. (2010). Retromer recycles vacuolar sorting receptors from the trans-Golgi network. Plant J. 61, 107-121.

Nordmann, M., Cabrera, M., Perz, A., Bröcker, C., Ostrowicz, C.W., Engelbrecht-Vandre, S., and Ungermann, C. (2010). The Mon1-Ccz1 complex is the GEF for the Rab7 homolog Ypt7. Curr. Biol., 20(18):1654-9.

Ohi, M., Li, Y., Cheng, Y., Walz, T. (2004). Negative staining and image classification- Powerful tools in modern electron microscopy. Biol. Proced. Online. 6:23-34.

Ortiz, D., Medkova, M., Walch-Solimena, C., and Novick, P. (2002). Ypt32 recruits the Sec4p guanine nucleotide exchange factor, Sec2p, to secretory vesicles; evidence for a Rab cascade in yeast. J. Cell Biol. 157, 1005-1016.

Ostrowicz, C.W., Bröcker, C., Ahnert, F., Nordmann, M., Lachmann, J., Peplowska, K., Perz, A., Auffarth, K., Engelbrecht-Vandré, S., and Ungermann, C. (2010). Defined subunit arrangement and Rab interactions are required for functionality of the HOPS tethering complex. Traffic, 11(10):1334-46.

Panic, B., Perisic, O., Veprintsev, D.B., Williams, R.L., and Munro, S. (2003). Structural basis for Arl1-dependent targeting of homodimeric GRIP domains to the Golgi apparatus. Mol. Cell 12, 863-874.

Panic, B., Whyte, J.R., and Munro, S. (2003). The ARF-like GTPases Arl1p and Arl3p Act in a Pathway that Interacts with Vesicle-Tethering Factors at the Golgi Apparatus. Curr. Biol. 13, 405-410.

Pawelec, A., Arsic, J., and Kolling, R. (2010). Mapping of Vps21 and HOPS binding sites in Vps8 and effect of binding site mutants on endocytic trafficking. Eukaryot. Cell 9, 602-610.

Peplowska, K., Markgraf, D.F., Ostrowicz, C.W., Bange, G., and Ungermann, C. (2007). The CORVET Tethering Complex Interacts with the Yeast Rab5 Homolog Vps21 and Is Involved in Endo-Lysosomal Biogenesis. Dev. Cell 12, 739-750.

Perez-Victoria, F.J., Abascal-Palacios, G., Tascon, I., Kajava, A., Magadan, J.G., Pioro, E.P., Bonifacino, J.S., and Hierro, A. (2010). Structural basis for the wobbler mouse neurodegenerative disorder caused by mutation in the Vps54 subunit of the GARP complex. Proc. Natl. Acad. Sci. U. S. A. 107, 12860-12865.

Perez-Victoria, F.J., and Bonifacino, J.S. (2009). Dual roles of the mammalian GARP complex in tethering and SNARE complex assembly at the trans-golgi network. Mol. Cell Biol. 29, 5251-5263.

Perez-Victoria, F.J., Schindler, C., Magadan, J.G., Mardones, G.A., Delevoye, C., Romao, M., Raposo, G., and Bonifacino, J.S. (2010). Ang2/Fat-free Is a Conserved Subunit of the Golgi-associated Retrograde Protein (GARP) Complex. Mol. Biol. Cell., 21(19):3386-95.

Peterson, M.R., Emr, S.D. (2001). The Class C Vps-complex functions at multiple stages of the vacuolar transport pathway. Traffic. 2:476-86.

Pieren, M., Schmidt, A., and Mayer, A. (2010). The SM protein Vps33 and the t-SNARE H(abc) domain promote fusion pore opening. Nat. Struct. Mol. Biol. 17, 710-717.

Plemel, R.L., Lobingier, B.T., Brett, C.L., Angers, C.G., Nickerson, D.P., Paulsel, A., Sprague, D., Merz, A.J. (2011) Subunit organization and Rab interactions of Vps-C protein complexes that control endolysosomal membrane traffic. Mol. Biol. Cell (Epub ahead of print).

Poteryaev, D., Datta, S., Ackema, K., Zerial, M., and Spang, A. (2010). Identification of the switch in early-to-late endosome transition. Cell. 141, 497-508.

Puig, O., Caspary, F., Rigaut, G., Rutz, B., Bouveret, E., Bragado-Nilsson, E., Wilm M., Séraphin, B. (2001). The tandem affinity purification (TAP) method: a general procedure of protein complex purification. Methods. 24(3):218-29.

Puig, O., Rutz, B., Luukkonen, B.G., Kandels-Lewis, S., Bragado-Nilsson, E., Séraphin, B. (1998). New constructs and strategies for effiecient PCR-based gene manipulations in yeast. Yeast. 14(12):1139-46.

Radisky, D.C., Snyder, W.B., Emr, S.D., and Kaplan, J. (1997). Characterization of VPS41, a gene required for vacuolar trafficking and high-affinity iron transport in yeast. Proc. Natl. Acad. Sci. U. S. A. 94, 5662-5666.

Raiborg, C., Stenmark, H. (2009). The ESCRT machinery in endosomal sorting of ubiquitylated membrane proteins. Nature. 458(7237):445-52.

Raymond, C.K., O'Hara, P.J., Eichinger, G., Rothman, J.H., and Stevens, T.H. (1990). Molecular analysis of the yeast VPS3 gene and the role of its product in vacuolar protein sorting and vacuolar segregation during the cell cycle. J. Cell Biol. 111, 877-892.

Reggiori, F., Pelham, H.R. (2002). A transmembrane ubiquitin ligase required to sort membrane proteins into multivesicular bodies. Nat. Cell Biol. 4:117-23.

Rehling, P., Darsow, T., Katzmann, D.J., and Emr, S.D. (1999). Formation of AP-3 transport intermediates requires Vps41 function. Nat. Cell Biol. 1, 346-353.

Ren, Y., Yip, C.K., Tripathi, A., Huie, D., Jeffrey, P.D., Walz, T., and Hughson, F.M. (2009). A structure-based mechanism for vesicle capture by the multisubunit tethering complex Dsl1. Cell 139, 1119-1129.

Rice, L.M., Brunger, A.T. (1999). Crystal structure of the vesicular transport protein Sec17: implications for SNAP function in SNARE complex disassembly. Mol. Cell. 4(1):85-95.

Richardson, B.C., Smith, R.D., Ungar, D., Nakamura, A., Jeffrey, P.D., Lupashin, V.V., and Hughson, F.M. (2009). Structural basis for a human glycosylation disorder caused by mutation of the COG4 gene. Proc. Natl. Acad. Sci. U. S. A. 106, 13329-13334.

Rieder, S.E., and Emr, S.D. (1997). A novel RING finger protein complex essential for a late step in protein transport to the yeast vacuole. Mol. Biol. Cell 8, 2307-2327.

Rigaut, G., Shevchenko, A., Rutz, B., Wilm, M., Mann, M., Séraphin, B. (1999). Ageneric protein purification method for protein complex characterization and proteome exploration. Nat. Biotechnol. 17(10):1030-2.

Rink, J., Ghigo, E., Kalaidzidis, Y., and Zerial, M. (2005). Rab conversion as a mechanism of progression from early to late endosomes. Cell. 122, 735-749.

Robinson, D.G., Jiang, L., and Schumacher, K. (2008). The endosomal system of plants: charting new and familiar territories. Plant Physiol. 147, 1482-1492.

Rojas, R., van Vlijemen, T., Mardones, G.A., Prabhu, Y., Rojas, A.L., Mohammed, S., Heck, A.J., Raposo, G., van der Sluijs, P., Bonifacino, J.S. (2008). Regulation of retromer recuitment to endosomes by sequential action of Rab5 and Rab7. J. Cell Biol. 183(3):513-26.

Rothman, J.E., (1994) Mechanisms of intracellular protein transport. Nature. 372:55-63.

Rothman, J.E., Howald, I., Stevens, T.H. (1989). Charaterization of genes required for protein sorting and vacuolar function in the yeast Saccharomyces cerevisiae. EMBO J. 8:2057-65.

Roumanie, O., Wu, H., Molk, J.N., Rossi, G., Bloom, K., and Brennwald, P. (2005). Rho GTPase regulation of exocytosis in yeast is independent of GTP hydrolysis and polarization of the exocyst complex. J. Cell Biol. 170, 583-594.

Sato, T.K., Darsow, T., Emr, S.D. (1998). Vam7p, a SNAP-25-like molecule, and Vam3p, a syntaxin homolog, function together in yeast vacuolar protein trafficking. Mol. Biol. Cell. 18(9):5308-19.

Schöbel, S., Oesterlin, L.K., Blankenfeldt, W., Goody, R.S., and Itzen, A. (2009). RabGDI displacement by DrrA from Legionella is a consequence of its guanine nucleotide exchange activity. Mol. Cell 36, 1060-1072.

Scott, S.V., Baba, M., Ohsumi, Y., Klionski, D. (1997). Aminopeptidase I is targeted to the vacuole by a nonclassical vesicular mechanism. J. Cell. Biol. 138:37-44.

Scott, S.V., Hefner-Gravink, A., Morano, K.A., Noda, T., Ohsumi, Y., Klionski, D. (1996). Cytoplasm-to-vacuole targeting and autophagy employ the same machinery to deliver proteins to the yeast vacuole. Proc. Natl. Acad. Sci. USA. 93:12304-8.

Scott, S.V., Nice, D.C.,Nau, J.J., Weisman, L.S., Kamada, Y., Keizer-Gunnink, I., Funakoshi, T., Veenhuis, M., Ohsumi, Y., Klionski, D. (2000). Apg13p and Vac8p are part of a complex of phosphoproteins that are required for cytoplasm to vacuole targeting. J. Biol. Chem. 275:25840-9.

Seals, D.F., Eitzen, G., Margolis, N., Wickner, W.T., and Price, A. (2000). A Ypt/Rab effector complex containing the Sec1 homolog Vps33p is required for homotypic vacuole fusion. Proc. Natl. Acad. Sci. U. S. A. 97, 9402-9407.

Seaman, M.N. (2005) Recycle your receptors with retromer. Trends Cell Biol. 15(2):68-75.

Seaman, M.N., Habour, M.E, Tattersall, D., Read, E., Bright, N. (2009). Membrane recruitment of the cargo-selective retromer subcomplex is catalysed by small GTPase Rab7 and inhibited by the Rab-GAP TBC1D5. J. Cell Sci. 122(14):2371-82.

Seaman, M.N., McCaffery, J.M., Emr, S.D. (1998). A membrane coat complex essential for endosome-to-Golgi retrograde transport in yeast. J. Cell Bio. 142(3):665-81.

Shestakova, A., Suvorova, E., Pavliv, O., Khaidakova, G., and Lupashin, V. (2007). Interaction of the conserved oligomeric Golgi complex with t-SNARE Syntaxin5a/Sed5 enhances intra-Golgi SNARE complex stability. J. Cell Biol. 179, 1179-1192.

Simonsen, A., Lippe, R., Christoforidis, S., Gaullier, J.M., Brech, A., Callaghan, J., Toh, B.H., Murphy, C., Zerial, M., and Stenmark, H. (1998). EEA1 links PI(3)K function to Rab5 regulation of endosome fusion. Nature. 394, 494-498.

Siniossoglou, S., and Pelham, H.R. (2001). An effector of Ypt6p binds the SNARE Tlg1p and mediates selective fusion of vesicles with late Golgi membranes. EMBO J. 20, 5991-5998.

Siniossoglou, S., and Pelham, H.R. (2002). Vps51p Links the VFT Complex to the SNARE Tlg1p. J. Biol. Chem. 277, 48318-48324.

Sinka, R., Gillingham, A.K., Kondylis, V., and Munro, S. (2008). Golgi coiled-coil proteins contain multiple binding sites for Rab family G proteins. J. Cell Biol. 183, 607-615.

Sivaram, M.V., Furgason, M.L., Brewer, D.N., and Munson, M. (2006). The structure of the exocyst subunit Sec6p defines a conserved architecture with diverse roles. Nat. Struct. Mol. Biol. 13, 555-556.

Sivaram, M.V., Saporita, J.A., Furgason, M.L., Boettcher, A.J., and Munson, M. (2005). Dimerization of the exocyst protein Sec6p and its interaction with the t-SNARE Sec9p. Biochemistry 44, 6302-6311.

Smith, R.D., Willett, R., Kudlyk, T., Pokrovskaya, I., Paton, A.W., Paton, J.C., and Lupashin, V.V. (2009). The COG complex, Rab6 and COPI define a novel Golgi retrograde trafficking pathway that is exploited by SubAB toxin. Traffic. 10, 1502-1517.

Starai, V.J., Hickey, C.M., and Wickner, W. (2008). HOPS Proofreads the trans-SNARE Complex for Yeast Vacuole Fusion. Mol. Biol. Cell. 19, 2500-2508.

Starr, T., Sun, Y., Wilkins, N., and Storrie, B. (2010). Rab33b and Rab6 are functionally overlapping regulators of Golgi homeostasis and trafficking. Traffic. 11, 626-636.

Stevens, T., Esmon, B., Schekman, R. (1982). Early stages in the yeast secretory pathway are required for transport of carboxypeptidase Y to the vacuoles. Cell. 30:439-48.

Stroupe, C., Collins, K.M., Fratti, R.A., Wickner, W. (2006). Purification of active HOPS complex reveals its affinities for phosphoinositides and the SNARE Vam7p. EMBO J. 25(8):1579-89.

Stroupe, C., Hickey, C.M., Mima, J., Burfeind, A.S., and Wickner, W. (2009). Minimal membrane docking requirements revealed by reconstitution of Rab GTPase-dependent membrane fusion from purified components. Proc. Natl. Acad. Sci. U. S. A. 106, 17626-17633.

Sun, B., Chen, L., Cao, W., Roth, A.F., and Davis, N.G. (2004). The yeast casein kinase Yck3p is palmitoylated, then sorted to the vacuolar membrane with AP-3-dependent recognition of a YXXPhi adaptin sorting signal. Mol. Biol. Cell. 15, 1397-1406.

Sun, Y., Shestakova, A., Hunt, L., Sehgal, S., Lupashin, V., and Storrie, B. (2007). Rab6 regulates both ZW10/RINT-1 and conserved oligomeric Golgi complex-dependent Golgi trafficking and homeostasis. Mol. Biol. Cell. 18, 4129-4142.

Suvorova, E.S., Duden, R., and Lupashin, V.V. (2002). The Sec34/Sec35p complex, a Ypt1p effector required for retrograde intra-Golgi trafficking, interacts with Golgi SNAREs and COPI vesicle coat proteins. J. Cell Biol. 157, 631-643.

Sztul, E., and Lupashin, V. (2006). Role of tethering factors in secretory membrane traffic. Am. J. Physiol. Cell Physiol. 290, C11-26.

Teis, D., Saksena, S., Emr, S.D. (2008). Ordered assembly of the ESCRT-III complex on endosomes is required to sequester cargo during MVB formation. Dev. Cell. 15:578-589.

Thorngren, N., Collins, K.M., Fratti, R.A., Wickner, W., Merz, A.J. (2004). A soluble SNARE drives rapid docking, bypassing ATP and Sec17/18p for vacuole fusion. EMBO J. 23(14):2765-76.

Tripathi, A., Ren, Y., Jeffrey, P.D., and Hughson, F.M. (2009). Structural characterization of Tip20p and Dsl1p, subunits of the Dsl1p vesicle tethering complex. Nat. Struct. Mol. Biol. 16, 114-123.

Ungar, D., Oka, T., Krieger, M., and Hughson, F.M. (2006). Retrograde transport on the COG railway. Trends Cell Biol. 16, 113-120.

Ungermann, C. von Mollard, G.F., Jensen, O.N., Margolis, N., Stevens, T.H., Wickner, W. (1999). Three v-SNAREs and two t-SNAREs, present in a pentameric cis-SNARE complex on isolated vacuoles, are essential for homotypic fusion. J. Cell Biol. 145(7):1435-42.

Ungermann, C., Wickner, W. (1998). Vam7p, a vacuolar SNAP-25 homolog, is required for SNARE complex integrity and vacuole docking and fusion. EMBO J. 17(12):3269-76.

Vasan, N., Hutagalung, A., Novick, P., and Reinisch, K.M. (2010). Structure of a C-terminal fragment of its Vps53 subunit suggests similarity of Golgi-associated retrograde protein (GARP) complex to a family of tethering complexes. Proc. Natl. Acad. Sci. U. S. A. 107, 14176-14181.

Wang, L., Ungermann, C., Wickner, W. (2000). The docking of primed vacuoles can be reversibly arrested by excess Sec17p (alpha-SNAP). J. Biol. Chem. 275(30):22862-7.

Weber, T., Zemelman, B.V., McNew, J.A., Westermann, B., Gmachl, M., Parlati, F., Söllner, T.H., Rothman, J.E. (1998). SNAREpins: minimal machinery for membrane fusion. Cell. 92:759-72.

Weimbs, T., Low, S.H., Chapin, S.J., Mostov, K.E., Bucher, P., Hofmann, K. (1997). A conserved domain is present in different families of vesicular fusion proteins: a new superfamily. Proc. Natl. Acad. Sci. USA. 94:3046-51.

Weisman, L. (2006). Organelles on the move: insights from yeast vacuole inheritance. Nat. Rev. Mol. Cell Biol. 7:243-52.

Weisman, L.S., Bacallao, R., Wickner, W. (1987). Multiple methods of visualizing the yeast vacuole permit evaluation of its morphology and inheritance during the cell cycle. J. Cell Biol. 105:1539-47.

Weisman, L.S., Wickner, W. (1988). Intervacuole exchange in the yeast zygote: a new pathway in organelle communication. Science. 241:589-91.

Wen, W., Chen, L., Wu, H., Sun, X., Zhang, M., Banfield, D.K. (2006) Identification of the yeast R-SNARE Nyv1p as a novel longin domain-containing protein. Mol. Biol. Cell. 17:4282-99.

Whyte, J.R., and Munro, S. (2001). The Sec34/35 Golgi transport complex is related to the exocyst, defining a family of complexes involved in multiple steps of membrane traffic. Dev. Cell 1, 527-537.

Whyte, J.R., and Munro, S. (2002). Vesicle tethering complexes in membrane traffic. J. Cell Sci. 115, 2627-2637.

Wiederkehr, A., De Craene, J.O., Ferro-Novick, S., and Novick, P. (2004). Functional specialization within a vesicle tethering complex: bypass of a subset of exocyst deletion mutants by Sec1p or Sec4p. J. Cell Biol. 167, 875-887.

Wollert, T., Yang, D., Ren, X., Lee, H.H., Im, Y.J., Hurley, J.H. (2009). The ESCRT machinery at a glance. J. Cell Sci. 122:2163-2166.

Wu, H., Rossi, G., and Brennwald, P. (2008). The ghost in the machine: small GTPases as spatial regulators of exocytosis. Trends Cell Biol. 18, 397-404.

Wurmser, A.E., Sato, T.K., and Emr, S.D. (2000). New component of the vacuolar class C-Vps complex couples nucleotide exchange on the ypt7 GTPase to SNARE-dependent docking and fusion. J. Cell Biol. 151, 551-562.

Yamashita, M., Kurokawa, K., Sato, Y., Yamagata, A., Mimura, H., Yoshikawa, A., Sato, K., Nakano, A., and Fukai, S. (2010). Structural basis for the Rho- and phosphoinositide-dependent localization of the exocyst subunit Sec3. Nat. Struct. Mol. Biol. 17, 180-186.

Yip, C.K., Berscheminski, J., Walz, T. (2010). Molecular architecture of the TRAPPII complex and implications for vesicle tethering. Nat. Struct. Mol. Biol. 17(11):1298-304.

Yogosawa, S., Hatakeyama, S., Nakayama, K.I., Miyoshi, H., Kohsaka, S., and Akazawa, C. (2005). Ubiquitylation and degradation of serum-inducible kinase by hVPS18, a RING-H2 type ubiquitin ligase. J. Biol. Chem. 280, 41619-41627.

Yu, R.C., Jahn, R., Brunger, A.T. (1999). NSF N-terminal domain crystal structure: models of NSF function. Mol. Cell. 4(1):97-107.

Zhang, X., Orlando, K., He, B., Xi, F., Zhang, J., Zajac, A., and Guo, W. (2008). Membrane association and functional regulation of Sec3 by phospholipids and Cdc42. J. Cell Biol. 180, 145-158.

Zink, S., Wenzel, D., Wurm, C.A., and Schmitt, H.D. (2009). A link between ER tethering and COP-I vesicle uncoating. Dev. Cell. 17, 403-416.

8. Supplementary data

8.1 Yeast strain list

Strain	Genotype	Reference
BJ3505	MATa *pep4Δ::HIS3 prb1Δ1.6R lys2-208 trp1Δ101 ura3-52 gal2*	Jones et al., 1982
DKY6281	MATalpha *leu2-3 leu2-112 ura3-52 his3-52 his3Δ200 trp1-Δ101 lys2-801 suc2-Δ9 PHO8::TRP1*	Klionsky et al., 1990
BY4727	MATalpha *his3Δ200 leu2Δ0 met15Δ0 trp1Δ63 ura3Δ0*	Brachmann et al., 1998
BY4732	MATa *his3Δ200 leu2Δ0 met15Δ0 trp1Δ63 ura3Δ0*	Brachmann et al., 1998
BY4733	MATalpha *his3Δ200 leu2Δ0 met15Δ0 trp1Δ63 ura3Δ0*	Brachmann et al., 1998
BY4741	MATa *his3Δ200 leu2Δ200 met15Δ0 ura3Δ0*	Brachmann et al., 1998
CSY09	*vps11Δ::HIS3MX6 pep4Δ::KanMX6 VPS11-1-URA3*	Stroupe et al., 2006
CSY10	*vps11Δ::HIS3MX6 pho8Δ::KanMX6 VPS11-1-URA3*	Stroupe et al., 2006
CUY1772	BY4733 *VPS33::HIS3-GAL1pr*	Ostrowicz et al., 2010
CUY1801	BY4741 *VPS41::TAP-URA3*	Ostrowicz et al., 2010
CUY1953	BY4732 *VPS41::TRP1-GAL1pr VPS41::TAP-URA3 VPS39::KanMX6-GAL1pr VPS33::HIS3-GAL1pr*	Ostrowicz et al., 2010
CUY2152	BY4732 *VPS41::TRP1-GAL1pr VPS41::TAP-URA3*	Ostrowicz et al., 2010
CUY2489	BY4727 *VPS11::HIS3-GAL1pr VPS16::natNT2-GAL1pr VPS18::KanMX6-GAL1pr-3HA*	Ostrowicz et al., 2010
CUY2530	BY4732 *VPS33::TRP1-GAL1pr*	Ostrowicz et al., 2010
CUY2675	BY4732xBY4727 *VPS41::TRP1-GAL1pr VPS41::TAP-URA3 VPS39::KanMX6-GAL1pr VPS33::HIS3-GAL1pr VPS11::HIS3-GAL1pr VPS16::natNT2-GAL1pr VPS18::KanMX6-GAL1pr-3HA*	Ostrowicz et al., 2010
CUY2724	BY4727 *VPS39::natNT2-GAL1pr VPS39::TAP-URA3 VPS11::HIS3-GAL1pr*	Ostrowicz et al., 2010
CUY2836	BY4727 *VPS11::HIS3-GAL1pr VPS11::TAP-URA3 VPS16::natNT2-GAL1pr VPS18::KanMX6-GAL1-3HA*	Ostrowicz et al., 2010
CUY2837	BY4727 *VPS11::HIS3-GAP1pr VPS16::natNT2-GAL1pr VPS16::TAP-URA3 VPS18::KanMX6-GAL1pr*	Ostrowicz et al., 2010
CUY2838	BY4727 *VPS11::HIS3-GAL1pr VPS16::natNT2.GAL1pr VPS18::KanMX6-GAL1pr VPS18::TAP-URA3*	Ostrowicz et al., 2010
CUY2839	BY4732 *VPS33::TRP1-GAL1pr VPS33::TAP-URA3*	Ostrowicz et al., 2010
CUY2858	BY4732 *VPS16::KanMX6-GAL1pr VPS16::TAP-URA3*	Ostrowicz et al., 2010
CUY2873	BY4732 *VPS39::KanMX6-GAL1pr VPS39::TAP-URA3*	Ostrowicz et al., 2010

CUY2989	BY4727 *VPS11::HIS3-GAL1pr VPS16::natNT2-GAL1pr VPS18::KanMX6-GAL1pr-3HA VPS33::TAP-URA3*	Ostrowicz et al., 2010
CUY3021	BY4732xBY4727 *VPS33::TRP1-GAL1pr VPS11::HIS3-GAL1pr VPS16::natNT2-GAL1pr VPS18::KanMX6GAL1pr-3HA VPS11::TAP-URA3*	Ostrowicz et al., 2010
CUY3022	BY4732xBY4727 *VPS11::HIS3-GAL1pr VPS16::natNT2-GAL1pr VPS18::KanMX6-GAL1pr-3HA VPS16::TAP-URA3*	Ostrowicz et al., 2010
CUY3023	BY4732xBY4727 *VPS11::HIS3-GAL1pr VPS16::natNT2-GAL1pr VPS18::KanMX6-GAL1pr-3HA VPS18::TAP-URA3*	Ostrowicz et al., 2010
CUY3050	BY4727 *VPS11::HIS3-GAL1pr VPS18::KanMX6-GAL1pr-3HA*	Ostrowicz et al., 2010
CUY3238	BY4733xBY4732 *VPS33::HIS3-GAL1pr VPS16::KanMX6-GAL1pr VPS16::TAP-URA3*	This study
CUY3396	BY4727 *VPS11::HIS3-GAL1pr VPS39::natNT2-GAL1pr VPS39::TAP-URA3 VPS18::TRP1-GAL1pr*	Ostrowicz et al., 2010
CUY3435	BY4732 *VPS41::TRP1-GAL1pr VPS39::KanMX6-GAL1pr VPS39::TAP-URA3*	This study
CUY3447	BY4727xBY4732 *VPS11::HIS3-GAL1pr VPS18::KanMX6-GAL1pr-3HA VPS41::TRP1-GAL1pr VPS39::KanMX6-GAL1pr VPS39::TAP-URA3*	This study
CUY3798	BY4732 *VPS39::KanMX6-GAL1pr VPS33::HIS3-GAL1pr GAL1pr::GAL1pr-VPS41 aa366-377Δ-URA3 VPS41 aa366-377Δ::TAP-TRP1*	This study
CUY3799	BY4732 *VPS39::KanMX6-GAL1pr VPS33::HIS3-GAL1pr GAL1pr::GAL1pr-VPS41 aa356-379Δ-URA3 VPS41 aa356-379Δ::TAP-TRP1*	This study
CUY3801	BY4727xBY4732 *VPS11::HIS3-GAL1pr VPS16::natNT2-GAL1pr VPS18::KanMX6-GAL1pr-3HA VPS39::KanMX6-GAL1pr VPS33::HIS3-GAL1pr GAL1pr::GAL1pr-VPS41 aa366-377Δ-URA3 VPS41 aa366-377Δ::TAP-TRP1*	This study
CUY3802	BY4727xBY4732 *VPS11::HIS3-GAL1pr VPS16::natNT2-GAL1pr VPS18::KanMX6-GAL1pr-3HA VPS39::KanMX6-GAL1pr VPS33::HIS3-GAL1pr GAL1pr::GAL1pr-VPS41 aa356-379Δ-URA3 VPS41 aa356-379Δ::TAP-TRP1*	This study
CUY4391	BY4732xBY4727 *VPS41::TRP1-GAL1pr VPS41::TAP-URA3 VPS39::KanMX6-GAL1pr VPS39::yeGFP-hphNT1 VPS33::HIS3-GAL1pr VPS11::HIS3-GAL1pr VPS16::natNT2-GAL1pr VPS18::KanMX6-GAL1pr-3HA*	This study

CUY4392	BY4732xBY4727 *VPS41::TRP1-GAL1pr VPS41::TAP-URA3 VPS39::KanMX6-GAL1pr VPS33::HIS3-GAL1pr VPS11::HIS3-GAL1pr VPS11::yeGFP-hphNT1 VPS16::natNT2-GAL1pr VPS18::KanMX6-GAL1pr-3HA*	This study
CUY4393	BY4732xBY4727 *VPS41::TRP1-GAL1pr VPS41::TAP-URA3 VPS39::KanMX6-GAL1pr VPS33::HIS3-GAL1pr VPS11::HIS3-GAL1pr VPS16::natNT2-GAL1pr VPS16::yeGFP-hphNT1 VPS18::KanMX6-GAL1pr-3HA*	This study
CUY4394	BY4732xBY4727 *VPS41::TRP1-GAL1pr VPS41::TAP-URA3 VPS39::KanMX6-GAL1pr VPS33::HIS3-GAL1pr VPS11::HIS3-GAL1pr VPS16::natNT2-GAL1pr VPS18::KanMX6-GAL1pr-3HA VPS18::yeGFP-hphNT1*	This study
CUY4395	BY4732xBY4727 *VPS41::TRP1-GAL1pr VPS41::TAP-URA3 VPS39::KanMX6-GAL1pr VPS33::HIS3-GAL1pr VPS33::yeGFP-hphNT1 VPS11::HIS3-GAL1pr VPS16::natNT2-GAL1pr VPS18::KanMX6-GAL1pr-3HA*	This study
CUY4605	BY4727xBY4741 *VPS11::HIS3-GAL1pr VPS16::naNT2-GAL1pr VPS18::KanMX6-GAL1pr-3HA VPS33::TRP1-GAL1pr VPS3::KanMX6-GAL1pr VPS41::natNT2-GAL1pr VPS41::TAP-URA3*	This study
CUY4640	BY4727 *VPS11::HIS3-GAL1pr VPS16::naNT2-GAL1pr VPS18::KanMX6-GAL1pr-3HA VPS33::TRP1-GAL1pr*	This study
CUY4641	BY4741 *VPS3::KanMX6-GAL1pr VPS41::natNT2-GAL1pr VPS41::TAP-URA3*	This study
CUY4659	BJ3505 *YPT7::natNT2-GPDpr*	Balderhaar et al., 2010
CUY4661	DKY6281 *YPT7::natNT2-GPDpr*	Balderhaar et al., 2010
CUY5471	BJ3505 *VPS39::KanMX6-GPDpr*	This study
CUY5473	DXY6281 *VPS39::KanMX6-GPDpr*	This study

8.2 List of figures

8.3 List of tables

8.4 List of abbreviations

α-SNAP	α-soluble N-ethylmaleimide-sensitive factor attachment protein
ALP	alkaline phosphatase (Pho8)
ATP	adenosinetriphosphate
BAR domain	Bin/ Amphiphysin/ Rvs domain
CATCHR	complex associated with tethering containing helical rods
COG	Conserved oligomeric complex
CORVET	Class C core vacuole/endosome tethering
Cvt	cytoplasm to vacuole targeting
ddH20	distilled water
DIC	differential interference contrast
DNA	desoxyribonucleicacid
dNTP	desoxynucleotide
DTT	dithiotreitol
E.coli	*Escherichia coli*

ER	endoplasmatic reticulum
ESCRT	endosomal sorting complex required for transport
FM4-64	N- (3-triethylammoniumpropyl)-4-(6-(4-(diethylamino) phenyl) hexatrienyl) pyridinium dibromide
g	gravity
GAP	GTPase activating protein
GARP	Golgi-associated retrograde protein
Gdi	GTPase dissociation inhibitor
GDF	Gdi-displacement factor
GDP	Guanosine-nucleotide-diphosphate
GEF	GDP/GTP exchange factor
GFP	green fluorescent protein
GTP	Guanosine-nucleotide-triphosphate
h	hours
HOPS	Homotypic fusion and vacuole protein sorting
IPTG	Isopropyl-b-D-thiogalactopyranosid
kDa	kilo Dalton
M	Molarity (mol/l)
min	minutes
NSF	N-ethylmaleimide-sensitive factor
OD600nm	optical density at the wavelength of 600nm
PAGE	polyacrylamide gelelectrophoresis
PCR	polymerase chain reaction
pNPP	para-nitrophenylphosphate
rpm	rounds per minute
S.cerevisiae	*Saccharomyces cerevisiae*
SDS	Sodium-dodecylsulfate
sec	seconds
SNARE	soluble N-ethylmaleimide-sensitive attachment protein receptor
TGN	Trans-Golgi network
Tris	Tris-(hydroxymethyl)-aminomethane
U	Units of enzymatic activity
v/v	volume per volume
w/v	weight per volume

9. Acknowledgments

First of all, I would like to thank Christian Ungermann for offering me the opportunity to work in his lab. He is great supervisor and a never-ending source of ideas. He tought me to work efficiently in a scientific lab and to critically discuss science. Thank you for the possibility to work on this great project.

Furthermore, I would like to thank Sigfried Engelbrecht-Vandré for many scientific discussions and for being the referee of this thesis.

I would like to acknowledge Stefan Raunser and Anne Schwedt for the great cooperatios and the “discussions within hours in the dark”. I really appreciate the great correspondance within our cooperation and I am really looking forward to the final HOPS structure.

I would like to thank the “old Ungermann people” from Heidelberg, who supported me in the first year of my PhD. I especially want to thank Clemens Ostrowicz for his supervision and making my start in the lab as smooth as possible.

Finally, I would like to thank the “new Ungermann people” (mainly from Osnabrück) for the relaxed and inspiring atmosphere in the lab. Thank you Margarita Cabrera, Lars Langemeyer, Arun Thomas John Peter, Mirjana Nordmann, Jens Lachmann, Henning Balderhaar, Franziska Ahnert, Ralf Rethmeier, Nadine Epp, Johannes Numrich, Henning Arlt and Carina (Uschi) Hönscher for the great time together. I especially like to thank Angela Perz and Kathrin Auffarth for technical and mental support in every situation. Thanks to Christine Schimp for harvesting yeast cells. I would like to thank Lukas Krämer for being my office-mate and for lots of scientific and non-scientific discussions. I had a great time in the lab!

Danksagung

Ich möchte mich in erster Linie bei meinen Eltern bedanken, die mich während meines gesamten Studiums und der Promotion immer unterstützt haben. Vielen Dank, dass Ihr immer an mich geglaubt hab, auch wenn ich es mal nicht getan hab. Vielen Dank für die materielle/ finanzielle und mental Unterstützung.

Ich danke meinen “ehemaligen Lübeckern” für die vielen Anrufe, Mails und Postkarten seitdem wir nicht mehr in einer Stadt wohnen. Mein Dank gilt vorallem

Sandra Braren, Sylvia Merkert, Elli Gretschik und Birte Hansen für die regelmäßigen “Kontrollanrufe”. Ich hoffe wir schaffen es, in Kontakt zu bleiben.
Ich möchte mich bei Henning Balderhaar für die beiden letzten Jahre bedanken. Vielen Dank für’s Warten, Zuhören, Beruhigen und für’s einfach nur Dasein. Ich danke Wimbledon, der mich während meines gesamten Studiums begleitet und immer “auf Trap” gehalten hat.
Ohne Eure Unterstützung hätte ich diese Ausbildung nicht geschafft! Vielen Dank dafür!

10. Eidesstattliche Erklärung

Erklärung über die Eigenständigkeit der erbrachten wissenschaftlichen Leistung

Ich erkläre hiermit, dass ich die vorliegende Arbeit ohne unzulässige Hilfe Dritter und ohne Benutzung anderer als der angegebenen Hilfsmittel angefertigt habe. Die aus anderen Quellen direkt oder indirekt übernommenen Daten und Konzepte sind unter Angabe der Quelle gekennzeichnet.

Weitere Personen waren an der inhaltlichen materiellen Erstellung der vorliegenden Arbeit nicht beteiligt. Insbesondere habe ich hierfür nicht die entgeltliche Hilfe von Vermittlungs- bzw. Beratungsdiensten (Promotionsberater oder andere Personen) in Anspruch genommen. Niemand hat von mir unmittelbar oder mittelbar geldwerte Leistungen für Arbeiten erhalten, die im Zusammenhang mit dem Inhalt der vorgelegten Dissertation stehen.

Die Arbeit wurde bisher weder im In- noch im Ausland in gleicher oder ähnlicher Form einer anderen Prüfungsbehörde vorgelegt.

....
(Ort, Datum) (Unterschrift)